Finite Element Tool for Modelling Stent Deployment to Aid Stent Design

Pieter-André Keevy

Submitted to the University of Cape Town in partial fulfilment of the requirements for the degree of Master of Science in Biomedical Engineering

December 2004

DECLARATION

I, Pieter-André Keevy, declare that the work set out in thesis is essentially my own work and that no part has been submitted for a degree at any academic institution

Signed by candidate

Signature removed

Pieter-André Keevy

Cape Town, December 2004

ABSTRACT

Atherosclerosis, which is the underlying cause of most arterial blockage, is a major health care risk. The implantation of stents is a popular and effective technique used by cardiologists to treat the arterial stenosis. Currently the large balloon-inflatable stents used for iliac vessels have a tendency to slip off the delivery balloon when the stent is deployed. The project in hand deals with the use of finite element modelling to simulate the deployment system in an attempt to find a solution to the problem.

The modelling of stents by different finite element packages was carefully analysed and the results of various simulations described in the literature were reviewed. However, published work on the simulation of balloon-inflatable stents with computer programs is very scarce. For this study the ABAQUS finite element package was used to model the system. After carefully studying the folded balloon shape, the balloon was modelled with membrane elements, having square ends instead of the actual tapered ones. Two stents were modelled with the use of shell elements, the one being in the uncrimped form and the other having the dimensions of an already crimped stent. Shell elements were also used to create the inner lumen of the catheter. The guide wire that fits inside the lumen was modelled as a discrete rigid body. At first the already crimped stent was used in the assembly. The balloon, inner lumen and guide-wire were fixed in the axial direction, whereas the stent had free boundary conditions and was allowed to move in any direction. Pressure was applied to the inner surface of the balloon, which inflated and forced the stent to deploy.

A stent crimping machine was then studied and the mechanism modelled as 12 discrete rigid plates, which were arranged in circumferential fashion and moved radially inwards to mimic the crimping action. The already crimped stent was then replaced with the uncrimped one and the crimping tool model added. The stent was now crimped onto the outer surface of the balloon, the crimping tool removed and the balloon inflated to deploy the stent. In an attempt to cause the stent to shoot off the delivery balloon, the stent was

assembled so that it was located off-centre on the balloon and the balloon was then inflated.

The simulations yielded satisfactory results, although the simulations were found to be extremely expensive from a computational point of view, with run times of up to 2 weeks. The energies in the system as well as the stress distributions were computed and analysed. The deformation of the stent and balloon was closely watched throughout the simulation. The balloon was inflated and the pressure was large enough to overcome the reaction force of the stent and to deploy it. It was found that the balloon took on a triangular shape during inflation, which produced out-of-plane deformation of the stent's hairpin bends. This is an area of concern, since this could potentially cause injury to the vessel wherein it is to be deployed. The displacement of the stent during the whole simulation, both crimping and deployment, was calculated and analysed. It was found that stored inertial energy caused the stent to have a "spring back" motion and it began to oscillate when the crimping tool plates were removed. During crimping and deployment of the stent it was plastically deformed and thus work-hardened into its new shape. The use of a parallel computer cluster to decrease simulation times was also investigated, and found to be a feasible option, depending on the nature of the simulation.

Due to time constraints and the computationally expensive nature of the simulations, the exact reason for the dislodging of the stent could not be established. However, crucial knowledge was gained about possible reasons for this phenomenon. The areas where failure is likely to occur were identified as well as causes for possible vessel injury. The computer model that was created can also be used to investigate the effects of certain alterations in the stent design. These include, for instance, changes in stent strut dimensions and material properties, which could be useful when trying to achieve the optimal stent design. This finite element model thus opens the door to future simulation studies and makes it considerably easier to find a solution to the off-shooting stent.

ACKNOWLEDGEMENTS

The research that follows was completed with the support, encouragement and patience of a number of dynamic people. Thank you!

Professor C.L. Vaughan, head of the Department of Biomedical Engineering, UCT, for his guidance and patience as thesis supervisor and for organising financial assistance.

Hellmut Bowles, FEAS, for all his assistance, guidance and patience in helping me with the modelling of the system, as well as the use of their computers for the simulations.

Bruce Becker, UCT-CERN Research Centre, Physics Department, UCT, for allowing me to use the computer cluster and helping me set up ABAQUS on the system.

Victor Balden, FEAS, for assisting me with the setup of ABAQUS on the computer cluster and organizing a computer at CERECAM, UCT.

Damian Conway, DISA Vascular, for his ideas and input and for organizing financial support.

My girlfriend, parents, sister and grandmother who supported me throughout and who continue to be enthusiastic about my future plans.

TABLE OF CONTENTS

LIST OF FIGURES

LIST OF TABLES

CHAPTER ONE

INTRODUCTION

The arterial system is increasingly affected by atherosclerosis. It manifests itself through the gradual thickening of the arterial walls, where there is a deposit of fatty plaque. This leads to a decrease in the vessel luminal diameter. Atherosclerosis is the underlying chronic disease in most cases of artery stenosis or arterial blockage. This results in the narrowing or complete occlusion of the vessels, which in turn leads to restriction of blood supply to the tissues in the human body. Restoring adequate arterial blood flow to insufficiently oxygenated tissue areas will help to treat this problem. Presently there are different surgical and interventional approaches that could be taken. The most common are the interventional methods because they are minimally invasive. For this method catheters are used to access the diseased artery. Two different interventional methods are currently used: Percutaneous transluminal angioplasty (PTA) and stenting. With PTA a catheter, with a deflated balloon mounted onto it, is advanced in the artery to the area of blockage. The balloon is then inflated in the area of the occlusion to the original vessel diameter to widen the restriction and restore normal blood flow to the area.

A stent is a small, smooth, metallic tubular mesh, which is used to support arterial walls to minimize the blockage of arteries (Etave *et al.*, 2001 and Migliavacca *et al.*, 2002). There are two types of stents: self-expanding and balloon expandable. Practically, the self-expanding stent is crimped onto a balloon, which is then attached to a catheter. It is then advanced to the area of blockage, the balloon inflated and the stent deployed. The balloon is then deflated and the plastically deformed mesh maintains the dimension of the inflated balloon. The stent is thus left to support the damaged arterial wall after the balloon has been deflated and the delivery system removed. Figure 1.1 shows a typical stent in crimped and deployed form.

The use of stents is not without problems, however, and there are difficulties: migrations, clot formations, collapses and positioning are some of the serious issues (Migliavacca *et*

al., 2002). Different techniques have been used in the past to try and determine the mechanical properties and characteristics of the stents. This information helps the design of the stent and stent delivery systems to minimize the different problems involved with the use of stents.

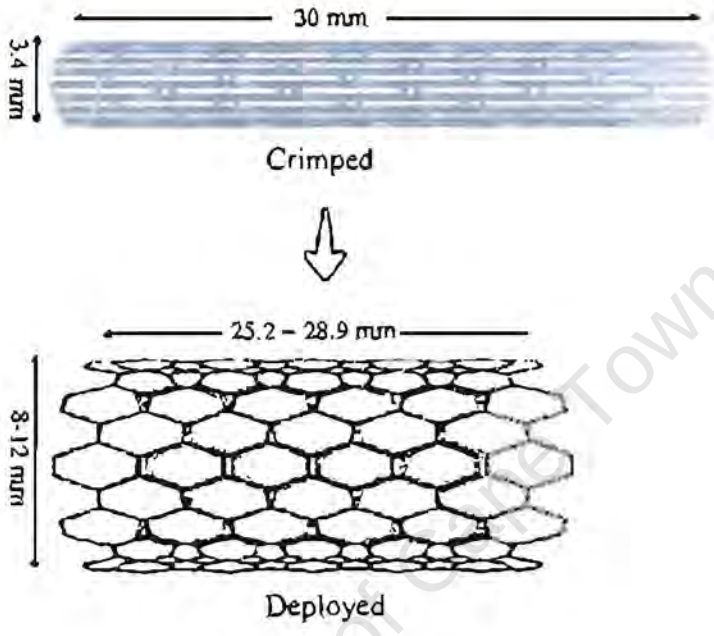

Figure 1.1 Typical stent in crimped and deployed shape (Dumoulin *et al.*, 2000)

This project was done in conjunction with the company DISA Vascular (Pty) Ltd that is based in Cape Town, South Africa. DISA Vascular specializes in the design and development of coronary and peripheral stents and related technologies. The company has developed a number of stent platforms, from stainless steel to cobalt-chromium. They have exploited the proven S-Flex coronary stent technology and developed a range of peripheral stents that combine the attributes of a leading coronary stent with the specific requirement for the peripheral vessels. The large balloon-inflatable stents used for iliac vessels (diameters of up to 12mm) have a tendency to slip off the delivery balloon when it is deployed. This could be very dangerous to the patient and could lead to major problems. The exact reason for this phenomenon is unknown, but it was believed that the asymmetrical initial opening of the balloon was one of the main causes. The one end of

the balloon opened up quicker than the other and this tended to push the stent off the balloon. Other reasons could be: the fact that the stent is not central on the folded balloon; internal pressure is not uniform; balloon folding is not uniform; and the fact that the stent is not uniformly in contact with the folded balloon. Understanding the physical mechanism and mechanical properties of the system is the first step in finding the reason for this phenomenon and solving this problem.

Finite element modelling is believed to be the right tool to use to solve this problem and therefore the ABAQUS finite element package (Hibbit Karlsson & Sorenses, Inc., Pawtucket, RI, USA) is used to model the system. An initial literature study of previous studies where Finite Element Analysis was used to model stents forms the foundation for the modelling of the system. Based on these findings the balloon, which is used to expand the stent, the stent itself, the inner lumen on which the balloon is fixed and the guide wire used to insert the catheter, will be modelled in detail. Pressure will then be applied to the inner surface of the balloon to model the deployment of the balloon.

The stent is actually crimped onto the folded balloon to ensure that the stent does not dislodge during the advancing of the catheter to the site of blockage in the vessel. After successful modelling of the stent deployment, the crimping tool will be modelled and the whole system assembled. The stent will then be crimped onto the balloon, the crimping tools removed and finally the balloon, with crimped stent on top of it, will be inflated and the stent deployed. Finally, imperfections will be added to the model to try and simulate the shooting off of the stent during deployment and to find the cause of this strange phenomenon.

Chapter Two will be a review of the relevant literature on the finite element modelling of stents. Chapters Three and Four will outline the actual modelling of the system, while Chapter Five will provide the simulation results and include an in-depth discussion. This will be followed by Chapters Seven and Eight, which will comprise of a conclusion and give recommendations on future work.

CHAPTER TWO

LITERATURE REVIEW

2.1 The Finite Element Method

In recent years, the finite element method has become widely accepted by the engineering professions as an extremely valuable method of analysis (Rockey *et al.,* 1975). At first it was applied to problems of stress analysis, but has subsequently been applied to many other problems of continua. The development of the finite element method thus ensures a rapidly widening field of application. Problems that were once regarded as insoluble can now be solved and satisfactory results obtained. The finite element (FE) analysis is a way of getting a numerical solution to a specific problem (Cook, 1995). However, the FE solution is approximate and it does not produce a formula as solution, nor does it solve a class of problems.

Cook (1995) gave an unsophisticated description of the FE method to try and explain what FE modelling is in laymen terms. Basically a structure is cut into several elements and the behaviour of each element then described in a simple way. The elements are reconnected via "nodes", which are like drops of glue holding the elements together. This process results in a set of simultaneous algebraic equations. There may be several thousand such equations, which must be analysed and solved by the computer. In stress analysis these equations are in equilibrium. Cook (1995) also provided a more sophisticated description of the FE method: it could be regarded as a piecewise polynomial interpolation. This means that, over an element, a field quantity such as displacement is interpolated from values of the field quantity at the nodes. If the elements are connected, the field quantity becomes interpolated over the whole structure in piecewise fashion. There are thus as many polynomial expressions as there are elements.

According to Cook *et al.* (2002) the general formulation of elements of finite element analysis relies on tools of stress analysis, which includes stress-strain relations, strain-

displacement relations and energy considerations. Stress-strain relations could be stated in the followings matrix forms for linear elasticity:

$$\{\sigma\} = [E]\{\varepsilon\} \tag{2.1}$$

where $\{\sigma\}$ and $\{\varepsilon\}$ are the vector arrays of stresses and strains, respectively and [E] is the matrix of the elastic modulus. In two dimensions, with x and y coordinates, the equation can be rewritten as:

Stresses = Constitutive matrix x Strains

$$\begin{Bmatrix} \sigma_x \\ \sigma_y \\ \tau_{xy} \end{Bmatrix} = \begin{bmatrix} E_{11} & E_{12} & E_{13} \\ E_{21} & E_{22} & E_{23} \\ E_{31} & E_{32} & E_{33} \end{bmatrix} \times \begin{Bmatrix} \varepsilon_x \\ \varepsilon_y \\ \tau_{xy} \end{Bmatrix} \tag{2.2}$$

To obtain the relations for the displacement field, the following definitions of strain could be used. Engineering normal strain is change in length divided by the original length while shear strain is the amount of change in a right angle. Figure 2.1 shows the formulas for strains ε_x, ε_y, γ_{xy} in the xy plane.

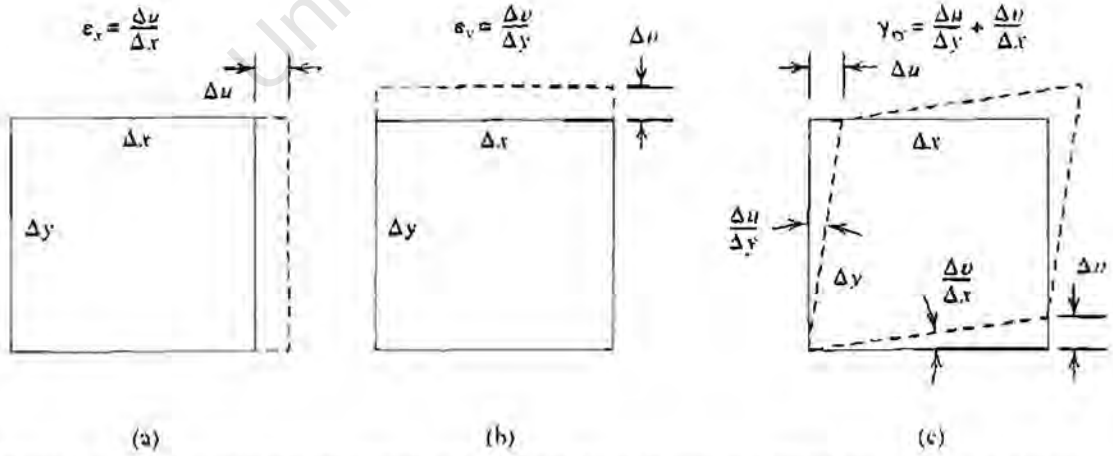

Figure 2.1 An infinitesimal rectangle, subjected to (a) x-direction normal strain, (b) y-direction normal strain, (c) shear strain (Cook *et al.*, 2002)

The two-dimensional strain-displacement relations could be written as:

$$\begin{aligned} \varepsilon_x &= \frac{\partial u}{\partial x} \\ \varepsilon_x &= \frac{\partial v}{\partial y} \\ \gamma_{xy} &= \frac{\partial u}{\partial y} + \frac{\partial v}{\partial x} \end{aligned} \tag{2.3}$$

For 2-D cases the strain-relationship could now be rewritten as:

$$\begin{Bmatrix} \varepsilon_x \\ \varepsilon_y \\ \gamma_{xy} \end{Bmatrix} = \begin{bmatrix} \frac{\partial}{\partial x} & 0 \\ 0 & \frac{\partial}{\partial y} \\ \frac{\partial}{\partial y} & \frac{\partial}{\partial x} \end{bmatrix} \times \begin{Bmatrix} u \\ v \end{Bmatrix} \tag{2.4}$$

or symbolically,

$$\{\varepsilon\} = [\partial] \times \{u\} \tag{2.5}$$

furthermore it was given that

$$\{u\} = [N] \times \{d\} \qquad \text{where} \qquad \{u\} = \lfloor u \quad v \quad w \rfloor^T \tag{2.6}$$

where {u} and {d} are the displacements and nodal displacement respectively and [N] the shape function matrix. If the two equations above are now combined, it could be shown that

$$\{\varepsilon\} = [B] \times \{d\} \qquad \text{where} \qquad [B] = [\partial] \times [N] \tag{2.7}$$

The stiffness matrix of the individual elements could be written as:

$$[k]_{elm} = \int [B]^T [E][B] dV \qquad (2.8)$$

For the assembly of the elements to form a finite element structure, the global stiffness matrix was given as:

$$[K]_{global} = \sum_{i=1}^{N_{els}} [k]_i \qquad (2.9)$$

where N_{els} is the number of elements in the structure. It could now also be shown that:

$$[K]_{global}\{D\} = \{F\}_{external} \qquad (2.10)$$

where {d} for each element is assembled into a global displacement vector {D}, the vector of degrees of freedom for the entire structure and $\{F\}_{external}$ is equal to the external forces applied to the structure nodes. This equation is for a linear static system.

This project involves a structure that is in movement; therefore it is useful to look at the equations for a system in motion. Bathe (1976) explained that for a finite element system in motion the equations for equilibrium could be written as:

$$[M]\{\ddot{D}\} + [C]\{\dot{D}\} + [K]\{D\} = \{F_{external}\} \qquad (2.11)$$

where M, C and K are the mass, damping and stiffness matrices, respectively, $F_{external}$ is the external load vector and U, $\dot{U}$ and $\ddot{U}$ are the displacement, velocity and acceleration vectors of the finite element assembly. All of these factors are time-dependant and the equation may be rewritten as:

$$F_I(t) + F_D(t) + F_E(t) = F(t) \qquad (2.12)$$

where $F_I(t)$, $F_D(t)$ and $F_E(t)$ are inertia, damping and elastic forces, respectively. For this reason, in dynamic analysis, the static equilibrium at time t is considered. Two types of numerical integration techniques may be used, implicit or explicit integration.

Bathe (1976) explained that explicit integration is aimed at satisfying only at discrete time intervals Δt. This means that equilibrium is sought at discrete time points. If the displacement, velocity and acceleration vectors at time 0 are known and the solution of the above equation is needed for time 0 to T. The time T is now subdivided into *n* equal time intervals Δt. The integration algorithm assumes that that the solutions at times 0, Δt, $2\Delta t$,...., t are known and that the solution at time $t + \Delta t$ is required next. The explicit integration method most commonly used is the central difference method. It was assumed that:

$$\{\ddot{D}\}_t = \frac{1}{\Delta t^2}(\{D\}_{t-\Delta t} - 2\{D\}_t + \{D\}_{t+\Delta t}) \qquad (2.13)$$

and

$$\{\dot{D}\}_t = \frac{1}{2\Delta t}(-\{D\}_{t-\Delta t} + \{D\}_{t+\Delta t}) \qquad (2.14)$$

now substituting for $\dot{D}$ and $\ddot{D}$ we obtain:

$$\{D\}_{t+\Delta t} = \left[\frac{1}{\Delta t^2}M + \frac{1}{2\Delta t}C\right]^{-1}\left(\{F\}_t - \left[K - \frac{2}{\Delta t^2}M\right]\{D\}_t - \left[\frac{1}{\Delta t^2}M - \frac{1}{2\Delta t}C\right]\{D\}_{t-\Delta t}\right)$$

or simply put

$$[M]\{\ddot{D}\}_t + [C]\{\dot{D}\}_t + [K]\{D\}_t = \{F_{external}\} \Rightarrow \{D\}_{t+\Delta t} \qquad (2.15)$$

The time step Δt is critical for the analysis. The integration scheme is conditionally stable and therefore $\Delta t \leq \Delta t_{crit}$ to prevent divergence. If Δt is too large, explicit integration fails and if Δt is too small, it is computationally too expensive. Cook *et al.* (2002) defined Δt_{crit} as follows:

$$\Delta t_{crit} \leq \frac{L}{\sqrt{\frac{E}{\rho}}} \tag{2.16}$$

This means that Δt must be small enough so that information does not propagate more than the distance between adjacent nodes during a single time step. For implicit integration equilibrium conditions are not used at time Δt but at time t + Δt. This could easily be explained by the following equation:

$$[M]\{\ddot{D}\}_{t+\Delta t} + [C]\{\dot{D}\}_{t+\Delta t} + [K]\{D\}_{t+\Delta t} = \{F_{external}\} \Rightarrow \{D\}_{t+\Delta t} \tag{2.17}$$

Different types of elements could be used to build up a finite element structure, but only two will be described here, namely: shell and membrane elements.

Cook *et al.* (2002) described a shell having a curved inner and outer surface, which is separated by a thickness t that is small in comparison with the overall dimensions of the shell. The mid-surface is a distance halfway between the outer and inner surfaces, in other words a distance t/2. Most finite element software packages make use of the mid-surface or mid-plane value to model the shell element. An illustration of this surface is shown in Figure 2.2.

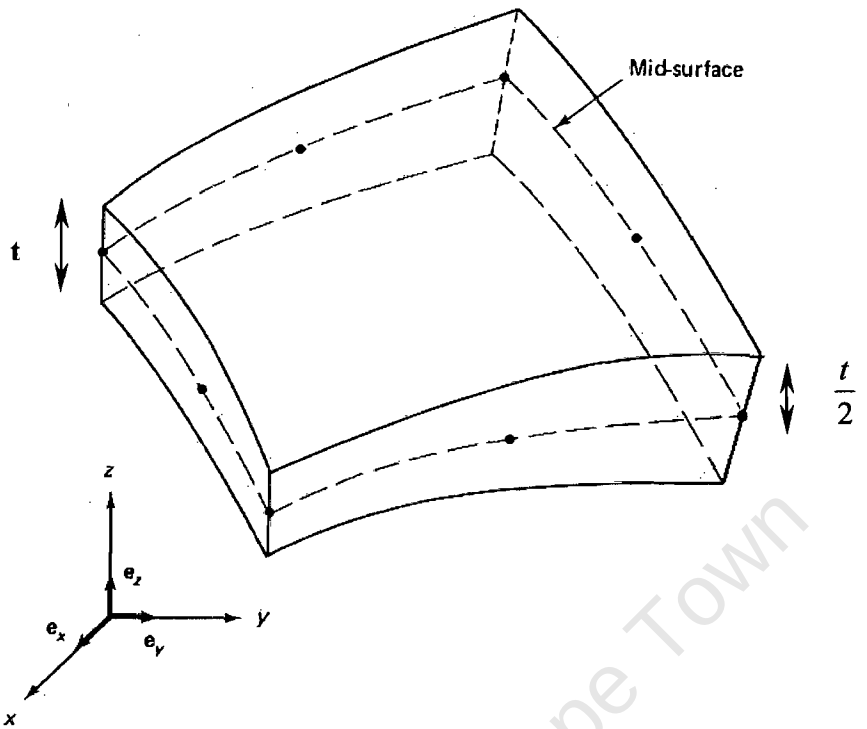

Figure 2.2 Mid-surface illustration (Bathe, 1982)

The general-purpose shell elements used in the finite element package ABAQUS are small-strain elements. The ABAQUS user's manual explained that these general-purpose elements provide robust and accurate solutions in all loading conditions for thin and thick shell problems. Thickness change as a function of in-plane deformation is allowed. The elements do not suffer from transverse shear locking, nor do they have any unconstrained hourglass modes. With the exception of the small-strain elements, all of these elements consider finite membrane strains. No hourglass control is required in the bending and membrane response of the fully integrated shell element. The membrane kinematics of the elements is based on an assumed-strain formulation that provides accurate solutions for in-plane bending behaviour. These elements are well suited for many impact dynamics problems, including structures undergoing large-scale buckling behaviour, which involves small-strains but large rotations and severe bending. These elements use simplified methods for strain calculation and hourglass control and offer significant advantages in computational speed.

On the other hand, membrane elements are sheets in space that can carry membrane force but do not have any bending or transverse shear stiffness, so that the only nonzero stress components in the membrane are those components parallel to the middle surface of the membrane. In other words, the membrane is in a state of plane stress.

The FE method is a very powerful tool due to its versatility. The structure that needs to be analysed can have arbitrary loads, supports and shape. The FE method includes matrix manipulations, numerical integration, equation solving, and other processes that are carried out automatically by commercial software (Cook, 1995). The user mainly deals with pre-processing, which includes: describing loads, supports and materials, as well as generating the FE mesh. The user also deals with post-processing, which includes: sorting out, listing and plotting the results. It is very easy to make mistakes in describing a problem to the computer program and therefore the user should be competent in mathematical modelling and have a good understanding of the problem at hand. This is necessary so that any problems that may occur can be detected and fixed without any real difficulty.

2.2 Stents

A stent is a small, smooth, metallic tubular mesh, which is used to support arterial walls to minimize the blockage of arteries due to plaque (Etave *et al.*, 2001 and Migliavacca *et al.*, 2002). A typical stent is shown in crimped and deployed form in Figure 2.3. The stent is necessary to restore blood flow perfusion to downstream tissues (Migliavacca *et al.*, 2002). Dotter (1969) described the first implanted stent that was used to treat arterial shrinkage. In later years stents were used as a replacement for balloon-angioplasty, due to the many limitations of this technique. The use of stents is not without problems, however, and there are several difficulties: migrations, clot formations, collapses and positioning are some of the serious issues (Migliavacca *et al.*, 2002).

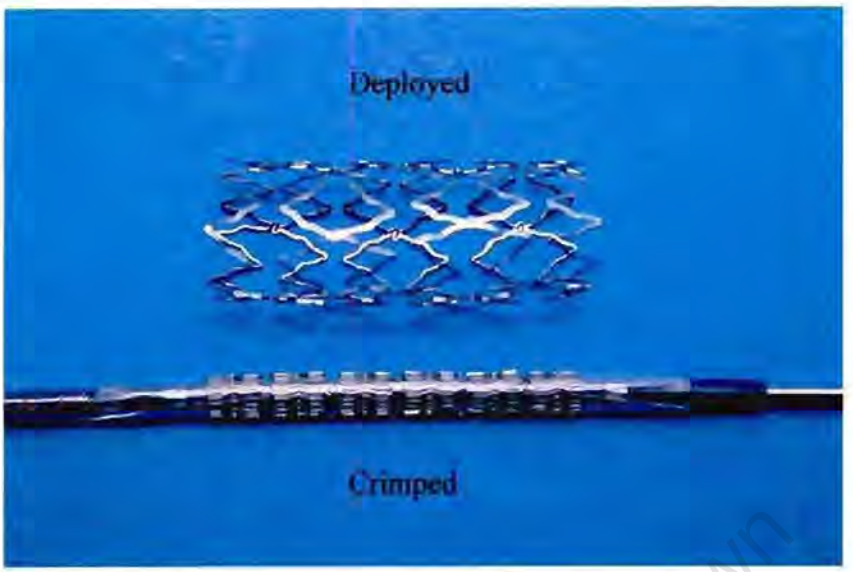

Figure 2.3 Typical stent in crimped and deployed shape (DISA Vascular photo archive)

According to Etave *et al.* (2001) at least 38 different types of stents were already available in Europe. Four of these are self-expanding and the other thirty-four are balloon-expandable. These stents also vary in terms of mechanical properties, depending on their design, material and the technology used. Dumoulin *et al.* (2000) distinguish between the following stents: mesh and mono-filament metallic balloon-expandable stents, which are expanded by the inflation of an angioplasty balloon; elastic and memory self-expandable stents, expanded by intrinsic force; silicone; and biodegradable devices. Practically the balloon-expandable stent is crimped onto a balloon, which is then attached to a catheter. This device is then advanced through the arteries to the site of blockage. Once it is in position, the stent is deployed by inflating the balloon. Its plastically deformable mesh maintains the same dimension as the inflated balloon, so that the stent is left to support the damaged arterial wall after the balloon has been deflated and the delivery system removed. The deployment process can be seen in Figure 2.4. When deployed, the stent's final diameter could be more than four times the initial one (Dumoulin *et al.*, 2002).

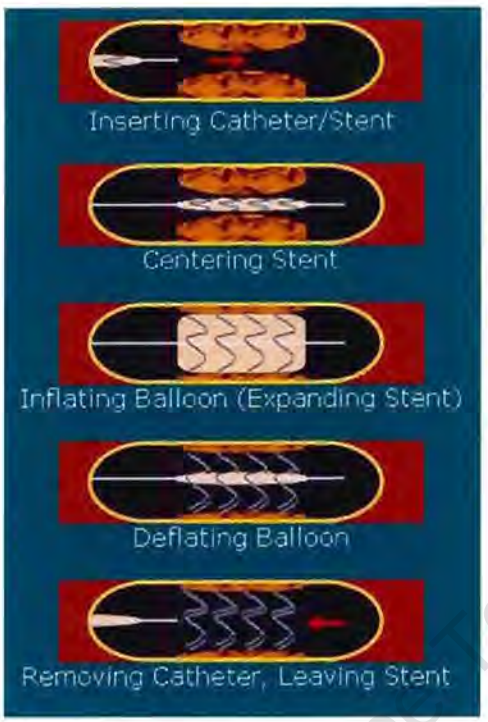

Figure 2.4 Stent deployment process (www.tu-tech.com/cs/htm)

2.3 Stents and Finite Element Modelling

The paper by Prendergast *et al.* (2003) outlined six different issues with respect to the design of stents:

1. Sufficient rigidity to resist compressive forces from the vessel wall
2. Stent must be able to support and hold open the vessel and scaffold the plaque
3. Minimal longitudinal contraction when expanded
4. Minimal shearing between the stent and the tissue
5. Flexibility to navigate tortuous vessels
6. Minimal activation of the re-stenosis mechanism

It is very difficult to meet all these issues in any stent design. To try and implement as many of these issues as possible, a rapid investigation method has to be used to

investigate design concepts prior to clinical trials. The mechanical characteristics of stents vary significantly and it is impossible to determine them from first principles or by extrapolation (Etave *et al.*, 2001). Therefore the finite element method (FEM) provides one possible answer to this problem and can be used to determine mechanical properties, and by doing this help with other issues concerning the design of stents.

According to Tan *et al.* (2001), two approaches could be taken when studying the mechanical characteristics of different stent designs. Firstly, direct mechanical measurements could be made on the individual stents. Typically one could take different stent sizes and expand them to different diameters, according to the size of the simulated diseased artery. Each artery would exhibit different characteristics, namely: angulations, compressibility of lesions, and contractibility or spasm of the vessel wall. This kind of study is very expensive and almost unachievable. Therefore, studies by computer analysis employing the finite element method (FEM) would seem to be the logical alternative. Simulations could be carried out to understand the response of different stents under different conditions. The results could be verified with targeted experimental measurements of the mechanical behaviour of stents. This method would be cheaper and definitely achievable.

In studies conducted to date, it can be seen that the FEM has been applied to different aspects of stent design. It has been used to investigate mechanical properties of balloon-expandable stents (Migliavacca *et al.*, 2002 and Dumoulin *et al.*, 2000) and in particular to address the deformation characteristics and stress distribution over the stent (Chua *et al.*, 2003). It has also been used to measure stent shortening on expansion and to measure the degree of elastic recoil as a function of expansion diameter (Prendergast *et al.*, 2003). Tan *et al.* (2001) and Etave *et al.* (2001) used the FEM technique to compare the performance of two different types of stents.

Rogers *et al.* (1999) described how the FEM technique was used to model balloon-artery contact stresses and to show how the stent strut geometry, balloon compliance and inflation pressure affects these stresses. Finally Prendergast *et al.* (2003) used FEM to

model the blood vessel/stent interaction. Three types of finite element packages were used, namely: ANSYS Version 5.5 (Canonsburg, PA, USA), ABAQUS (Hibbit Karlsson & Sorenses, Inc., Pawtucket, RI, USA) and Autonomic Dynamic Incremental Nonlinear Analysis (ADINA 7.0, ADINA R&D, Inc.)

Balloon modelling has really been neglected in most modelling of balloon-expandable stents, due to the difficulty of modelling the balloon in its crimped form. When pressure is applied to the inner surface of the balloon, it will start to unfold, creating friction between the surfaces of the balloon due to its surfaces sliding over one another. The inflation pressure, transmitted through the balloon membrane is locally uniform, but its direction follows the deformed stent and its magnitude depends on the balloon compliance (Dumoulin *et al.,* 2000). This and the interaction between the balloon and the stent are very difficult to model and therefore only very simple balloon models have been created in the past.

From what was said in the previous paragraph it could be seen that the FEM has a number of different applications concerning the design and development of stents and in particular balloon-expandable stents. The rest of this review focuses on these previous studies to give a clearer understanding of exactly how this technique was used to aid with stent development.

2.3.1 Geometrical Model

Stent Model

Different types of stents have been modelled, and thus different geometrical models were created to model these stents. Chua *et al.* (2003) used the ANSYS Finite Element package to design the geometric model of the balloon-expandable stent with an outer diameter of 3 mm, inner diameter of 2.9 mm and length of 10 mm. The stent model consisted of 66 slots or cells, which were equally spaced throughout the entire length of the model. ABAQUS was used to create a 3D FE model of a typical diamond shaped

stent (Palmaz-Schatz[1]). It was assumed to be a tube with rectangular slots on its surface, 5 in the longitudinal direction and 12 in the circumferential direction. The stent has a length of 16 mm, outer diameter of 1.2 mm and wall thickness of 0.1 mm. The slot length and stent thickness were varied to see what influence changes to the mechanical parameters would have on the physical performance of the stent. The stent performance was evaluated in terms of radial recoil, longitudinal recoil, foreshortening and dogboning. Due the circumferential symmetry of the stent, only one-twelfth of the stent was modelled and because of the presence of longitudinal symmetry it was possible to model and study only half of the length of the stent. Prendergast *et al.* (2003) also used ANSYS to model the stent and the arterial tissue surrounding the stent when deployed. The ideal case of a cylindrical vessel was assumed for simplification of the problem.

Tan *et al.* (2001) and Etave *et al.* (2001) used FEM to model two different stent configurations. This was done to investigate and compare the structural behaviour of the two different stent geometries. The first of the two stents modelled was a typical tubular stent namely: Palmaz-Schatz[1] and the second was a typical coil stent namely: Freedom[2].

Etave *et al.* (2001) used the ABAQUS software to model both of these geometries. Two tubular stent models were created; the first model consisted of a slotted tube, 8 mm in length. It was made up of six identical units, each comprising of two openwork struts and two solid metal struts.

The second model had the same overall geometry, but its struts were twice the size. The coil stent was modelled in the form of a helical round wire. Two different coil stent models were created, the only difference between the two being that the second had a height twice that of the first. Two models of each stent geometry were created to investigate the impact of changing parameters on the stent's mechanical properties.

[1] Johnson & Johnson Interventional System, Warren, NJ.
[2] Global Therapeutics Inc., Broomfield, CO, USA.

Balloon model

Chua *et al.* (2003) used the ANSYS finite element package to design the geometric model of the balloon with an outer diameter of 2.9 mm. It had a wall thickness of approximately 0.1 mm. Oh *et al.* (1994) used the ABAQUS finite element software to model the balloon used for Balloon Angioplasty[3]. Since the balloon is crimped in the same way as that of the balloon-expandable stent's balloon, and will respond in the same way when pressure is applied to its inner surface, it is worthwhile to see how this balloon was modelled. Rogers *et al.* (1999) also used the ANSYS package to create a 2-dimensional FEA model of the balloon. The balloon was assumed to have no thickness and the contact between the balloon, artery and stent was assumed to be frictionless.

Another assumption was made: no other substances, such as blood, were present between the balloon and arterial wall. From what can be gleaned from the literature, the balloons were all modelled as a simple cylinder, which had a small diameter when crimped, and then expanded to a bigger diameter when inflated. As mentioned above, this is not a true reflection of the balloon shape when crimped; it is actually folded, so that its surfaces fold over one another. This special folding technique is later explained in detail in Section 3.2.

2.3.2 Material Model

Stent Material

Chua *et al.* (2003) used a bi-linear elasto-plastic material model, with stainless steel 304, to represent the material properties of the stent. Migliavacca *et al.* (2002) on the other hand, used stainless steel 316LN. A Von Mises-Hill plasticity model, with isotropic hardening, was used to describe the inelastic constitutive response of the material.

[3] Balloon Angioplasty is the process in which an inflatable balloon, mounted on the tip of a flexible catheter, is placed within the lumen of the obstructed vessel, under X-ray control. On inflation of the balloon, the lumen is reopened.

Stainless steel 316LN was also used in the study done by Etave *et al.* (2001) and Dumoulin *et al.* (2000). The material properties of both these materials can be seen in Table 2.1.

Table 2.1 Material properties of two types of stainless steel

Material property	**Stainless steel 304**	**Stainless steel 316LN**
Young' modulus	193 GPa	196 GPa
Shear modulus	$75x10^{6}$ MPa	
Tangent modulus	692 MPa	670 MPa
Density	$7.86x10^{-6}$ kg/mm^3	$7.85x10^{-6}$ kg/mm^3
Yield strength	207 MPa	205 MPa
Poisson's ratio	0.27	0.3

Balloon Material

Two types of materials are currently used to manufacture balloons, namely: Nylon and polyester or polyethylene terephthalate (PET). Nylon balloons are softer than PET balloons, but are not as strong. Due to this characteristic, the nylon balloon has to have a thicker wall and will thus have a larger profile. A comparison between PET and Nylon balloons can be seen in Table 2.2.

Table 2.2 Comparison of two High-Pressure Balloons

Materials	**Tensile Strength**	**Compliance**	**Stiffness**	**Profile**	**Max. Rated Pressure**	
					ATM	**PSI**
PET	High - Very High	Low - Medium	High	Low	20	294
Nylon	Medium - High	Medium	Medium	Low - Medium	16	235

Chua *et al.* (2003) used a polyurethane rubber type material to represent the balloon. A hyperelastic material model in ANSYS was chosen to represent the balloon. Two Moonley-Rivlin model constants were derived and used: C(10) = 0.106881×10^{-2} and C(01) = 0.710918×10^{-3}. The density of polyurethane rubber was taken as 1.07×10^{-6} kg/mm^3 and the Poisson's ratio as 0.495. As mentioned above, Oh *et al.* (1994) modelled the Balloon Angioplasty balloon. The non-linear solution option in the ABAQUS software package was used to create the material properties for the balloon. A non-linear hyper-elastic material was assumed to model the stent. Rogers *et al.* (1998) made use of a strain-stress measurement instrument (Instron), with a 50 kg load, to measure the Young's modulus of balloon materials. The Young's modulus was 2.58×10^4 kPa for a compliant balloon and 7.03×10^5 kPa for a semi-compliant balloon. It is very difficult to measure the Young's modulus of the non-compliant balloon and therefore a value was estimated on the basis of its material properties. For the FEA, three values, within the normal range, were chosen for low-compliant, semi-compliant and compliant balloons. These values were 1.38×10^6 kPa, 6.9×10^5 kPa, and 3.45×10^5 kPa respectively. A Poisson's ratio of 0.3 was chosen for all three types of balloon. Dumoulin *et al.* (2000) assumed the stent material to be elastic and perfectly plastic.

2.3.3 Boundary Conditions

Symmetry conditions made it possible for simplification of some of the models. Chua *et al.* (2003) only modelled a quarter of the stent and balloon. Symmetric boundary conditions were imposed on the nodes in the planes of symmetry. Nodes were not allowed to move in the direction perpendicular to the plane of symmetry. The ends of the stent were unconstrained, to be able to observe its expansion and shortening behaviour. The balloon was assumed to be fully tethered at both ends, so that expansion in the radial direction was the only movement allowed. An autonomic surface-to-surface algorithm approach was used to cope with the non-linear contact problem between the surfaces of the stent and balloon. Migliavacca *et al.* (2002) only modelled one-twelfth of the stent in the circumferential direction and half of the length due to symmetry. Similarly to Chua *et*

al. (2003), nodes on the symmetry plane were fixed in the direction normal to the symmetry plane. Etave *et al.* (2001) applied boundary conditions to the model that corresponded to radial shifts. The shifts were made on all the nodes of the coil stent model and only on specific ones for the tubular stent model so as to limit flexion effects. Both of these models were piloted with such shifts to calculate what forces arose from these changes.

2.3.4 Meshing

Meshing the model is a very important step in the FEM process. It is important to get the correct balance between a fine and a coarse mesh. Typically you want to have a finer mesh in the areas of interest and high stress concentration. A fine mesh is unnecessary in the areas with low stress concentrations and will only increase the computational time; therefore a coarse mesh is ideal for these areas. Different approaches have been taken in previous studies, and in the following paragraphs I try to outline these approaches and see if there is any comparison between them.

Stent Mesh

Chau *et al.* (2003) meshed the stent model with tetrahedral, reduced integration elements. It comprised of 7,881 elements and 3,473 nodes. The models created by Migliavacca *et al.* (2002) and Chua *et al.* (2002) were meshed with eight-node explicit solid brick elements that were fully integrated. Migliavacca *et al.* (2002) used the commercial code GAMBIT[5] to automatically generate a mesh for the model. It comprised of 3,840 brick elements and 6,560 nodes. The model by Chua *et al.* (2002) consisted of 9,504 elements, discretized by 200 elements along its length, 88 elements in circumference and one element in thickness.

[5] Fluent Inc., Lebanon, NH, USA.

Etave *et al.* (2001) made use of Visual Basic software[6] to program all the nodes and their coordinates, since the specific version of ABAQUS used did not have automatic grid generation. Quadratic continuum elements in two or three dimensions were used to mesh the model, which Dumoulin *et al.* (2000) investigated. It was done in two or three dimensions depending on the case they investigated.

Balloon Mesh

The balloon model created by Chua *et al.* (2003) was meshed using eight-node three dimensional explicit dynamic solid brick elements. The model consisted of a total of 2400 elements. It was discretized by 60 elements along its length and 40 elements in circumference with 1 element in thickness. On the other hand, Rogers *et al.* (1999) used two-node isobeam plane-strain elements to mesh the model.

2.3.5 Loading and Solution

Different approaches have been taken to simulate the loading of the stent and balloon. The following section outlines these approaches and the differences between them.

Chua *et al.* (2003) applied a uniform pressure load to the inner surface of the balloon. This caused the balloon and the stent to expand radially. The pressure increased constantly from 0 to 0.409 MPa at a constant rate for 1.635 ms. Figure 2.5 illustrates the loading curve. The balloon was loaded until the stent reached its failure stress at the maximum diameter, passing its elastic limit in the process. According to Chua *et al.* (2003), using ramp loading at a sufficiently low rate provides the opportunity to find the relationship of pressure level to ultimate tensile strength of the stent material. This is due to the fact that at a slow loading rate, there is small kinetic energy and small oscillations.

[6] Windows®, Microsoft Corporation, Redmond, WA, USA.

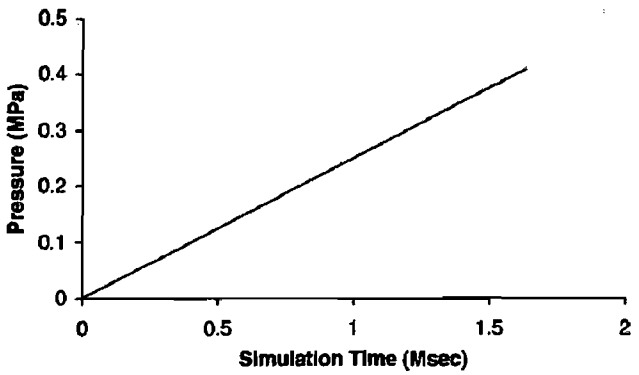

Figure 2.5 Loading curve (Chua *et al.*, 2003)

Different damping coefficients were used to try and keep the dynamic effects to a minimum. In the end a damping coefficient of 10 was found to give the best results. To try and reduce the computational time, a short simulation time was chosen for this analysis. The time chosen was a lot less than the actual time for stent deployment, but the kinetic energy was checked throughout to ensure that it was negligible compared to the internal energy. Chua *et al.* (2002), Rogers *et al.* (1999) and Oh *et al.* (1994) also applied pressure to the inner surface of the balloon. According to the paper by Chua *et al.* (2002), two cases were investigated. In the first case, the stent was subjected to uniform internal pressure at a rate of 400 MPa/ms and in the second case the rate was changed to 11.3 MPa/ms. Rogers *et al.* (1999) used a deployment pressure of 0.8106 MPa to inflate the balloon.

Migliavacca *et al.* (2002) organised their simulations in three levels. First a uniform linearly increasing radial pressure was applied to the inner surface of the stent to simulate the free expansion of the stent. This pressure was applied until a 2 mm radius was reached in the central region. The pressure and distal radius were now calculated. Next, the model was loaded by an internal uniform radial pressure to investigate the behaviour of the stent up to a diameter of 3 mm. This corresponds to the typical diameter of a coronary vessel. At this stage the pressure, longitudinal length and distal radius were calculated. Finally, a simulation was performed to check the mechanical properties of the

stent after load removal. The pressure was thus decreased until zero. Again, the pressure, longitudinal length and distal radius were calculated.

Etave *et al.* (2001) ran three different simulations to model three stents with different deployment diameters. One of their main concerns was to find the pressure required for stent deployment. To try and calculate this pressure and other mechanical properties of the stent the following simulations were done:

- Each of the stent's nodes was subjected to a positive radial displacement. This was done to model stent deployment. Eight different calculations were performed in modelling the stent from its crimped position to a variety of deployment diameters.
- Stent compression was modelled by submitting each of the nodes of the various deployed stents to a negative radial displacement. Four different calculations were performed.
- Conformability was modelled by positioning the stent on two supports, with a negative radial force applied to the opposite generatrix.

Dumoulin *et al.* (2000) considered an infinite prosthesis under uniform radial internal pressure. This approach, together with loading symmetries and periodic boundary conditions, allowed investigation on a generic part of the model. Two types of analysis were performed (Figure 2.6). Firstly, internal pressure was applied to the inner surface ot the three-dimensional curved cells of the stent model. They found that during expansion of the stent the circumferential stresses were greater than the radial stresses. This allowed them to consider the same cells, but unrolled on a plane. These cells were deployed by a prescribed displacement under plane stress assumptions.

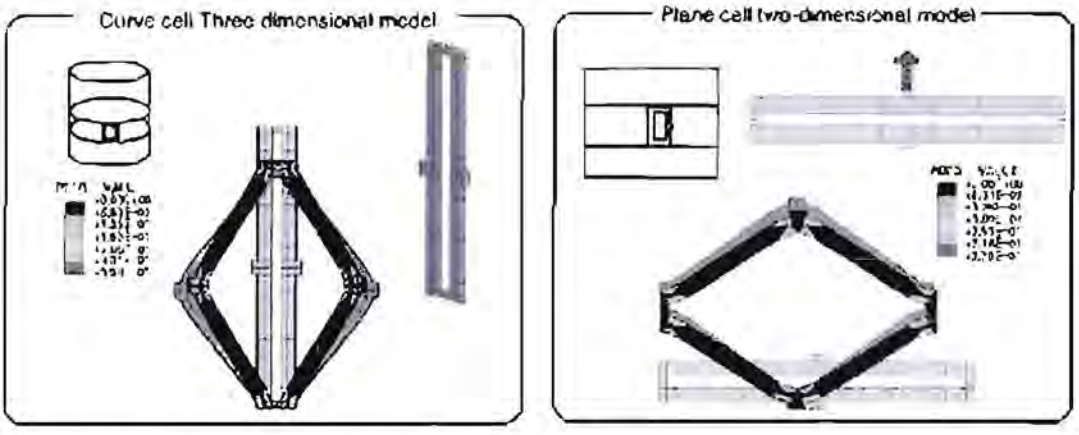

Figure 2.6 Three- and two-dimensional stent models (Dumoulin *et al.* (2000)

Tan *et al.* (2001), showed the following responses of the stent to the loading by the balloon:

- Extension of the stent loop due to the change in radius of the balloon
- Extension of the stent loop due to the shape change of the parabola, of which it is made
- Rotation about the plastic hinge to accommodate the above mentioned changes

2.3.6 Modelling Parameters

Chua *et al.* (2003) tried to determine the maximum radial displacement of the stent by radially expanding the model until the onset of plastic deformation was observed and the ultimate tensile strength reached. The values for radial displacement were measured by taking the displacement values of the nodes in the radial direction. Etave *et al.* (2001) studied seven mechanical properties of the balloon-expandable stent model:

- The pressure needed for full stent deployment, meaning the pressure needed to achieve plastic deformation
- The intrinsic elastic recoil, thus the amount of reduction in diameter after the balloon has been deflated
- The resistance of the stent to external forces
- The amount of stent foreshortening due to expansion in the radial direction
- The stent flexibility by calculating the stent stiffness. The stiffness was calculated by dividing the force required for stent deployment by the maximum radial displacement
- Stress and strain in the stent after deployment

Rogers *et al.* (1998) performed a study with FEA to investigate the effects of distance between strent struts, balloon and stent material properties and balloon inflation pressures on the balloon-artery surface stress and contact area. Dumoulin *et al.* (2000) focused on the following cases: the plastic limit load, assuming small displacements and strains; the linear buckling limit, assuming elastic material behaviour and small displacements; non-linear analysis; post-buckling analysis; elastic-plastic collapse analysis; and lastly the measurement of sensitivity of critical load to geometric imperfections.

2.3.7 Results and Discussion

Chua *et al.* (2003) found that the development of stress in their model closely resembles the bi-linear stress-strain relationship of the stent material, which indicates that the solution is reliable. What was evident however was the fact that the stress development was fairly unstable at the beginning of the simulation. After a time of 0.251 ms, the yield point was reached and the stress began to stabilise. Chua *et al.* (2003) also found that the deployment of the stent and balloon is a volume-controlled process. This can be seen from the fact that during the initial inflation of the balloon there is almost no dilatation of the stent diameter. This phenomenon occurs until the pressure reaches approximately 0.06 MPa, from where the balloon starts to bulge at its ends. As the pressure increases the

forces are transmitted towards the centre of the balloon which distributes the force throughout the whole model. According to Chua *et al.* (2003) this is a direct result of the difference in material properties between the balloon and stent and the resistance of the stent. When the pressure increases sufficiently, the reaction force of the stent is no longer able to hold the balloon down and the balloon starts to expand towards its central part and now dilates the diameter of the stent. Chua *et al.* (2003) found that the stress was typically high in some areas. It was found that the stress at the corners of the cells and in the middle of the cells was high. This can clearly be seen in Figure 2.7 and can be explained by the fact that the struts of the stent are being pulled apart as it dilates.

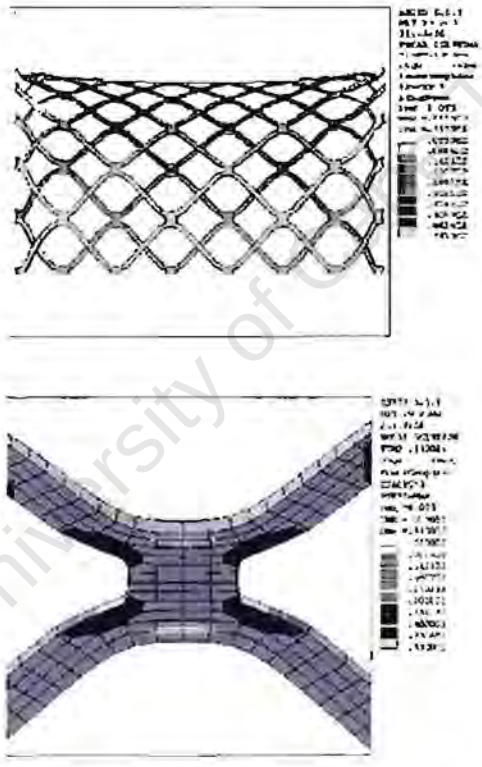

Figure 2.7 Stress distribution on stent model (Chua *et al.*, 2002)

As the stent expands it goes through a stage of elastic deformation and then eventually it is plastically deformed into its new shape. A common problem in stent deployment is the foreshortening at the edge of the stent. Chua *et al.* (2003) found that foreshortening happens in three phases. It starts off very slowly, while the stent is waiting for the balloon to make good contact. In the second stage the foreshortening happens a little bit faster,

and in the third stage it picks up very quickly due to the rapid expansion in the radial direction. The development of foreshortening can clearly be seen in Fig. 2.8. Another interesting phenomenon that was observed was that there was no contact between the end of the stent and the balloon at maximum pressure. Migliavacca *et al.* (2002) defined a metal-to-artery index (α_P / α_V) (Figure 2.8). It was found that this factor influenced the pressure required to expand the balloon. For example, if α_P / α_V = 0.2, then 0.12 MPa is enough to expand the stent, but when α_P / α_V = 1.46, then 0.57 MPa is only enough to start the expansion process and another 0.34 MPa is needed to complete the expansion of the stent. Another common effect, which happens during the stent expansion, is the so-called *dogboning* effect (Migliavacca *et al.*, 2002 and Tan *et al.*, 2000). *Dogboning* happens when there is stronger expansion of the stent at its distal ends than in the central region. Migliavacca *et al.* (2002) looked at changing some of the crucial parameters of the stent to try and see if this would have a significant influence on effects like *dogboning* and foreshortening of the stent. When α_P / α_V was increased, the foreshortening and dogboning increased, while the radial and longitudinal recoil decreased. When the thickness s was increased, it was found that the foreshortening, dogboning and longitudinal recoil all increased. An increase in slot length increased the radial recoil, but did not have any real effects on the other quantities.

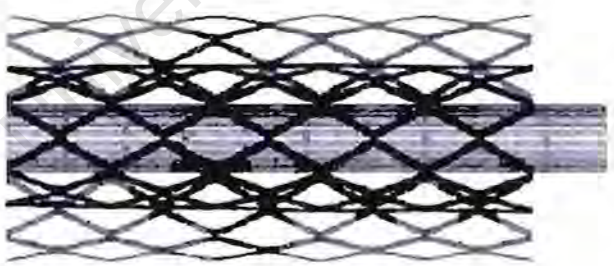

Figure 2.8 Foreshortening of stent (Dumoulin *et al.*, 2000)

Chua *et al.* (2002) showed that stresses in the stent developed at a faster rate during the first millimetre of radial expansion, regardless of the pressure rates applied. It was also found that foreshortening of the stent occurs at a slower rate than the radial displacement, but that at the maximum pressure they were almost equal in value. The speed of pressure

application was also found to have a direct effect on the foreshortening of the stent during expansion, i.e. the faster the speed of pressure application the greater the foreshortening. According to Tan *et al.* (2001), the stent becomes stiffer as the number of convolutes making up the stent increases, meaning that higher pressures are required to deploy the stent as the number of convolutes is increased. It was also found that an increase of stent wire diameter and foundation elastic modulus increases the deployment pressure considerably. Etave *et al.* (2001) found that the deployment pressure required for a tubular stent is almost 3 times as much as that for the coil stent. The stent strut thickness was also found to have a large influence on the deployment pressure, the thicker the struts the higher the pressure required to deploy the stent. The thickness also had a significant influence on the stent stiffness. After the deflation of the balloon, there was definite elastic recoil and thus shrinkage in the diameter of the deployed stent (Etave *et al.,* 2001 and Dumoulin *et al.,* 2000). It was also shown that the degree of foreshortening increased with an increase of the deployment diameter.

The papers by Etave *et al.* (2001) and Dumoulin *et al.* (2000) showed the mechanical role of the balloon in the stent deployment process. The pressure required to deform the balloon was shown to be the difference between the external and internal pressures (Etave *et al.,* 2001). The balloon's linear compliance curve was used to relate these pressures with the relative balloon diameters. The balloon manufacturers define this pressure as the nominal balloon inflation pressure (NBP). Once the stent is mounted onto the balloon the external force on the balloon is no longer zero. The total inflation pressure of the balloon now becomes the nominal inflation pressure plus the pressure required to deploy the stent. As shown earlier, this pressure depends on a number of factors, which include the stent strut thickness and mechanical properties of the stent and balloon. Dumoulin *et al.* (2000) used a slightly different approach. They assumed that the balloon is subjected to pressure exerted by the internal fluid (P_i) on the open surface (S_i), pressure exerted by the stent (P_s) on the covered area (S_s) and external pressure (P_e) on the tube's exterior ($S_e = S_i + S_s$) while at equilibrium. The following equation was used to describe the energy balance in the balloon:

$$P_eS_eU_e = P_iS_iU_i + P_sS_sU_s + W_{def} \quad (2.18)$$

where U is the displacement on surface S and

$$W_{def} = \frac{1}{2} \int_{\Omega} \sigma_{ij}\varepsilon_{ij}\, d\Omega \quad (2.19)$$

is the energy accumulated during wall deformation. If the balloon is assumed to be uniformly deformed, and if the wall stays thin and soft and displacement is kept to a minimum, then the external pressure can be estimated by looking at the ratio between surfaces in contact. The study by Rogers *et al.* (1998) also showed that small alterations in inflation pressure, stent design or balloon material could have major effects on the balloon-artery contact and stress applied to the arterial wall by the balloon. FEA was used to determine this stress in the arterial wall. Interstrut distance and balloon pressure and compliance were used as input variables. By changing these variables it was clear that increasing the geometric complexity of the stent design or increasing the number of struts would reduce the surface-contact stress. When the interstrut distance and balloon compliance was kept constant, the surface-contact stress grew in a non-linear fashion as the pressure in the balloon increased. With an increase in balloon compliance the surface-contact stress and contact area increased and visa versa. As mentioned earlier, Dumoulin *et al.* (2000) studied the sensitivity of the critical load to geometric imperfections. A point load was added to the radial pressure, which was applied to the inside of the stent, by the balloon. This load involved a displacement equal to the stent wall thickness. This added load suggested that the stent is not very sensitive to imperfections.

2.4 Study Limitations

From all the papers studied it is clear that there are still a lot of limitations and shortcomings when using FEM as a tool to solve issues concerning stent design. The FEM process does use a theoretical model, which means there are definite limitations which come with this type of analysis. Due to the complexity of modelling the balloon

and stent, various assumptions have been made along the road to simplify the models and to decrease computation times.

Chua *et al.* (2003) and Migliavacca *et al.* (2002) did not model the interaction between the balloon and stent, but rather applied a uniform pressure directly to the inside surface of the balloon. In reality the stent is actually crimped onto the balloon before the deployment process. To actually represent the model, the crimping process will also have to be modelled. The results obtained from the simulations were simply validated by standard general checks with smooth load development, smooth continuity of contour lines and similarity of stress-strain plots of the structure against its material property data (Chua *et al.*, 2003). In the study done by Etave *et al.* (2001) a balloon model was used to simulate the actual balloon, but to simplify the model, perfectly radial and homogeneous balloon deployment was assumed. The model ignored friction between the balloon, stent and arterial wall. The analysis should also include an appropriate model for the arterial vessel and atherosclerotic plaque, so that a simulation of the interaction between these elements and the stent can be run during deployment (Migliavacca *et al.*, 2002).

CHAPTER THREE

FINITE ELEMENT MODELS

The first task was to create a model for both the balloon and stent, which was similar to the actual balloon and stent. The ABAQUS finite element package (Hibbit Karlsson & Sorenses, Inc., Pawtucket, RI, USA) would be used to create these models. The models could not be an exact presentation of reality due to computational restraints. The models had to be simplified in order to decrease computational time, cost and difficulty in modelling. However, these simplifications could not be done at random and had to be well thought out and judged, so that the model would react in the same way as the real system.

3.1 Test Model

Initially the possible modelling of this type of application was tested with a very simple model. A simple 3-D structure was created within ABAQUS. The balloon was modelled as a cylindrical surface with a few kinks in it and the stent as an octagon. Only half a model was simulated with axi-symmetric boundary conditions imposed on the side of the model. The stent's outer diameter was larger than the balloon's and the two were then assembled. Two different material properties were chosen, the one for the stent being significantly stiffer than the balloon's. Pressure was then applied to the inner surface of the balloon, to see if the balloon would open and push the stent outwards. This was done successfully and the real system could now be modelled. The assembled model is shown in Figure 3.1.

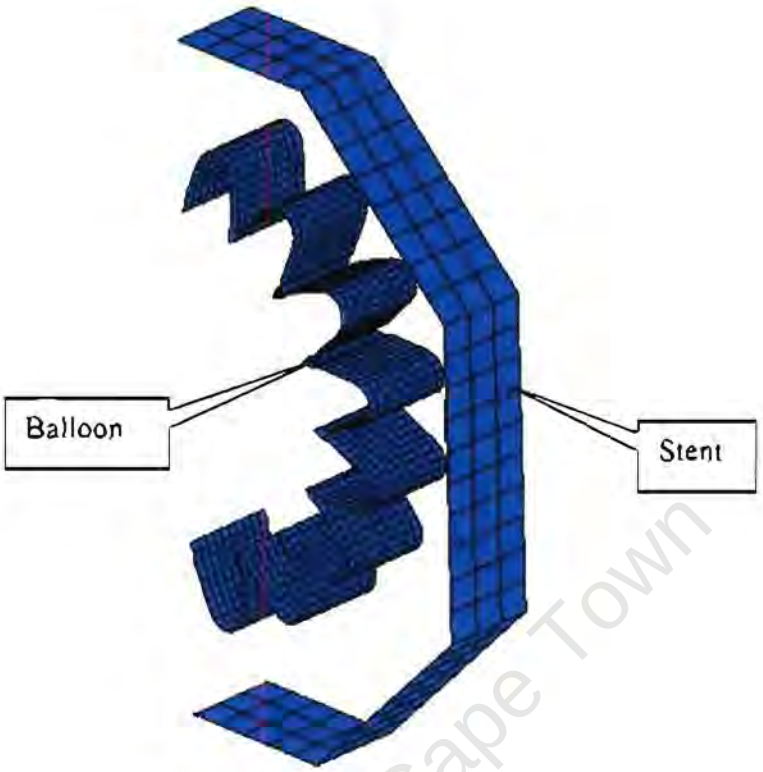

Figure 3.1 Test model assembly

3.2 Balloon Model

The physical balloon is folded in such a way that its outside diameter decreases from 10 mm in its unfolded state, to more or less 1 mm when folded. This is necessary to allow the catheter, with the balloon and stent crimped onto it, to enter into an artery with ease. To create the actual geometry of the folded balloon is a difficult task, but this is crucial in order to model the balloon correctly. The way the folding is currently done is with a special tri-folding method, where the balloon is folded in such a way that it has 3 flaps, which are folded around one another to create the correct geometry (Figure 3.2). In actual fact it is very difficult to predict the exact shape of the balloon in folded form. The presence of air gaps and the amount of overlap seriously influence the geometry.

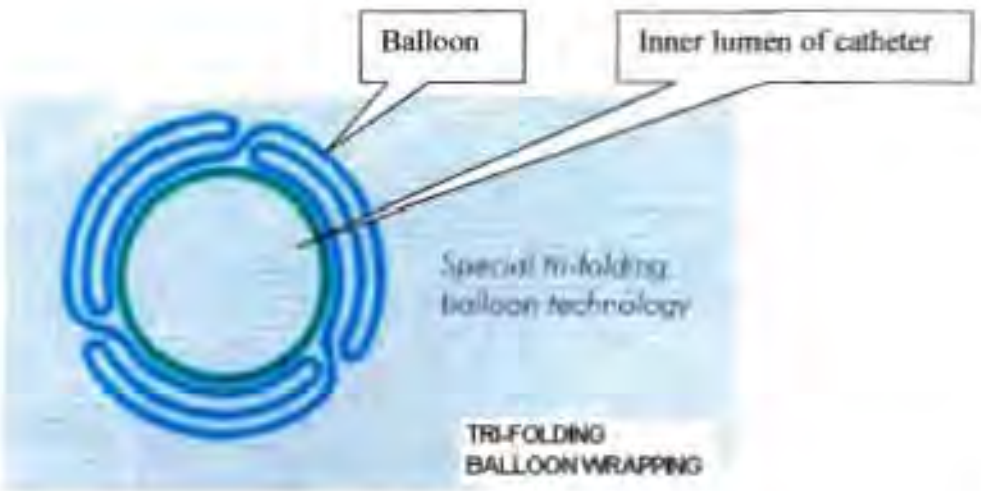

Figure 3.2 Tri-folded shape (Endovascular Angioplasty Materials Catalogue: 2003)

A few methods can be used to obtain a reasonable idea of the exact shape of the balloon in folded form.

3.2.1 Resin Cast

A folded balloon was cast in resin. The idea was that the casting would prevent the balloon from deforming when a cross-section was made, and would reflect the true folded shape of the balloon. A cross section was made with a cutter and the surface of interest polished with a special polishing disk. The polished surface was then inspected under a microscope. Digital photographs were taken to capture the geometry of the balloon and these photographs could now be used to measure critical distances (Figure 3.3). With every change of zoom of the camera a calibration mesh was photographed. The photograph of the mesh was used to calibrate the balloon photographs to ensure that the measurements taken were exact. Due to the cutting and polishing process the edges of the balloon were smudged and it was very difficult to get a clear understanding of the folded geometry.

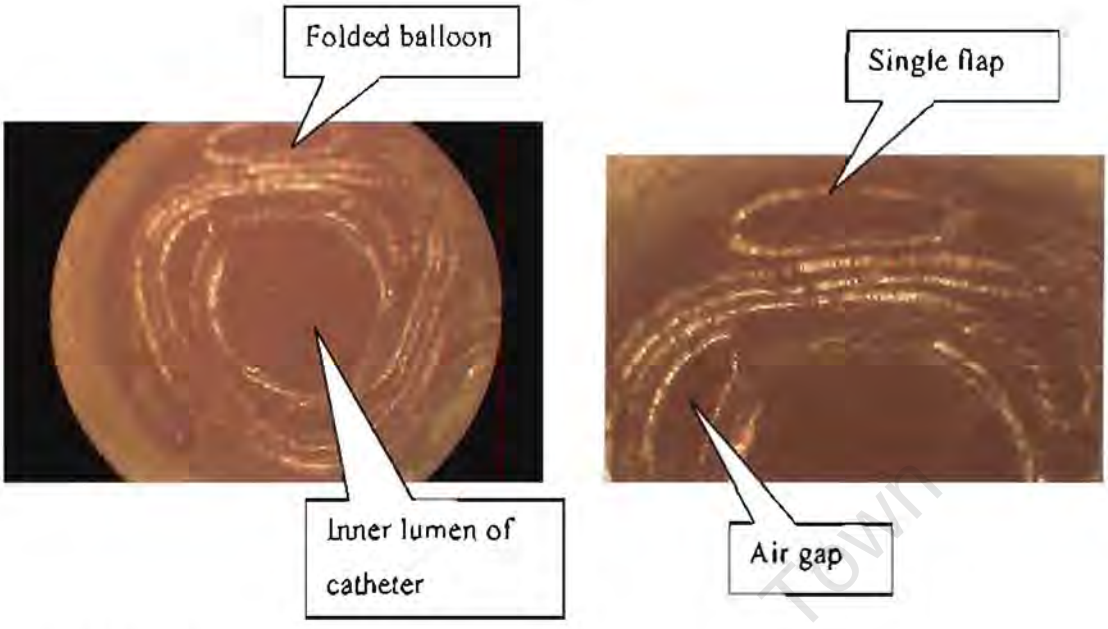

Figure 3.3 Microscope images of resin cast balloon

3.2.2 Plain Cross-section

Peripheral balloons are generally stiffer than the cardiac ones, and therefore a plain folded balloon could be sectioned and studied under the microscope. The same set of digital photographs was taken, which could be used to acquire the true geometry of the balloon (Figure 3.4). The geometry was more complex than initially anticipated and had to be simplified. The following measurements were taken and could be used to create a smooth balloon geometry:

- Outside diameter
- Lumen outside diameter
- Air gap between each overlapping portion of the wings
- Wall thickness of the balloon

To verify these measurements a piece of the actual balloon was taken and the wall thickness was measured with a micrometer. This thickness compared well with the thickness obtained from the microscopic images and so the measurements could thus be assumed as accurate. The wall thickness was taken as 60 μm. A simplified balloon geometry could now be created for the ABAQUS finite element model.

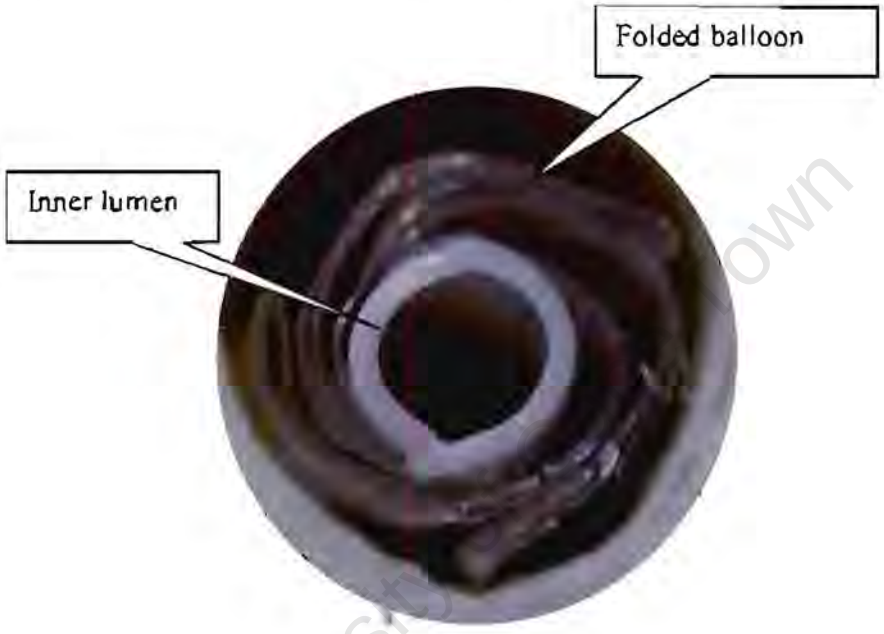

Figure 3.4 Plain cross section of folded balloon

Initially this was done with a drawing board and compasses. A set of curves and half circles, which were connected, was used to create the shape of the folded balloon. These curves could then be used to generate a set of mathematical equations that described the balloon geometry. The drawing was broken up into small pieces or a set of variables and each one named. These consisted of large and small arc lengths, large and small radii and a number of angles. The set of equations was then described in terms of these unique variables. The folded balloon consists of three balloon folds as described above, meaning that only one third of the balloon had to be drawn and the same values could be assumed for the other two thirds. The initial drawing without any named variables is shown in Figure 3.5.

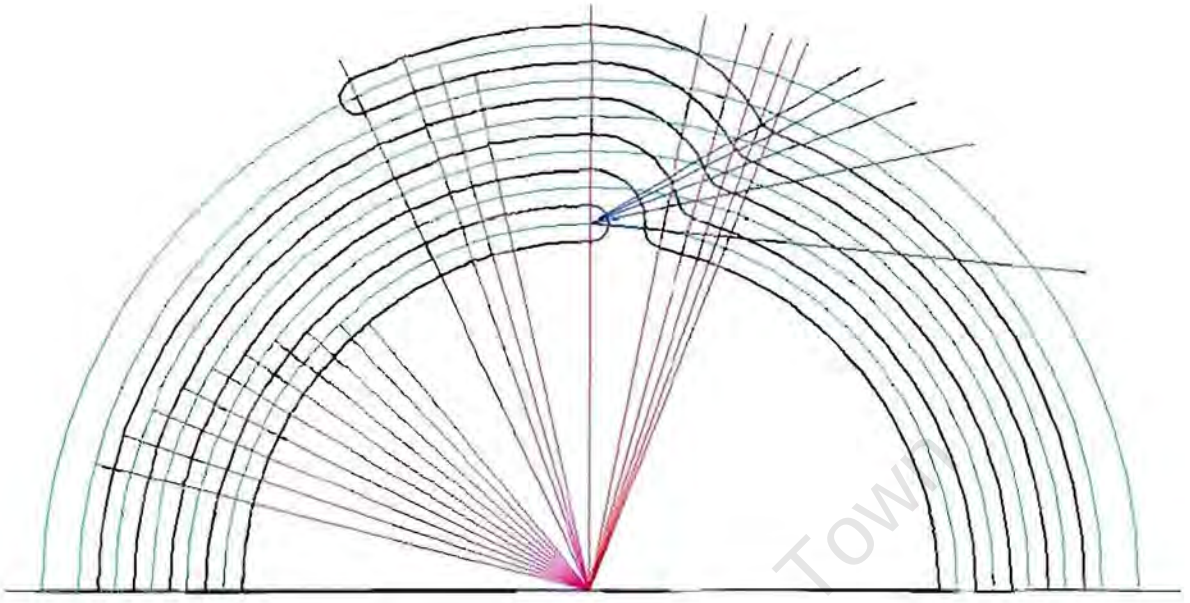

Figure 3.5 Initial folded balloon drawing

The drawing was done as the mid-plane surface of the balloon, meaning that the actual wall of the balloon was not drawn, but instead a line midway between the thickness of the balloon wall. The first variable that was described was:

$$t = a + b \qquad (3.1)$$

where a and b are the air gap and balloon wall thickness, respectively, meaning that t was the gap between each of the mid-plane lines of the balloon. The radius of the bends that connect each of the mid-plane lines could then be defined as:

$$r = \frac{t}{2} \qquad (3.2)$$

Figure 3.6 clearly shows the location of both r and t.

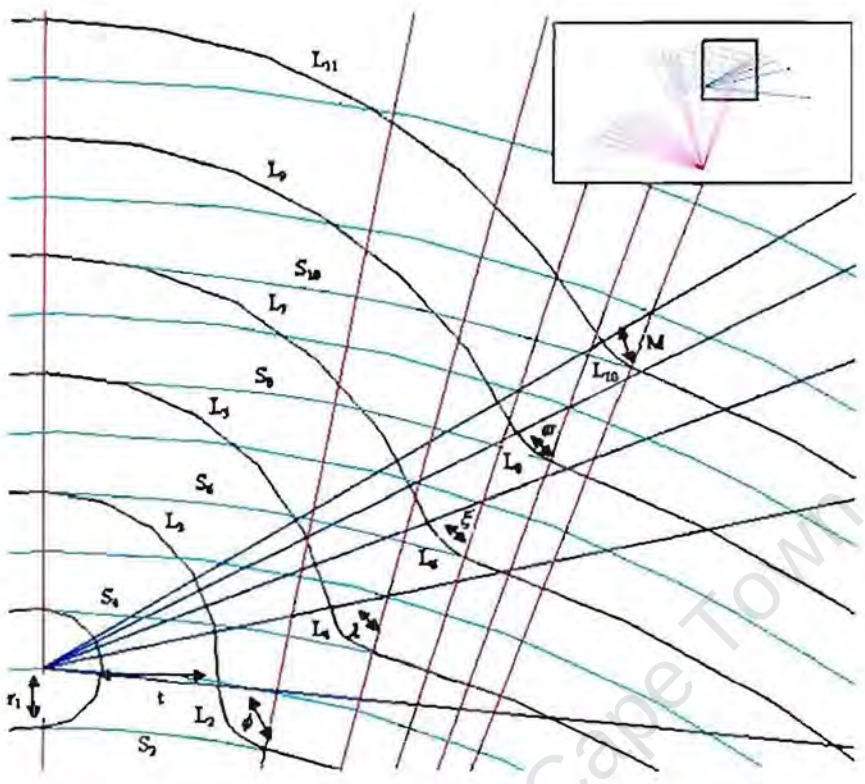

Figure 3.6 First section of the balloon drawing

Next all the angles in the drawing were described in terms of the radii and the variable t:

$$\alpha = \cos^{-1}\left(1 - \frac{(2r+t)^2}{2R_2^{\,2}}\right) \tag{3.3}$$

$$\Psi = \cos^{-1}\left(\frac{R_2^{\,2} + R_4^{\,2} - (2r+2t)^2}{2R_2R_4}\right) \tag{3.4}$$

$$\beta = \cos^{-1}\left(\frac{R_2^{\,2} + R_6^{\,2} - (2r+3t)^2}{2R_2R_6}\right) \tag{3.5}$$

$$\Sigma = \cos^{-1}\left(\frac{R_2^{\,2} + R_8^{\,2} - (2r+4t)^2}{2R_2R_8}\right) \tag{3.6}$$

$$\Omega = \cos^{-1}\left(\frac{R_2{}^2 + R_{10}{}^2 - (2r+5t)^2}{2R_2R_{10}}\right) \tag{3.7}$$

$$\lambda = \cos^{-1}\left(\frac{R_4{}^2 - R_2{}^2 + (2r+2t)^2}{2(2r+2t)R_4}\right) \tag{3.8}$$

$$\xi = \cos^{-1}\left(\frac{R_6{}^2 - R_2{}^2 + (2r+3t)^2}{2(2r+3t)R_6}\right) \tag{3.9}$$

$$\omega = \cos^{-1}\left(\frac{R_8{}^2 - R_2{}^2 + (2r+4t)^2}{2(2r+4t)R_8}\right) \tag{3.10}$$

$$\mathrm{M} = \cos^{-1}\left(\frac{R_{10}{}^2 - R_2{}^2 + (2r+5t)^2}{2(2r+5t)R_{10}}\right) \tag{3.11}$$

$$\phi = \frac{\pi - \alpha}{2} \tag{3.12}$$

$$\eta = \pi - \psi - \lambda \tag{3.13}$$

$$\rho = \pi - \beta - \xi \tag{3.14}$$

$$\sigma = \pi - \Sigma - \omega \tag{3.15}$$

$$\upsilon = \pi - \Omega - \mathrm{M} \tag{3.16}$$

The location of these angles can be seen in Figures 3.6, 3.7 and 3.8

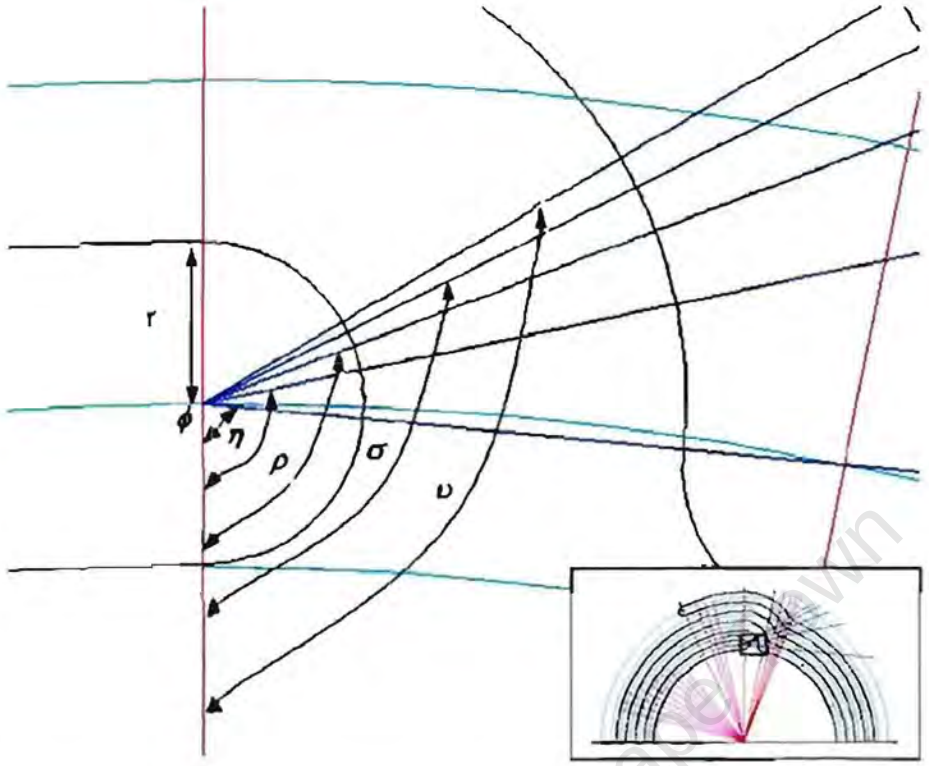

Figure 3.7 Second section of the balloon drawing

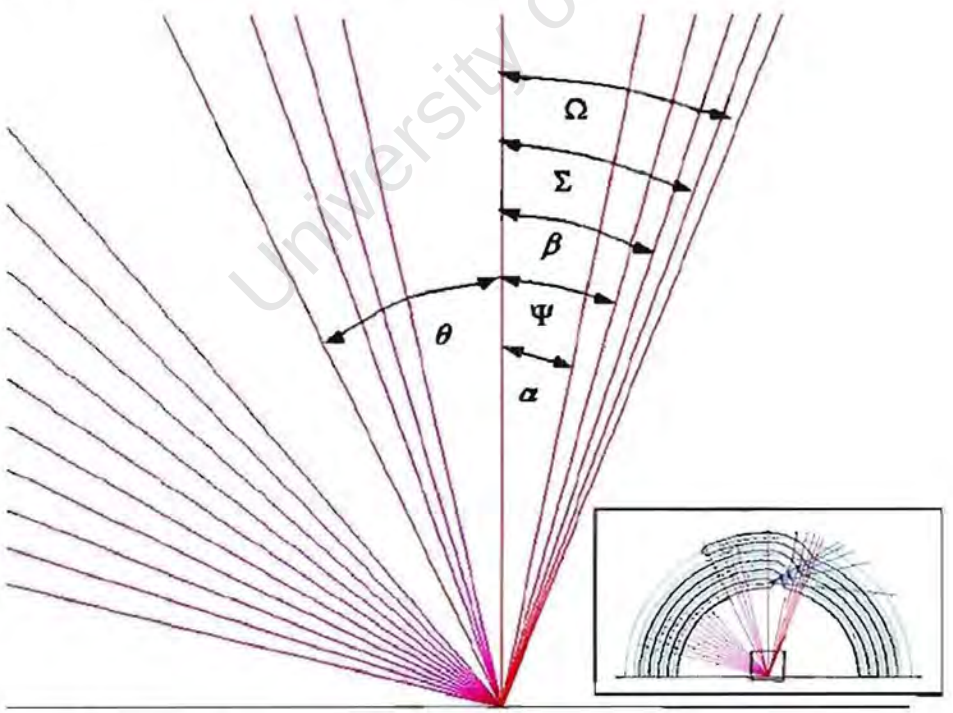

Figure 3.8 Third section of the balloon drawing

Two sets of equations were generated for the arcs making up the bulk of the drawing, one set for the large arcs and another for the small ones. The lengths of the large arcs could be described as:

$$S_1 = 2\pi R_1 - 3S_2 \tag{3.17}$$

$$S_2 = R_1\alpha \tag{3.18}$$

$$S_3 = 2\pi R_3 - 3S_4 \tag{3.19}$$

$$S_4 = R_3\Psi \tag{3.20}$$

$$S_5 = 2\pi R_5 - 3S_6 \tag{3.21}$$

$$S_6 = R_5\beta \tag{3.22}$$

$$S_7 = 2\pi R_7 - 3S_8 \tag{3.23}$$

$$S_8 = R_7\Sigma \tag{3.24}$$

$$S_9 = 2\pi R_9 - 3S_{10} \tag{3.25}$$

$$S_{10} = R_9\Omega \tag{3.26}$$

$$S_{11} = R_{11}\theta \tag{3.27}$$

$$S_{12} = R_{13}\theta \tag{3.28}$$

and the lengths of the small arcs as:

$$L_1 = \pi r \tag{3.29}$$

$$L_2 = \phi r \tag{3.30}$$

$$L_3 = (r+t)(\pi - \phi) \tag{3.31}$$

$$L_8 = \lambda r \tag{3.32}$$

$$L_9 = (r + 2t)(\pi - \eta) \tag{3.33}$$

$$L_{10} = \xi r \tag{3.34}$$

$$L_7 = (r + 3t)(\pi - \rho) \tag{3.35}$$

$$L_6 = \varpi r \tag{3.36}$$

$$L_5 = (r + 4t)(\pi - \sigma) \tag{3.37}$$

$$L_{12} = \mathrm{M} r \tag{3.38}$$

$$L_{11} = (r + 5t)(\pi - \upsilon) \tag{3.39}$$

The locations of the small and large arc lengths are clearly illustrated in Figure 3.6 and 3.9.

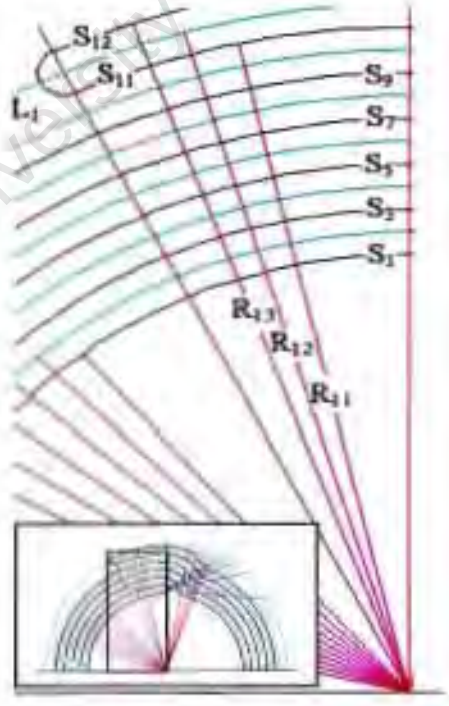

Figure 3.9 Fourth section of the balloon drawing

All the radii of the curves were defined next. The inner line of the balloon was at a radius:

$$R_1 = \frac{1}{2}(lumenOD) + a + \frac{1}{2}b \qquad (3.40)$$

where half of the lumen's outside diameter was added to a and b, the air gap and wall thickness of the balloon, respectively. The rest of the radii seen in Figures 3.9 and 3.10 were then calculated by adding half of the t value each time. All of these equations could now be used to calculate the angle θ, which determines the amount of overlap of the outer fold of the balloon, as seen in Figure 3.7. The angle θ can be described by the follwing equation:

$$\theta = \frac{\pi D - S_1 - S_3 - S_5 - S_7 - S_9 - 6L_1 - 3L_2 - 3L_3 - 3L_4 - 3L_5 - 3L_6 - 3L_7 - 3L_8 - 3L_9 - 3L_{10} - 3L_{11}}{(3R_{11} + 3R_{13})} \qquad (3.41)$$

where D is the diameter of the inflated balloon. With this set of mathematical equations, the desired inflated diameter of the balloon, the air gap between the balloon folds and the wall thickness of the balloon can be altered. They will then calculate all the values needed to draw up the correct balloon geometry for the specific set of variables.

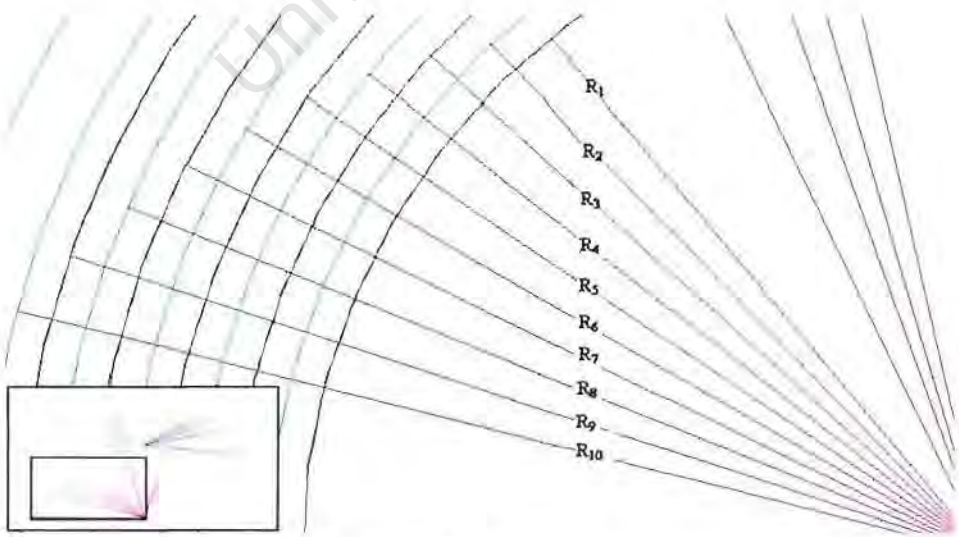

Figure 3.10 Fifth section of the balloon drawing

Eventually this gave the final folded balloon geometry that could now be used to create the model in the finite element package. The final geometry is shown in Figure 3.11.

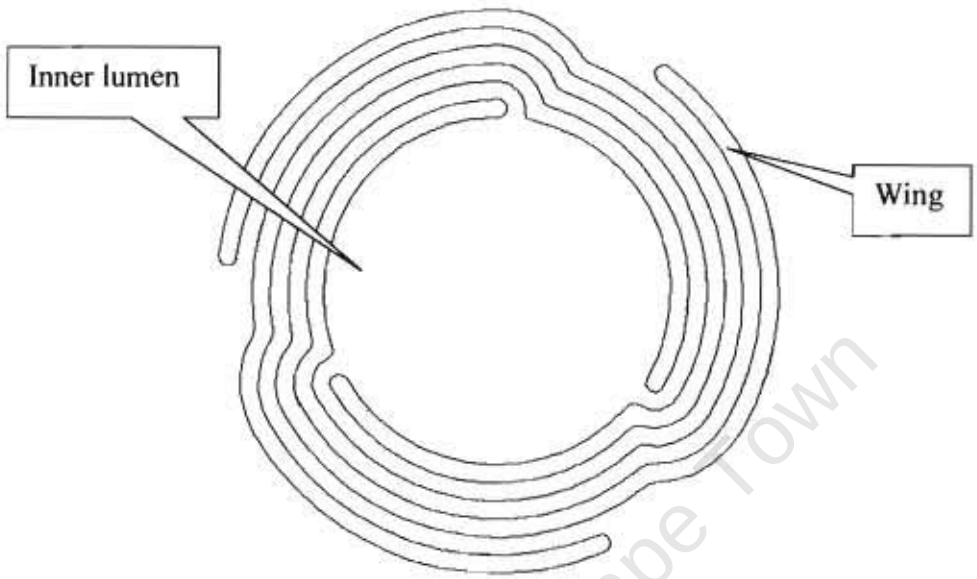

Figure 3.11 Final geometry of folded balloon

ABAQUS/CAE was now used to create the balloon model. Firstly, the 2-dimensional balloon geometry was created. With the sketch function a drawing of the folded balloon was made, since all the distances for the curves were known. One thing that has to be kept in mind is that ABAQUS works with the mid-plane values, as described in Section 2.1. This meant that fine calculations had to be done to draw the balloon surfaces at half the wall thickness. A 3-D deformable extrusion membrane element was chosen as base, where the extrusion depth was equal to the length of the balloon. Figure 3.12 shows the extruded balloon model. The balloon has an inside diameter of 1.1 mm, an outside diameter of 1.94 mm and a length of 20.72 mm.

The actual balloon tapers off towards its furthest extremities, where it is fixed to the inner lumen (Figure 3.13). To model this taper would be extremely difficult, since it would be almost impossible to predict and model the geometry of the tapered pieces. The problem is created by the fact that the balloon twists as it tapers. The balloon has a part that is not tapered before the part where the stent sits. This part is more or less the same length as

the tapered part. It was thus assumed that the role of the tapered parts in the deployment of the stent would be negligible and therefore the tapers were left out in the balloon model.

Figure 3.12 Section of the balloon model within ABAQUS

These balloons are made from ATOFINA RILSAN Nylon 11 (ClearStream Technologies Ltd., Moyne Upper, Enniscorthy, Co. Wexford, Ireland). The complete material properties of Nylon 11 are shown in Appendix B. One of the main problems in numerical modelling is obtaining appropriate material properties, to accurately model the actual material behaviour. This is especially important for the balloon properties, since the balloon would undergo large strains and deformations. DISA Vascular could not supply the actual properties of the balloon and the manufacturer of these balloons was hesitant in providing this information to a student. The following properties were obtained from the literature:

- Young's Modulus: 1.2×10^{9} Pa
- Density: 1.04×10^{-6} kg/mm^3
- Poisson's ratio: 0.4

By calculating the Young's Modulus from experimental data, the validity of these values was tested. The wall thickness, inflation pressure, % elongation and the nominal diameter of the balloon were known. By using the following equations the Young's Modulus could be calculated,

$$E = \frac{\sigma}{\varepsilon} \tag{3.42}$$

where σ and ε are the internal stress and % elongation, respectively. This equation can now be rewritten as follows,

$$E = \frac{\left(\frac{PD}{2t}\right)}{\varepsilon} \tag{3.43}$$

where P, D and t are the inflation pressure, nominal diameter and wall thickness, respectively. These values were used in equation 3.43 and the Young's Modulus calculated as 1.1 x 10^9 Pa, which closely correlates with the given value. These values were thus taken as sufficient to represent the Nylon 11 used for these balloons.

Next, this material had to be assigned to the 3-D model as a membrane shell section with a wall thickness of 0.06 mm. The reason for using membrane shell elements was that the balloon's bending stiffness was assumed to be negligible in comparison with its own membrane stiffness and the bending stiffness of the stent. The model then had to be meshed. It is difficult to know when a mesh is fine or coarse enough and that a specific mesh density will deliver accurate results without complicating the model too much or increasing the computational time by too large a factor.

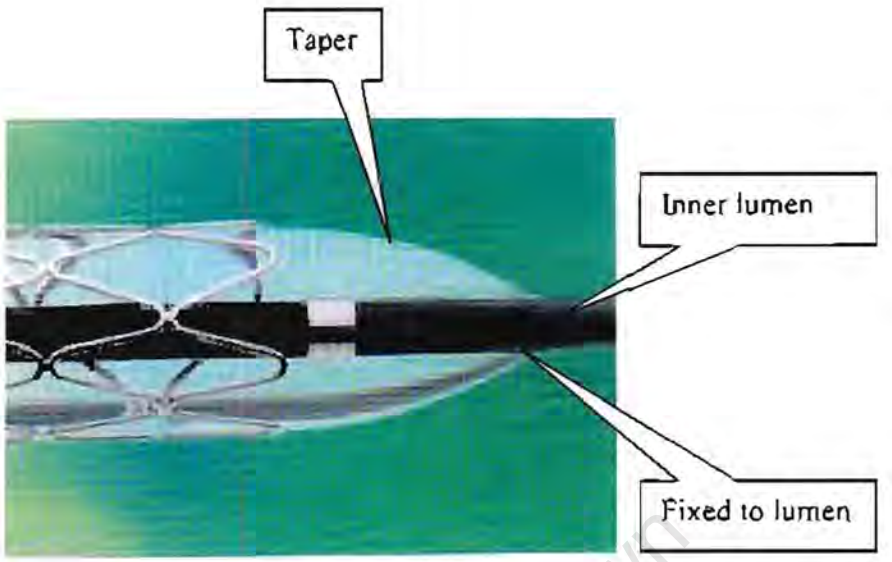

Figure 3.13 Balloon taper.(Endovascular Angioplasty Materials Catalogue: 2003)

One way to validate whether the mesh used rendered accurate results is to compare it to physical results. A rule of thumb in finite element modelling is to increase the density of the mesh in the areas where the highest stress concentration or displacement are expected and to decrease the density of the mesh in the other areas of lesser importance. This should allow the computational time to stay within reasonable limits and the results to be accurate and of practical use. For this reason the number of elements was increased on the bend of the balloon folds, thus increasing the density of the mesh. In the other areas a fairly coarse mesh was taken as satisfactory. One thing that would slow the simulation time down considerably, though, was the element length. The explicit integration scheme used for this analysis is dominated by Δt_{crit} as explained in Section 2.1. This means that the smaller the element length the smaller the critical time step. A small critical time step will cause the simulation time to slow down considerably. The right balance between too fine or too coarse a mesh had to be found. The balloon was meshed with linear quadrilateral elements. Figure 3.14 shows the discretized finite element model of the balloon, which was comprised of 97,650 elements and 98,301 nodes.

Figure 3.14 Meshed balloon model

3.3 Stent Model

Standard drawings of a flat or unrolled stent had already been created in Solid Works®, meaning that these drawings were in 2-D and that the stent was folded open and flat (Figure 3.15). These drawings could be altered to either represent a stent in its crimped or uncrimped state, depending on what was required for the model. The stent strut thicknesses will obviously change if there is a change in diameter of the stent, with the one in crimped form having a slightly smaller diameter. These drawings could easily be imported into ABAQUS® in DXF format. DXF is a text file format containing drawing information that can be read by other CAD systems or programs outside Solid Works®. The drawings were imported as sketches and could now be edited within ABAQUS®. The first model that was created was only one quarter of the full model. Six of the stent rings were cut, leaving two of the initial eight. The sketch was now ready and an element type for the stent model could be assigned. A 3-D deformable planar shell element was chosen for the stent.

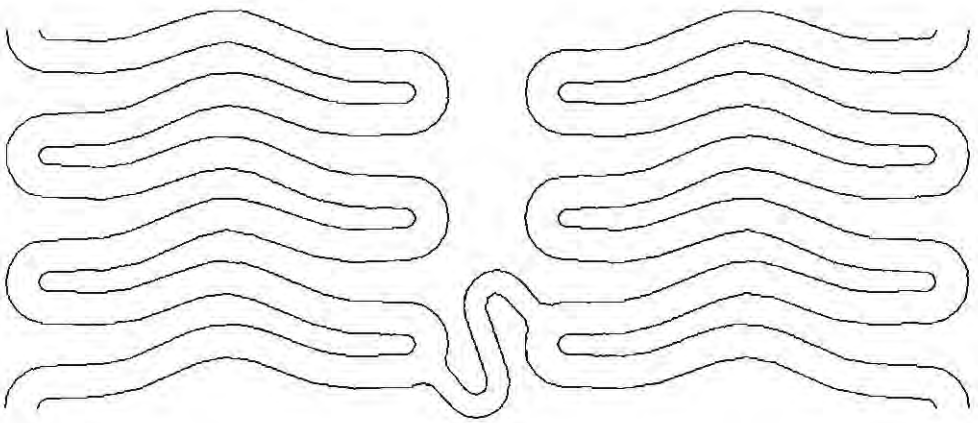

Figure 3.15 DXF drawing of a section of flat stent

The ABAQUS Theory Manual explains that ABAQUS shell elements allow the modelling of curved, intersecting shells that can exhibit non-linear material response and undergo large translations and rotations. These shell elements can also model the bending behaviour of the stainless steel and are formulated for large-strain analysis. Since ABAQUS/Explicit was used, general-purpose shell elements were employed. These general-purpose elements provide robust and accurate solutions in all loading conditions. Thickness change as a function of in-plane deformation is allowed and the elements do not suffer from shear locking and do not have unconstrained hourglass modes. In ABAQUS/Explicit the thickness change is based on the "effective section Poisson's ratio" for all shell elements in large-deformation analyses. The thickness change based on the "effective section Poisson's ratio" is calculated as follows.

In plane stress $\sigma_{33} = 0$ and linear elasticity gives

$$\varepsilon_{33} = -\frac{\upsilon}{1-\upsilon}(\varepsilon_{11} + \varepsilon_{22}) \qquad (3.44)$$

Treating these as logarithmic strains,

$$\ln\left(\frac{t}{t_0}\right) = -\frac{\upsilon}{1-\upsilon}\left(\ln\left(\frac{l_1}{l_1^0}\right) + \ln\left(\frac{l_2}{l_2^0}\right)\right) = -\frac{\upsilon}{1-\upsilon}\ln\left(\frac{A}{A^0}\right) \qquad (3.45)$$

where A is the area on the shell's reference surface. This non-linear analogy with linear elasticity leads to the thickness change relationship:

$$\frac{t}{t_0} = \left(\frac{A}{A_0}\right)^{-\frac{\upsilon}{1-\upsilon}} \qquad (3.46)$$

For υ = 0.5 the material is incompressible; for υ = 0 the section thickness does not change. These shell elements were thus the best-suited element to use for the stent model. Since the stent elements had to undergo large displacements and rotations during the deployment process, large strains and stresses would be present within the stent. These elements thus allow fairly smooth displacement fields and an accurate solution. The model of the flat stent can be seen in Figure 3.16.

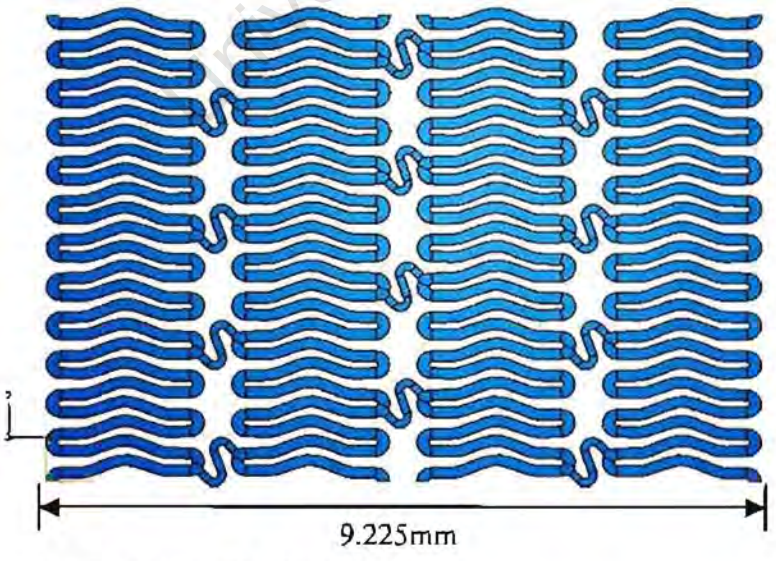

Figure 3.16 Flat stent model (Half stent)

An alternative would be to use 8-noded continuum brick elements, but this would be computationally too expensive.

These stents are made from Stainless Steel 316L and the material properties were chosen to approximately represent this material. The material was modelled using a Von Mises type bilinear elasto-plastic material model. The elastic and plastic responses are distinguished by separating the deformation into recoverable (elastic) and non-recoverable (plastic) parts. This separation is based on the assumption that there is an additive relationship between strain rates:

$$\dot{\varepsilon} = \dot{\varepsilon}^{el} + \dot{\varepsilon}^{pl} \tag{3.47}$$

where $\dot{\varepsilon}$ is the total strain rate, $\dot{\varepsilon}^{el}$ is the rate of change of the elastic strain, and $\dot{\varepsilon}^{pl}$ is the rate of change of the plastic strain. Belytschko *et al.* (2000) explain that the elastic strain is always related to the elastic modulus:

$$\dot{\sigma} = E\dot{\varepsilon}^{el} \tag{3.48}$$

where E is the elastic or Young's modulus. The above relations are homogeneous in the rates of stress and strain, meaning that the time can be scaled by any factor, but the constitutive relation will remain unchanged. This means that the material chosen is rate-independent even though it is expressed in terms of strain rate. The plastic strain rate is given by:

$$\dot{\varepsilon}^{pl} = \dot{\lambda}\frac{\partial \Psi}{\partial \sigma} \tag{3.49}$$

where $\dot{\lambda}$ and Ψ are the plastic rate parameter and plastic flow potential, respectively. The yield condition can now be described by:

$$f = \bar{\sigma} - \sigma_Y(\bar{\varepsilon}) = 0 \tag{3.50}$$

where $\bar{\sigma}, \sigma_y$ and $\bar{\varepsilon}$ are the effective stress, yield strength and effective plastic strain, respectively.

The following material properties were used (Appendix B):

- Young's Modulus: 193 GPa
- Density: 785 g/m^3
- Poisson's ratio: 0.3
- Yield Stress: 330 MPa
- Plastic Strain: 0.48

The material was then assigned to the model as a homogenous shell section with a wall thickness of 14 x 10^{-2} mm. The wall thickness of the stent was obtained from data provided by DISA Vascular. The stent has a length of 18.45 mm. The stent model could now be meshed. As explained previously, the meshing process is very difficult and requires good judgment. Areas that are expected to have the highest stress concentration usually have the densest meshing. For this reason the mesh was refined around all the curves of the stent struts where the highest stress concentrations were likely to occur (Figure 3.17). The stent was meshed with linear quadrilateral elements. The stent was comprised of 49,587 elements and 61,845 nodes.

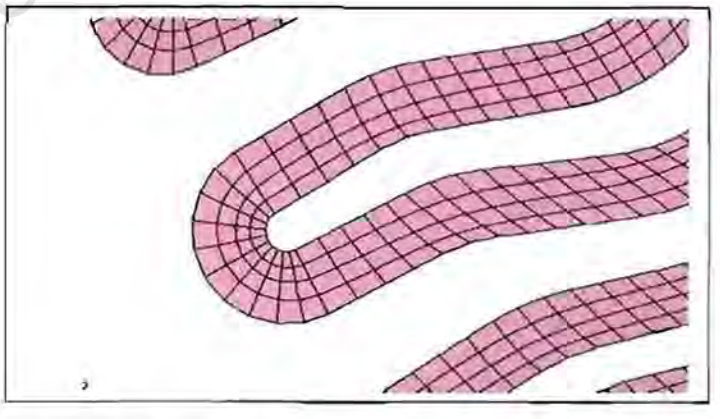

Figure 3.17 Close-up to show variable mesh density

The two outer edges of the flat stent had to be connected to form a closed and round stent. A Python script, programmed by Mr. Hellmut Bowles from Finite Element Analysis Services (Pty) Ltd, a company based in Mowbray, South Africa was used to map the flat 2D stent onto a circular 3D model. This program took all the nodes of the flat stent and mapped them into a cylindrical coordinate system so that the two outer edges lined up and a closed stent was formed. The circumference of the stent had to be specified in order for the two edges to align perfectly and the respective nodes to join up. Due to a set tolerance within ABAQUS the nodes of the two edges did not fall exactly on one another. A simple alteration to this tolerance was made and the nodes could then be merged and the stent fully closed. The stent model was now ready to be used in the full catheter assembly. Figure 3.18 shows the discretized finite element model of half the round stent.

Figure 3.18 Meshed model of half a stent

3.4 Inner Lumen Model

The inner lumen is a piece of rubber piping which houses the guide wire for the catheter. This lumen fits tightly over the guide wire of the catheter. An illustration of the assembly of these three items can be seen in Figure 3.19. The first idea was to model the lumen and guide wire as one rigid body, since the guide wire would not budge under the pressure from the balloon and stent.

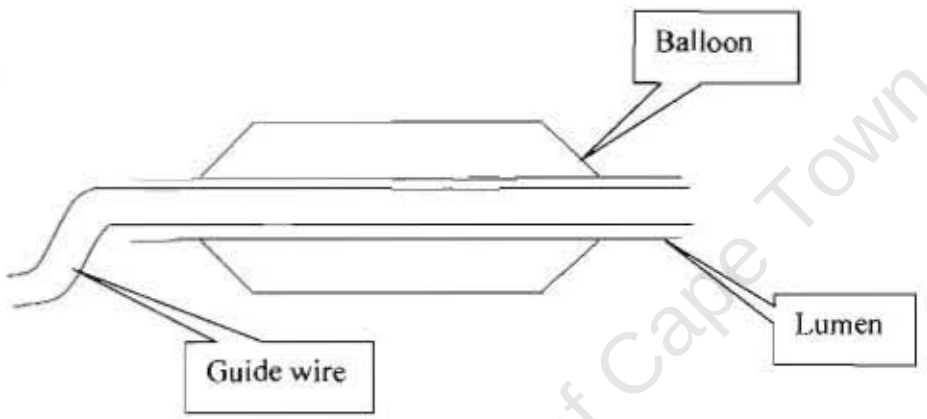

Figure 3.19 Section of balloon, lumen and guide wire assembly

To create a more realistic model, the two were modelled separately though. The rubbery lumen was modelled using a 3-D deformable planar shell element as base element with an extrusion length equal to that of the balloon model. The lumen model has an outside diameter of 1.1 mm and length of 20.72 mm. The lumen is made from a material called PEBAX and the material properties for this model were chosen to approximately represent PEBAX. The following material properties were used (Appendix B):

- Young's Modulus: 3.38×10^{8} Pa
- Density: 1.01×10^{-6} kg/mm^3
- Poisson's ratio: 0.35

Next this material had to be assigned to the 3-D model as a membrane shell section with a wall thickness of 6 x 10^{-2} mm. The lumen was meshed with linear quadrilateral elements and the model discretized into 3,540 nodes and 3,520 linear quadrilateral elements.

A 3-D discrete rigid shell extrusion part was created for the guide wire. The extrusion depth was the same as that for the lumen, which was in fact equal to the length of the balloon. The guide wire has an outside diameter of 0.8 mm and length of 20.72 mm. The lumen was meshed with linear quadrilateral elements and the model discretized into 5,612 nodes and 5,589 linear quadrilateral elements.

3.5 Crimping Tool Model

The actual stent is crimped onto the folded balloon. An uncrimped stent and folded balloon are placed inside a specially designed crimping machine. The machine works on a collet-based system consisting of 12 triangular beams which are arranged circumferentially. This creates the central canal where the stent and balloon can be placed and where the stent is crimped onto the balloon. As the triangular beams are displaced centrally, they slide over each other, keeping the central canal circular and ensuring that a regular and smooth crimped stent is created. A picture of the crimping machine mechanism can be seen in Figure 3.20. As the stent is crimped onto the balloon it is deformed plastically, meaning that it keeps its deformed or crimped shaped after the crimping process. This also causes the stent to be pre-loaded, so that the stent is internally stressed even before the balloon is inflated. Creating a stent model in ABAQUS that is already the crimped size, and assembling it onto the folded balloon model, will not reflect the true behaviour of the system. This stent will be the right size, but will not be pre-loaded. For this reason a model of the crimping machine had to be created to crimp the stent model onto the folded balloon model within ABAQUS.

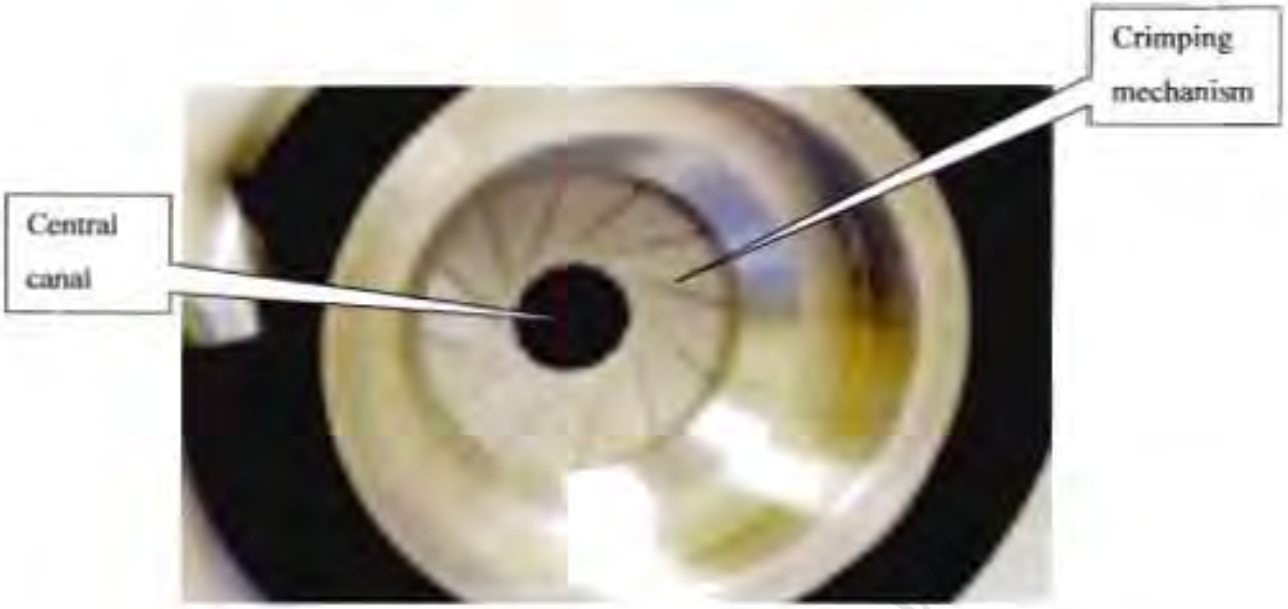

Figure 3.20 Crimping machine mechanism

The actual crimping machine is fairly complex and the challenge was to create a simplified model of the crimping machine, which would crimp the stent in exactly the same manner as the real machine. Discrete rigid surface elements were used to create twelve similar plates, 28 mm in length and 1 mm in width (Figure 3.21). They were meshed with 40 linear quadrilateral elements and had 63 nodes each. Rigid surfaces were used so no material properties had to be specified.

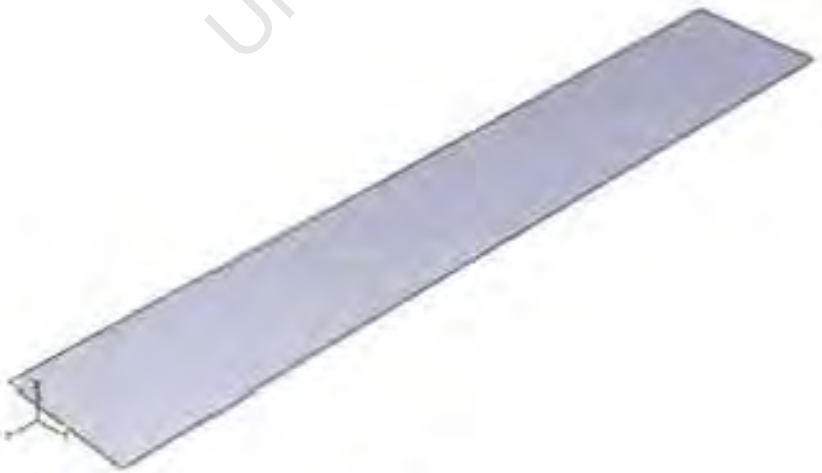

Figure 3.21 Crimping tool plate model

3.6 Assembly

3.6.1 Crimping Tool Assembly

The twelve rigid body plates were arranged circumferentially in such a way that each of them was positioned at a different angle. The angular difference between each of the plates was 30 degrees. This allowed the 12 plates to be arranged in such a way that the central area within the plates formed a canal of similar dimensions as the one formed in the actual crimping machine. This assembly can be seen in Figure 3.22. The diameter of the inner canal was made big enough so that an uncrimped stent could easily fit inside it.

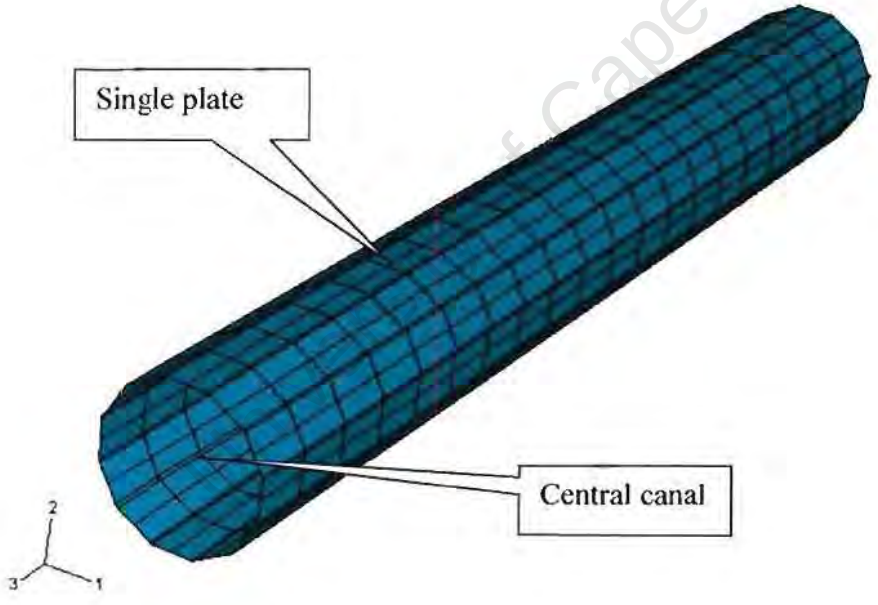

Figure 3.22 Assembled crimping tool

3.6.2 Balloon, Inner Lumen and Guide Wire Assembly

The balloon and inner lumen were assembled first by placing the crimped balloon over the inner lumen. The inner lumen's outside diameter was chosen to fit exactly inside the folded balloon. When assembled, there was no gap between the balloon and the inner lumen. This was a reflection of how the actual balloon fitted onto the inner lumen of the catheter. The guide wire was then inserted into the lumen. The guide wire was modelled in such a way that it fitted loosely into the central canal, like the real guide wire. This would allow some radial movement for the lumen and balloon, if it was necessary for them to move inwards during the crimping of the stent onto the balloon. This assembly can be seen in Figure 3.23.

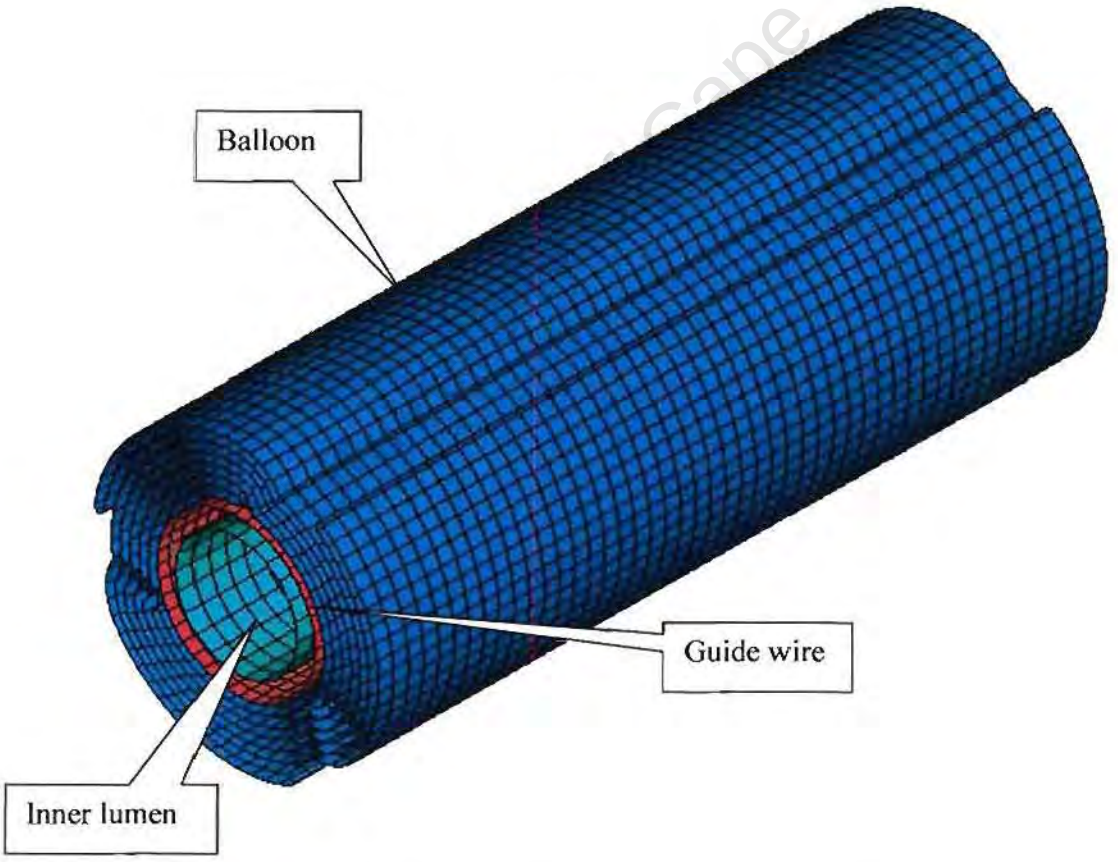

Figure 3.23 Balloon, lumen & guide wire assembly (1/4 of the model)

3.6.3 Stent Assembly

The balloon, inner lumen and guide wire assembly, were now assembled with the uncrimped stent. They were all positioned on the central axis, so that the stent was positioned furthest from the centre. In the actual stent and balloon assembly it is very clear that the ends of the balloon stick out underneath the stent. This is very influential during the deployment process, since the ends of the balloon tend to bulge first, and this could be the main cause for the stent shooting off the balloon. For this reason the stent model was made substantially shorter in length than the balloon. During assembly the stent was placed centrally on the balloon, allowing the same distance of balloon sticking out on each end of the stent. This could later be offset by a certain amount to see if a non-centrally assembled stent would cause the one side of the balloon to open up quicker than the other. This assembly can easily be seen in Figure 3.24.

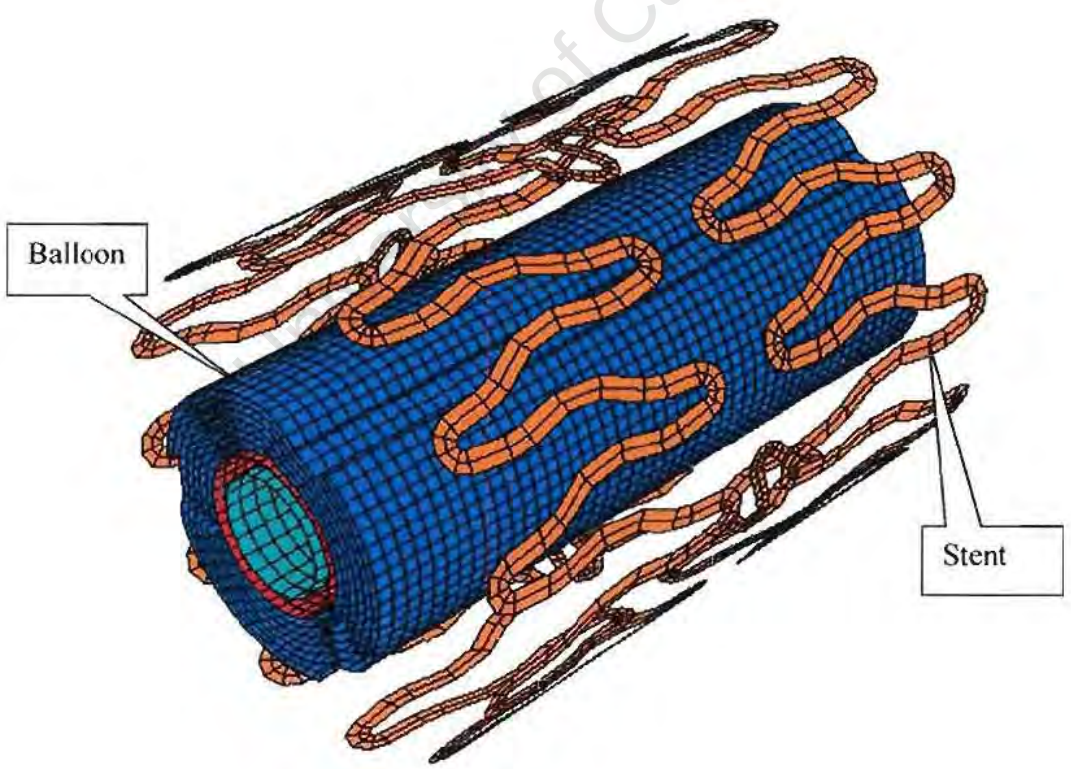

Figure 3.24 Main assembly without crimping tool (1/4 of the model)

3.6.4 Main Assembly

All the individual assemblies were now joined to form one large assembly, similar to the actual stent and balloon inside a crimping machine, waiting to be crimped. The crimping tools were placed on the outside of the other parts, since they have to move radially inward to crimp the stent onto the balloon. One quarter of the final assembly can be seen in Figure 3.25.

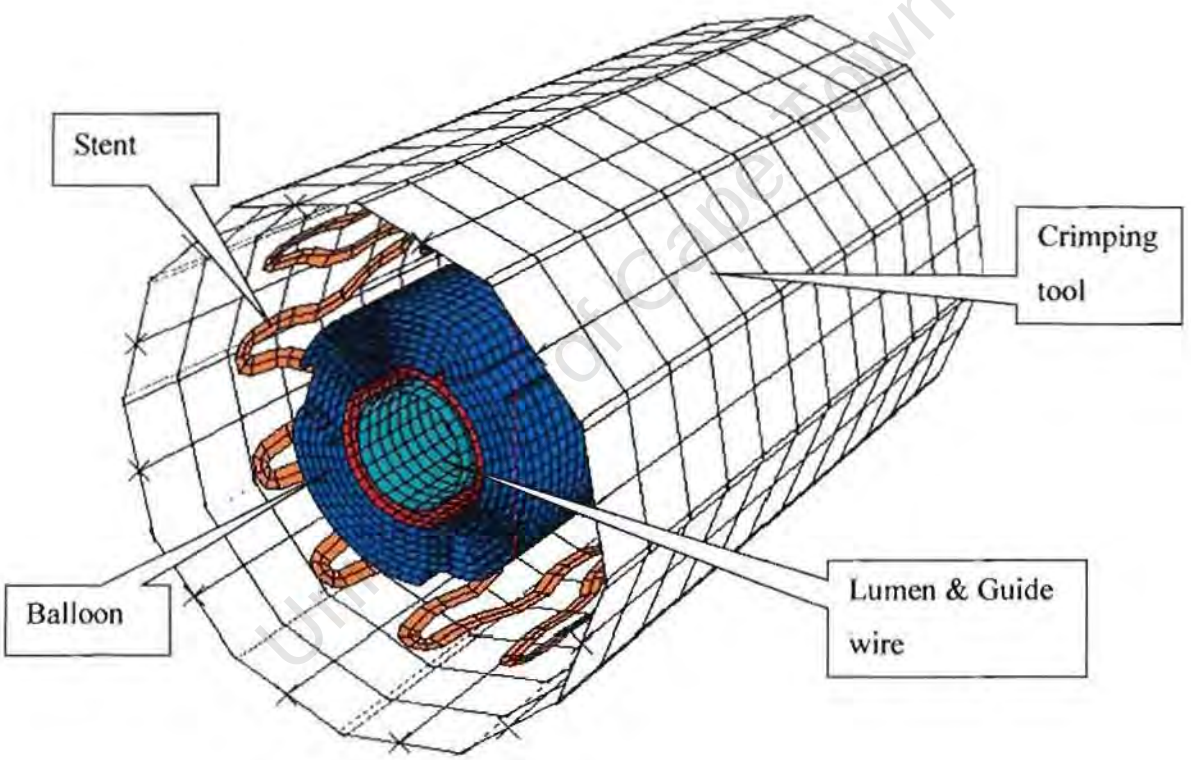

Figure 3.25 Main assembly with crimping tool

CHAPTER FOUR

LOADING AND SOLUTION

The correct boundary conditions had to be created for the model, in order to achieve accurate and real results after running the simulation. The guide wire was fixed in all degrees of freedom, since it remains stationary during the crimping of the stent and during the deployment of the balloon when the stent is delivered. The balloon and lumen were fixed in the axial direction, since the lumen is stationary in the axial direction and the balloon is fixed to the lumen. No actual boundary conditions were placed on the stent for the full model; it was free to move in any direction during the crimping and deployment processes. Due to computational time limits a smaller model had to be created. Initially the idea was to model only half of the complete stent model and to impose symmetrical boundary conditions on the one side. Symmetrical boundary conditions would cause the nodes in the plane of symmetry to have no displacement in the direction normal to the plane and impose rotational restrictions on the nodes in the plane of symmetry. To impose symmetrical boundary conditions one would assume that the model is symmetrical. To make this assumption would not be a true reflection of reality. As previously mentioned one of the main causes for the stent shooting off the balloon could be the asymmetrical placement of the crimped stent on the balloon. Therefore it was decided to duplicate the model, but to scale it down to one quarter of the length.

The coordinate system was transformed to a cylindrical system for the crimping tool. The plates of the crimping tool were fixed in all degrees of freedom except for the one in the radial direction, meaning that the plates could only move radially inwards. The boundary conditions imposed on these plates allowed them to move through one another when they were displaced centrally, and this was necessary to mimic the actual behaviour of the crimping machine during the crimping of the stent and to keep the central canal circular. In order for the stent to be crimped uniformly, the plates had to move inward smoothly and be kept at the same angle.

Another important consideration was the effect of contact between all the surfaces. All the contact had to be specified within ABAQUS. Here is a list of the contact pairs:

- Crimping tool and stent outer surface
- Stent inner surface and balloon outer surface
- Balloon self contact
- Balloon inner surface with lumen outer surface
- Lumen inner surface with guide wire outer surface

To simplify these contact definitions, ABAQUS's generalized contact function was used to create a general contact definition for all the contact surfaces. This contact algorithm uses a penalty method to enforce the contact constraints. The ABAQUS user's manual explains it as follows.

The two deformable bodies or deformable body and a rigid body that take part in the contact are named. With this approach one surface definition provides the "master" surface and the other surface definition provides the "slave" surface. The penalty contact algorithm searches for slave node penetrations in the current model. Contact forces that are a function of the penetration distance are applied to the slave nodes to oppose the penetration, while equal and opposite forces act on the master surface at the penetration point.

When the element faces form the master surface, the master surface contact forces are distributed to the nodes of the master faces being penetrated. In the case of an analytical rigid master surface, the master surface forces are applied as forces and moments on the associated rigid body. An illustration showing the master and slave surfaces is shown in Figure 4.1.

The "spring" stiffness that relates the contact force to the penetration distance is chosen automatically by ABAQUS/Explicit for hard penalty contact, such that the effect on the time increment is minimal yet the allowed penetration is not significant in most analyses.

Since the penalty algorithm introduces additional stiffness behaviour into the model, this stiffness can influence the stable time increment. ABAQUS/Explicit automatically accounts for the effect of the penalty stiffnesses in the automatic time incrementation, although this effect is usually small. The penalty contact algorithm for a balanced master-slave contact pair computes contact forces that are linear combinations of pure master-slave forces calculated in the manner outlined above. One set of forces is calculated considering one surface as the master surface, and the other forces are calculated considering that same surface as the slave surface. ABAQUS/Explicit then applies a weighted average of the two values. The weighting used with each set of forces depends on the value given to the WEIGHT parameter defining the contact pair. The default for balanced master-slave contact is to weight each of the two sets of forces equally. The penetration distance will typically be an order of magnitude greater than the parent element's elastic deformation normal to the contact interface.

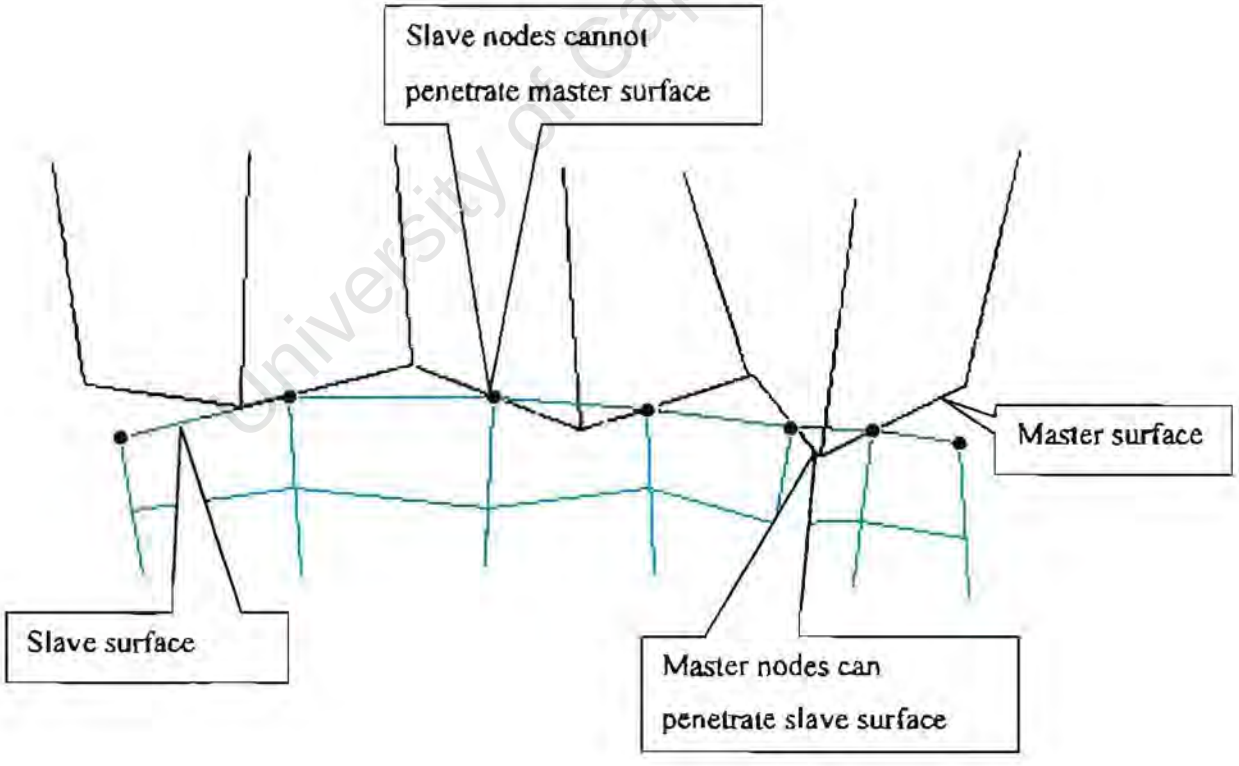

Figure 4.1 Contact definition (ABAQUS user's manual)

The distance that the crimping tool plates move determines the size of the crimped stent: the more they move inward the smaller the outside diameter of the stent, and the bigger the crimp. After careful calculation, it was concluded that each plate had to be displaced by 0.60 mm. This ensured that the stent was crimped tightly onto the folded balloon.

Frictional contact was defined between the outer surface of the balloon and the inner surface of the stent. The friction was modelled using a standard Mohr-Coloumb model, where the maximum allowable frictional shear stress is linearly proportional to the contact pressure:

$$\tau_{friction} \leq \mu P \qquad (4.1)$$

where μ and P are the frictional coefficient and the contact pressure respectively.

A set of fixed steps was created to simulate the response of the real system. The time scale is important in a dynamic analysis, and an accurate representation of the physical mass and inertia in the model is required to give a true response in the simulation. However, this model has many very small elements, which will force ABAQUS/Explicit to use a small time increment to integrate the entire model in time. These small elements are the result of a dense mesh, which gives a difficult mesh generation task. Mass scaling is often used in ABAQUS/Explicit for computational efficiency in quasi-static analyses and in some dynamic analyses that contain a few very small elements that control the stable time increment. By scaling the masses of these controlling elements at the beginning of the steps, the stable time increment can be increased significantly, yet the effect on the overall dynamic behaviour of the model may be negligible. During an impact analysis like this, where there is a lot of contact, elements at the contact zone typically experience large amounts of deformation. The reduced characteristic lengths of these elements result in a smaller global time increment. Scaling the mass of these elements as required throughout the simulation can significantly decrease the computation time. For this exact reason, mass scaling was used to increase computational

efficiency. There was however the danger that with the increase of the overall mass properties of the model, it would degrade the accuracy of the dynamic solution. The masses of the elements were scaled once at the beginning of the first step by the chosen scaling factor of 100. The following four steps were taken for the analysis.

4.1 Crimp Step

In this step the crimping tool plates were moved inward and the stent crimped onto the balloon. A smooth step amplitude was created for the displacement of the crimping tool plates. This was to ensure that the crimping velocities and accelerations were kept under control. A typical smooth step curve can be seen in Figure 4.2. Due to computational time limits the time step taken for this step was very small. The step time was taken as 0.005 seconds. The distance by which the crimping tool plates had to be displaced radially was specified in the load step. They were displaced by 0.6 mm, which was the distance that was required to crimp the stent tightly onto the folded balloon.

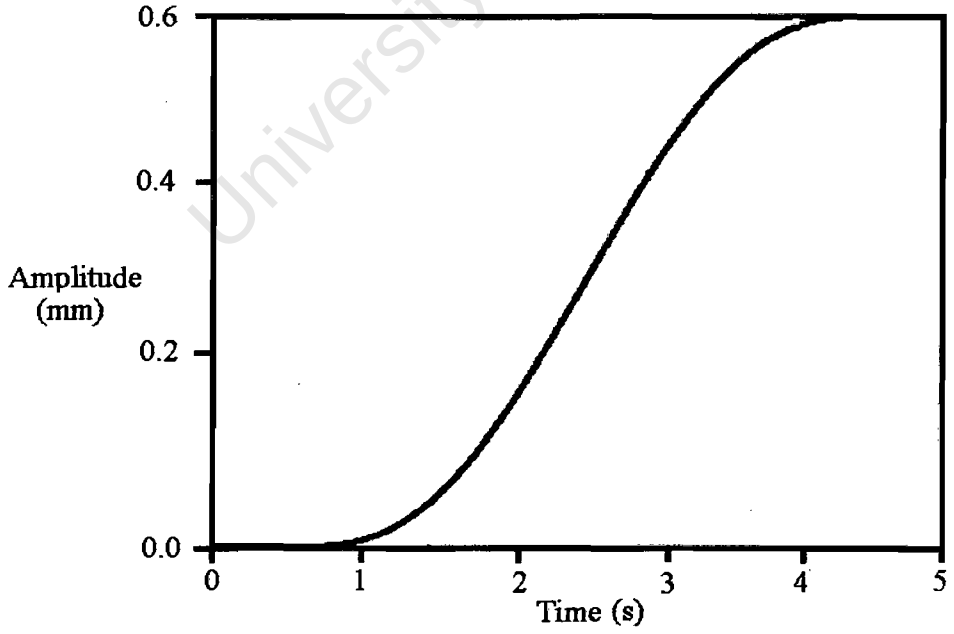

Figure 4.2 Graph of smooth step function

4.2 Zero Velocity Step

After the crimping step the velocities of both the stent and balloon had to be zeroed. Due to the fixed mass scaling the inertial effects were increased by a considerable factor, which caused the stent and the balloon to keep moving radially inwards after the crimping tool plates had stopped. By imposing a zero velocity boundary condition for a time of 1×10^{-5} seconds, this was corrected and the velocities of the stent and balloon equalled zero.

4.3 Release Step

After the zero velocity step another step had to be taken where the crimping tool plates were removed. This was done to allow the balloon to open up properly during inflation and the deployment of the stent to a diameter of 10 mm. A fixed radial distance in the opposite direction was specified and the crimping tools were then moved out of the way. The stent had internal energy after the crimping step and would oscillate until a stage of equilibrium was reached after the crimping tool was removed. To try and correct for this, the crimping tool was taken away in two stages. The first part of the removal was slow to allow the stent to move out gradually with the tools until an equilibrium state was reached. This was also done with a smooth step function over a time of 0.009 seconds. During this time the crimping tool plates were only moved outwards by a distance of 0.01 mm. After that the plates were moved out of the way completely by 9.6 mm in 0.001 seconds.

4.4 Deployment Step

The pressure load required to inflate the balloon was approximately 8 bar. The pressure was applied to the inner surfaces of the balloon as a uniform surface load. A smooth step function was chosen to ramp up the pressure. A step time of 0.08 seconds was selected, where the pressure was ramped up to 8 bar within 0.001 seconds and then kept constant for the rest of the inflation time. The kinetic and internal energies were checked

throughout to ensure that the balloon-loading rate was not too high. The kinetic energy had to be negligible for this to be true (Chua *et al.*, 2003). This allowed the balloon to be opened fully and the stent to be deployed to the required diameter.

CHAPTER FIVE

RESULTS AND DISCUSSION

5.1 Test model simulation

As explained in section 3.1 a simple test model was created to test the possibility of modelling the stent and balloon interaction in ABAQUS. As the pressure on the inner surface of the balloon increased, it inflated. In other words its surface moved radially outwards. The start of the inflation can clearly be seen in Figure 5.1 (b).

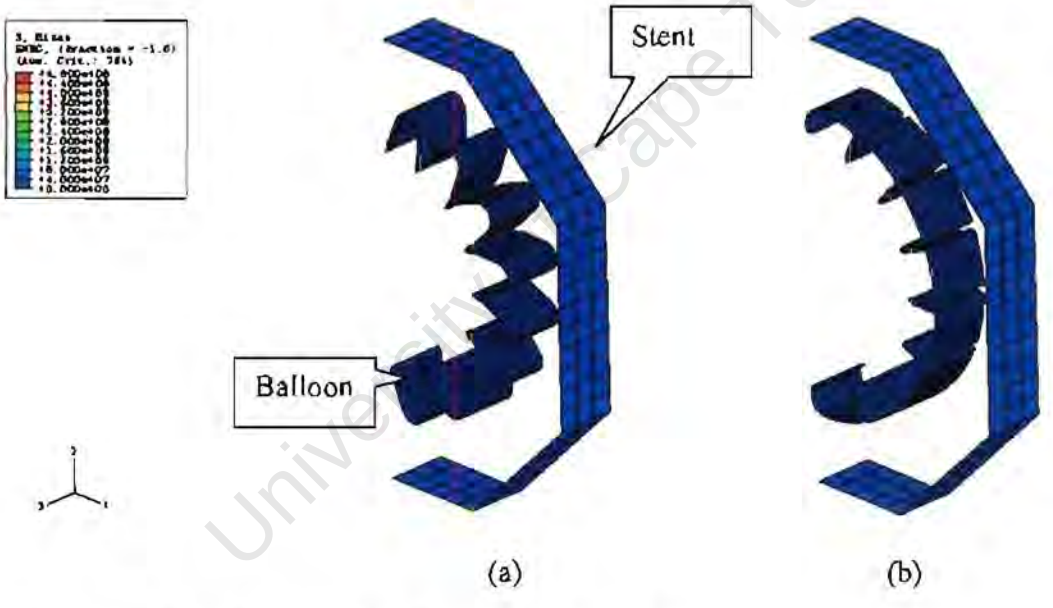

Figure 5.1 (a) Before inflation (b) 1st step of test model run

This outward radial movement continued until contact was made with the inner surface of the stent. The inflation of the balloon halted for a while until the pressure increased sufficiently to overcome the reaction force of the stent. The stent was now no longer able to hold the balloon down and the stent was also forced to expand radially. The deployment of the stent is shown clearly in Figure 5.2 (c). The bends in the original stent surface disappear, meaning that it is expanded radially. This inflation continued until the

balloon was fully deployed and all its kinks had disappeared (Figure 5.3). This simulation showed that the inflation process and deployment of the balloon could definitely be modelled in ABAQUS by using the same principles as used in the test model, just on a bigger scale.

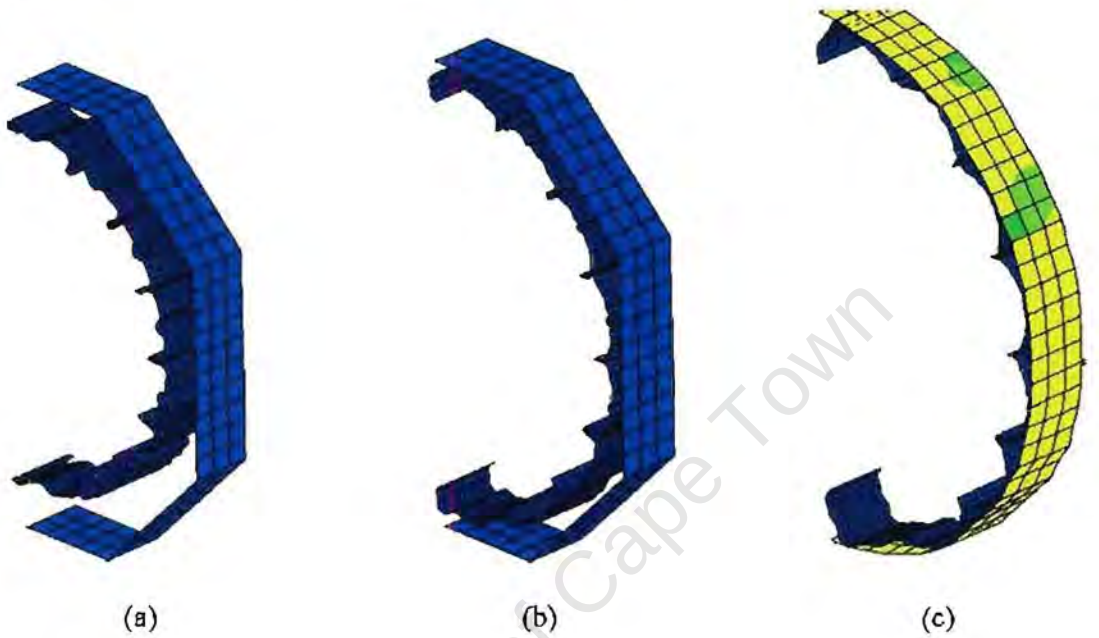

Figure 5.2 (a) 2nd, (b) 3rd, (c) 4th steps of test model run

Figure 5.3 Final step of test model run

5.2 First Small Assembly Simulation

Due to the computational limits, it was decided to model one quarter of the assembly only. The stent used for this assembly was modelled in the form of an already crimped stent, meaning that the stent had the same diameter of a stent that has already been crimped onto the balloon. The only difference is that this model had no internal strains and was thus not preloaded. This stent model was then taken and assembled onto the folded balloon model (Figure 5.4). The model had exactly the same properties as the full size model, the only difference being the shorter length of the balloon and the fewer number of stent rings.

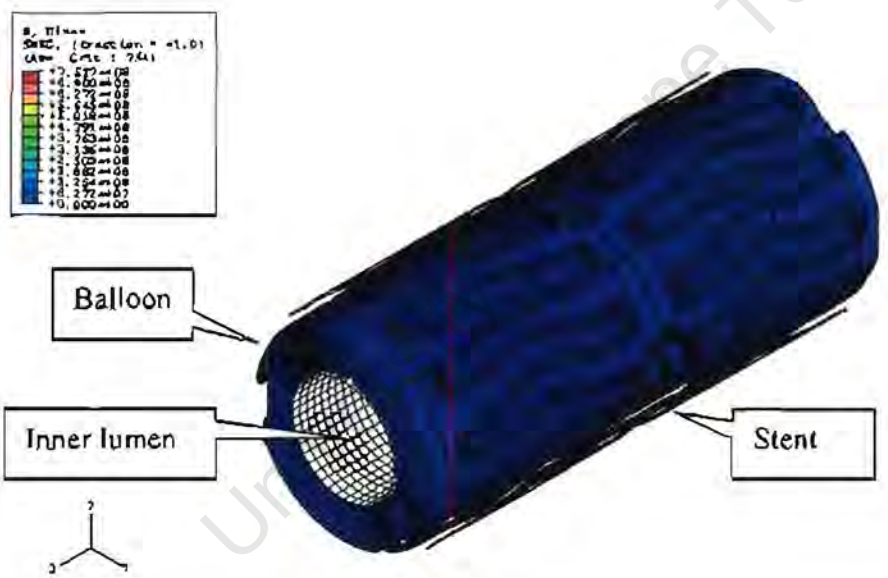

Figure 5.4 Small model run: Before inflation

As the pressure was applied to the inner surface of the balloon, it pushed against the inner surface of the stent. The balloon was initially held down by the reaction force of the stent and the balloon bulged slightly at its ends where it was not held down by the stent. As the pressure increased, the stent could no longer hold the balloon down and the stent started to deploy. This corresponds well with the finding by Chua *et al.* (2003). As the balloon

inflates and the stent is expanded, the stent goes through a stage of elastic deformation. This can clearly be seen in Figures 5.5 (a) and 5.5 (b).

Figure 5.5 Small model run: (a) $\frac{1}{8}$ of the way, (b) $\frac{1}{4}$ of way through

As the expansion of the balloon continues, parts of the stent start to deform plastically. The yield stress is reached at about 330 MPa, and this can be observed in Figure 5.6 (a) and (b). The stress seems to be more localised in some areas of the stent. This can particularly be observed in the corners of the stent struts as illustrated in Figure 5.7.

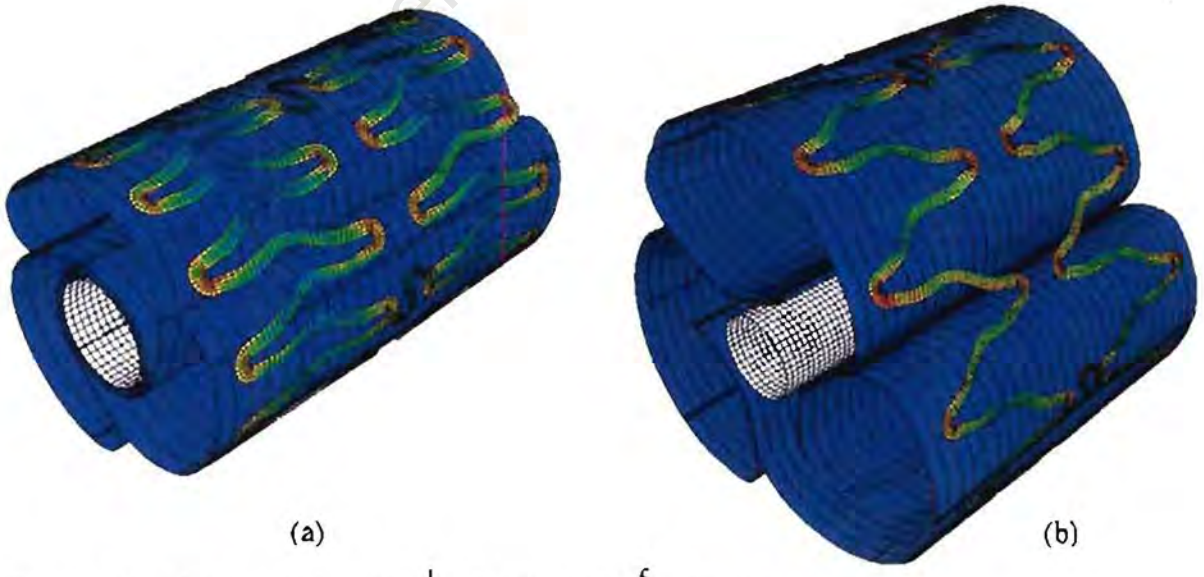

Figure 5.6 Small model run: (a) $\frac{1}{2}$ of the way, (b) $\frac{5}{8}$ of way through

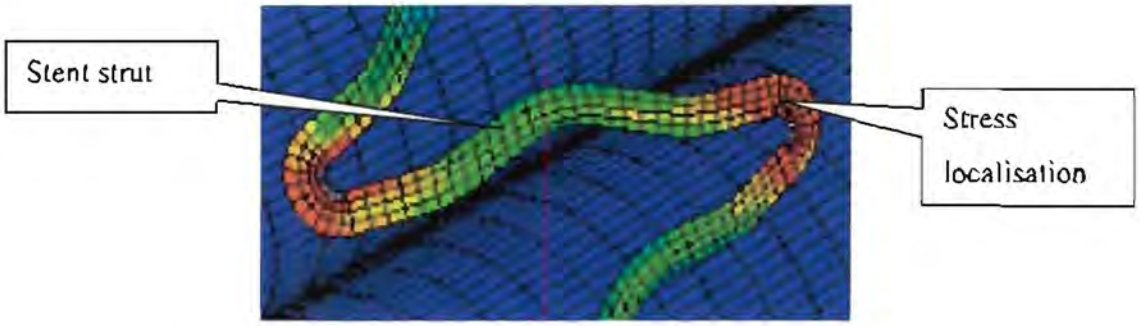

Figure 5.7 Stress localisation in stent strut corners

This stress localisation in the corners of the stent struts can be ascribed to the fact that the stent struts are pulled apart as the stent is deployed. This pulling process causes tension on the inside and compression on the outside of the bend or corners where the stent struts are connected. In return this causes the stress to rise considerably in these hairpin bends, especially on the outsides were the compressive forces are being exerted. This would imply that these are the areas were failure of the stent is most likely to occur, meaning that special attention must be given to the design of these hairpin bends to ensure that failure will not occur with the crimping or deployment of the stent. Failure could be life-threatening to the patient who receives the stent in an attempt to restore the blood flow in blocked vessel. Chua *et al.* (2003) found the same type of stress distribution.

Figure 5.8 Small model run: (a) $\frac{3}{4}$ of the way, (b) $\frac{7}{8}$ of way through

Figure 5.9 shows a plot of the stress development in one of the corner elements, where the stress is the greatest. The development of stress in the graph is very similar to the stress-strain relationship of an elasto-plastic material as described by Belytschko *et al.* (2000). This would suggest that the results are reliable and accurate. The increase of the yield strength after the initial yield is called work or strain hardening and helps the stent to keep its deployed shape after deflation of the balloon. This also implies that it becomes harder to expand the stent the further it is pushed beyond its yield point. The plastic deformation spread to the rest of the stent as its expansion continued, until the entire stent was plastically deformed into its permanent expanded shape. The elastic part of the stress-strain curve shows a few spikes. The cause of these could be the initial hard contact and frictional interaction between the balloon's outer surface and the stent. As the balloon's flaps started to unfold they made contact with the stent's inner surface. This sliding of the balloon surface on the stent could cause resistance to the opening of the stent and balloon, due to the frictional forces, which is a result of the interaction between the two surfaces. This could also contribute to the spiky appearance of the elastic portion of the stress-strain graph.

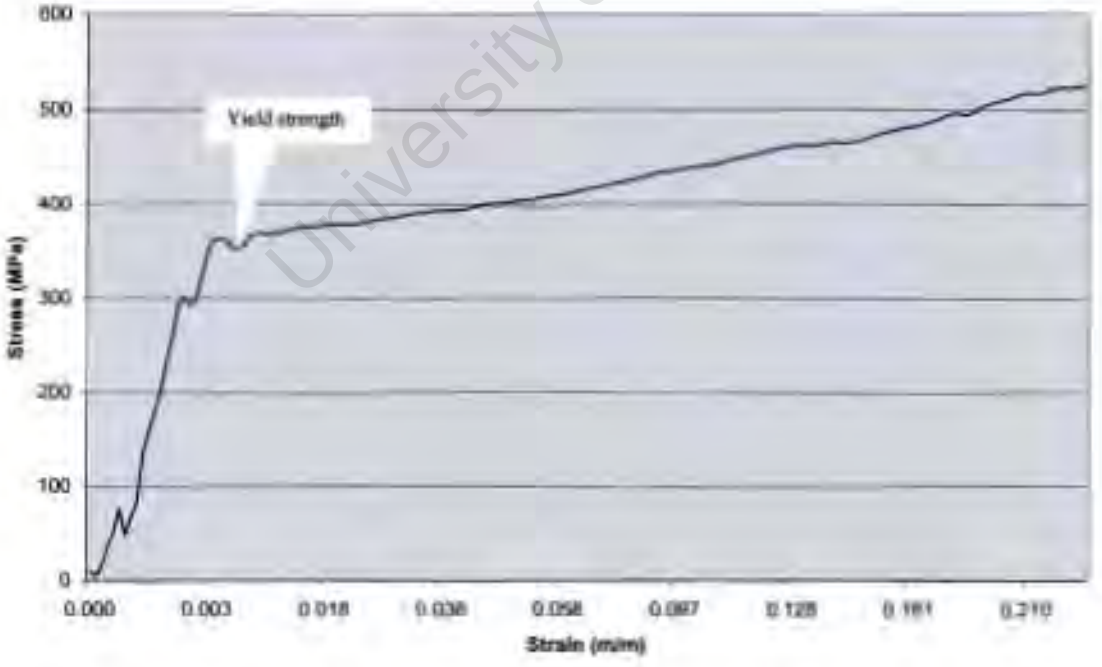

Figure 5.9 Stress vs strain plot for a corner element

The balloon was now fully deployed and the stent had reached its fully expanded diameter of about 10.35 mm in 0.025 seconds. A short simulation time was selected to compensate for the computational expense of having a very fine mesh and having a high mass scaling. As explained in Section 3.3 the material chosen was rate-independent, meaning that by shortening the step times the accuracy of the results would not be influenced. However as explained in Section 2.1, the length of the smallest element determines the size of the critical time step. Since a fine mesh was selected, the smallest element length caused the critical time step to be 2.085×10^{-9} seconds and the simulation to run for approximately 9 hours. In order to achieve an economical solution, it was either useful to reduce the step time of the analysis or to artificially increase the mass of the model with mass scaling. For quasi-static cases, a limited amount of mass scaling is usually possible and does result in a corresponding increase in the time increment used by ABAQUS/Explicit and a corresponding reduction in computational time. Both alternatives yield similar results for rate-independent materials, such as the materials used in this analysis. However, one must ensure that changes in the mass and consequent increases in the inertial forces do not alter the solution significantly. A limited amount of mass scaling is usually possible for most quasi-static cases and would result in a corresponding increase in the time increment used by ABAQUS/Explicit and a corresponding reduction in computational time. A combination of a mass-scaling factor of 100 and a decreased step time was used in this analysis to yield respectable run times with reliable results.

Although the selected simulation time was considerably shorter than the actual time required to expand the stent, the kinetic and internal energies were checked throughout to ensure that the kinetic energy was negligible when compared to the internal energy. This also meant that chosen fixed mass scaling was chosen correctly. The same approach was taken by Chua *et al.* (2003). The fully expanded balloon and stent are shown in Figure 5.10.

Figure 5.10 Small model run: Fully deployed (scaled)

The conventional wisdom was that the stent was circular when it was deployed. This was however not found to be the case. Although the fully deployed stent and balloon were more or less circular, the expanding stent took on a triangular shape. This phenomenon could be ascribed to the way that the balloon flaps were folded. The special tri-folding technique was explained in Section 3.2. As the balloon was inflated the three flaps of the balloon unfolded and caused the stent to expand more over the areas of the unfolding flaps. The folded balloon and assembled stent before the deployment are shown in Figure 5.11 (a). After some inflation of the balloon, it could clearly be seen that the balloon forced the stent to take on a triangular shape Figure 5.11 (b).

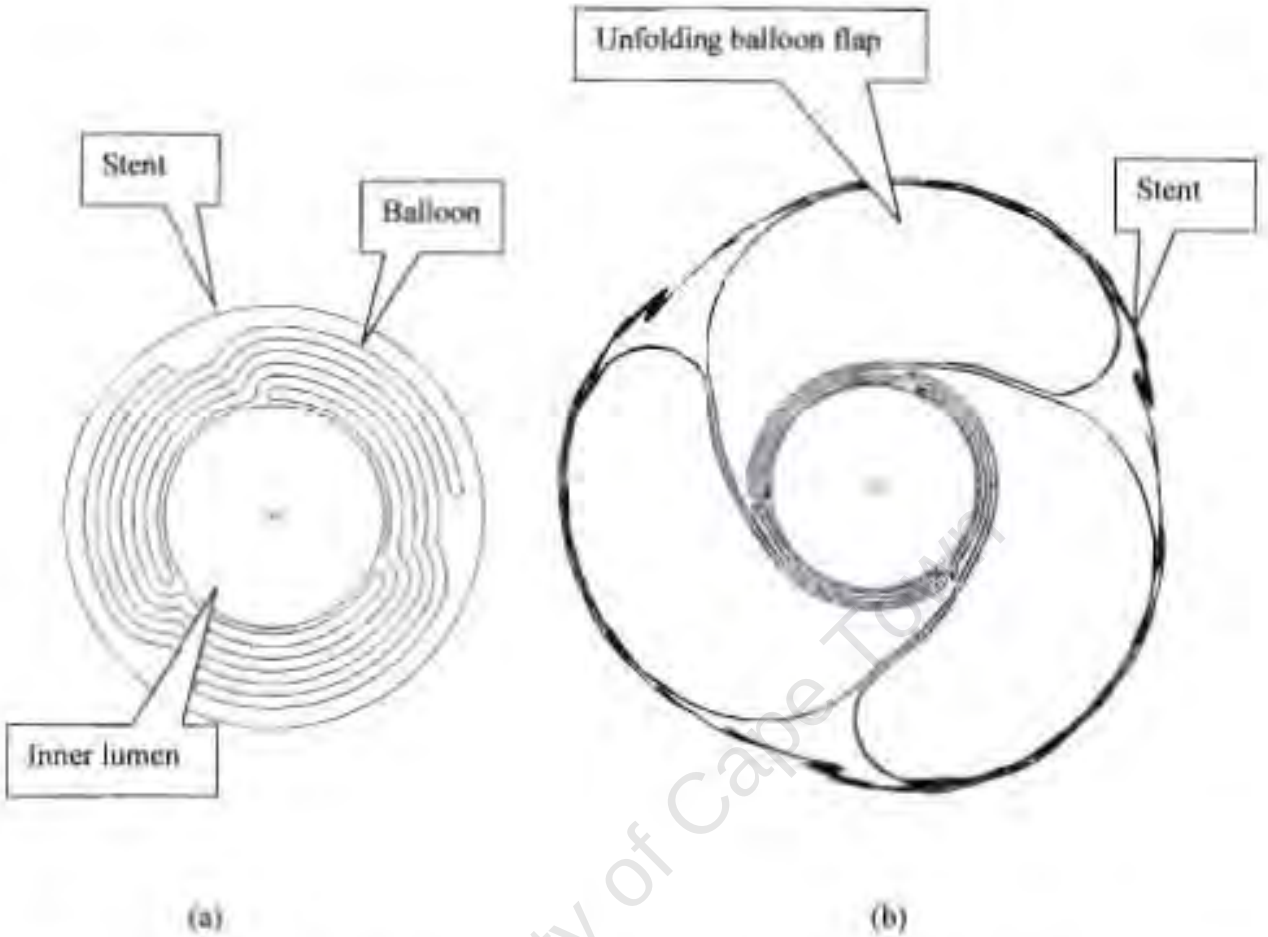

Figure 5.11 (a) Side view of assembled balloon and stent before deployment, (b) Partially inflated balloon with triangular shape

Another interesting point to note was the fact that there were sharp edges sticking out to the sides of the deploying stent. As the stent opened up the stent struts were forced to open up or move away from each other. As mentioned above they were connected via a hairpin bend. The opening of the stent caused a bending moment to form at these bends and the opening of the stent struts forced this to increase. The stent struts are relatively thin in the radial direction and therefore it responded to the increases in bending moment by introducing an out-of-plane deformation at the bends. This automatically compensated for and decreased the bending moments at the bends and ensured that chances of failure decreased considerably. The out-of-plane deformation of the stent at the hairpin bends is an area of great concern, since this could be very harmful to the patient receiving such a

stent. The parts of the stent sticking out could puncture the vessel wherein it is deployed and cause considerable bleeding as well as trigger the restenosis process at the site of injury. It is thus important that the stent hairpin bends are carefully polished, so that they are not sharp and would not injure the diseased vessel. This out-of-plane deformation of the stent can clearly be seen in Figure 5.12. These sharp outstanding edges could be harmful to the vessel wherein the stent will be deployed. This is an area of great concern, because injury to the vessel wall could cause local restenosis. This means that instead of effectively restoring the blood flow to the tissues supplied by the artery, which was blocked, the injury to the vessel wall would cause plaque to start forming at the site of injury. This would result in the closing of the artery, and blockage would yet again occur, and might even be more severe than it was before the stent was inserted. This triangular shape of the stent during the deployment process could also influence the effectiveness of the stent in pushing away or removing the plaque from the obstructed vessel. This triangular shape could cause uneven clearing of the plaque or push it away to one side instead of clearing it all away smoothly. This could start the forming of new plaque and a re-blockage of the vessel. The areas directly over the unfolding flaps were smoother and less out-of-plane bending occured.

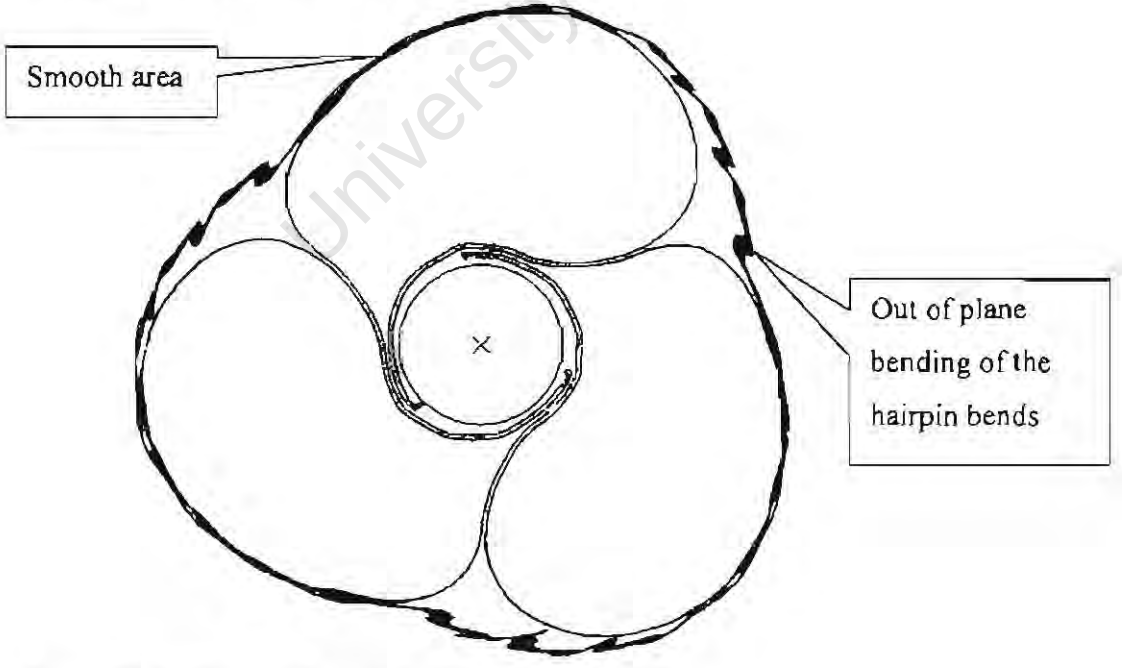

Figure 5.12 Halfway through the deployment process

As the deployment process continued the sharp edges seemed to lessen. This happened as the balloon flaps unfolded further and more of the stent's inner surface came in contact with the outer surface of the balloon (Figure 5.13). One thing that should also be noted was that the stent more or less regained a circular shape at the end of deployment. A scaled side view of the fully deployed stent and balloon is displayed in Figure 5.14.

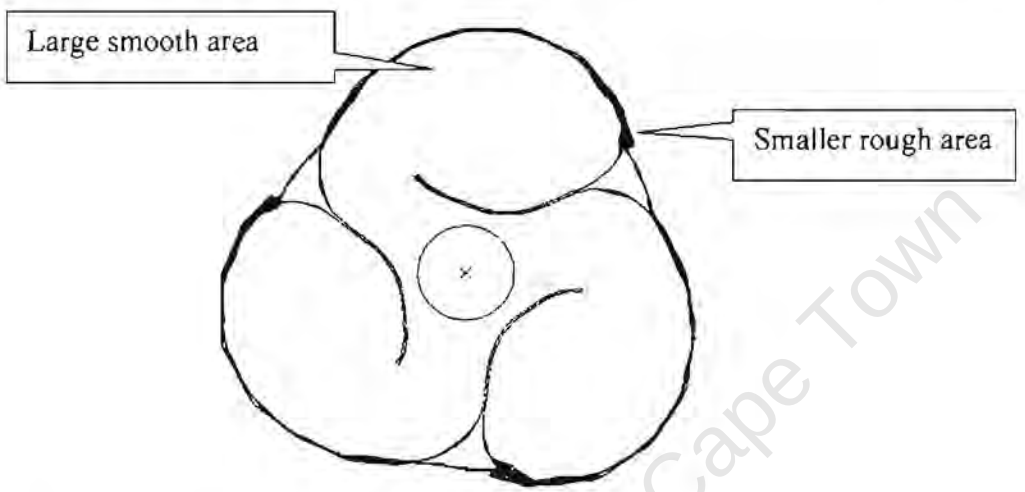

Figure 5.13 $\frac{3}{4}$ of the way deployed

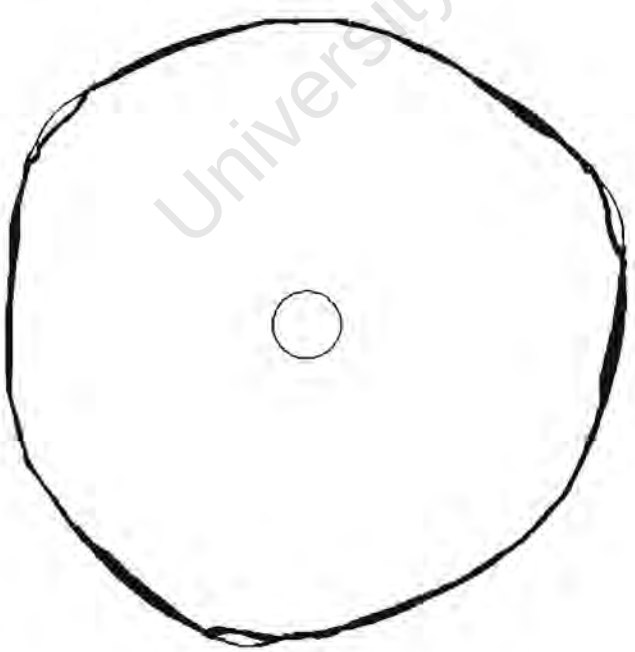

Figure 5.14 Fully deployed stent and balloon (scaled)

Something that could be considered for future work is to model an obstructed artery around the stent and balloon. The stent could then be deployed in exactly the same way as the above simulation. Its effectiveness to remove the plaque, which obstructs the vessel, could then be checked. The effect of the sharp out sticking parts of the deploying stent could be monitored to see if any damage would be caused to the vessel itself.

The difficulty however will be to find the material properties of an artery and the plaque which obstructs it. It will also be extremely difficult to predict when injury would occur to the inner surface of the artery, due to its unknown characteristics and the difficulty to model its reaction accurately. One of the biggest questions will be how one would determine under which inner pressure or compressive force the artery will fail or get injured.

Some finite element studies where the stent artery contact has been modelled has already been done by Prendergast *et al.* (2003), Tan *et al.*, (2001) and Rogers *et al.* (1999) and it was shown that this kind of study would be feasible.

5.3 Crimping Tool Simulation

The crimping tool mechanism was first tested without actually crimping a stent. The idea was to allow the 12 rigid body plates to move through one another displacing them radially inward by a fixed distance. Because of the angular offset of each one of the 12 plates, their inward movement caused the central canal to become smaller and smaller and eventually disappear. This is a very good reflection of what happens in the actual crimping machine and this model would be a suitable representation of the actual crimping mechanism. The crimping simulation is shown in Figures 5.15, 5.16 and 5.17.

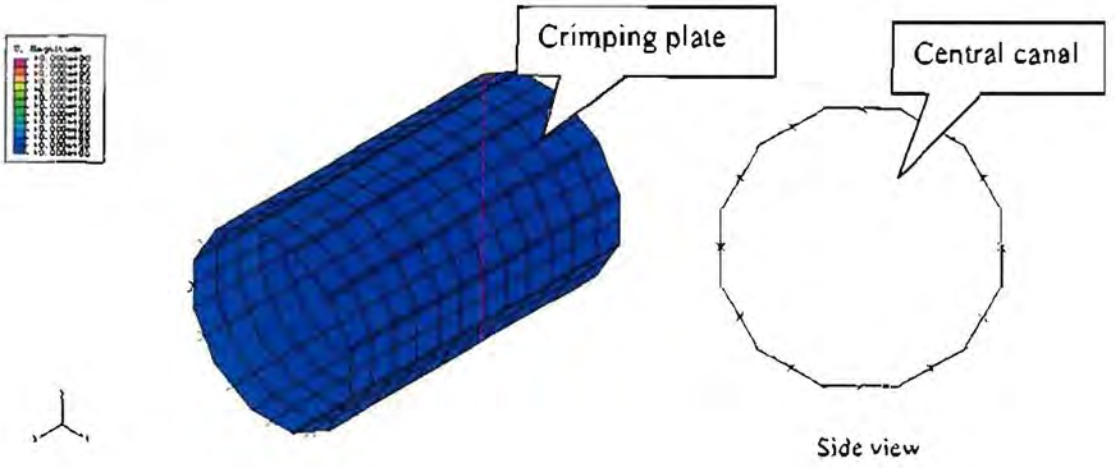

Figure 5.15 Crimping tool simulation: Before closing

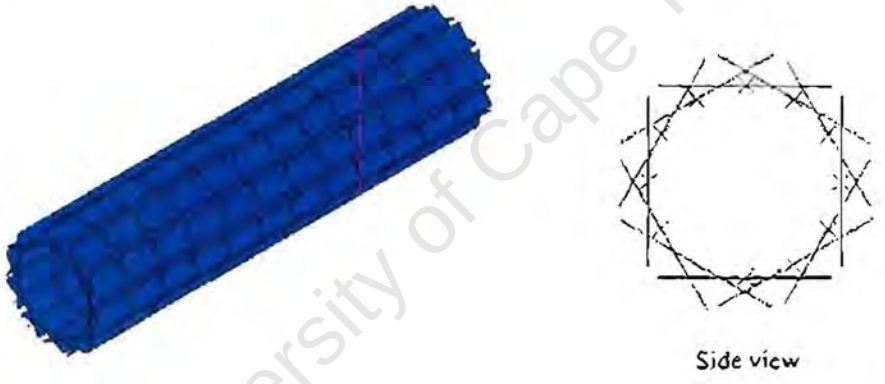

Figure 5.16 Crimping tool simulation: Halfway closed

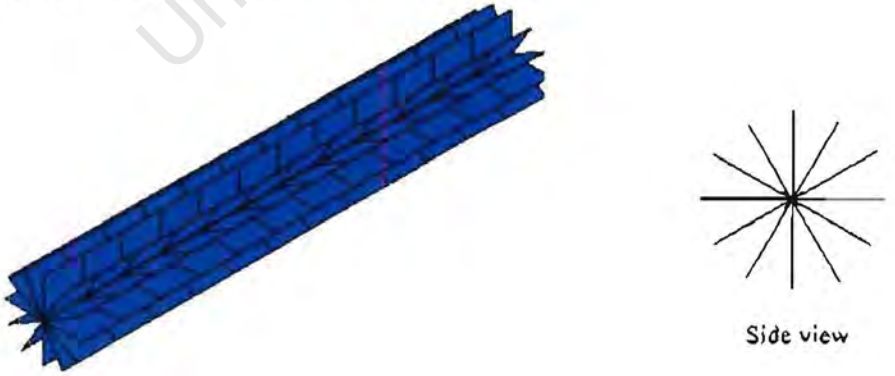

Figure 5.17 Crimping tool simulation: Fully closed

5.4 Full Assembly Simulation

As mentioned in Section 3.3 an uncrimped stent model was now used in the assembly. The initial model had a very fine mesh in order to obtain accurate and true results. This, however, resulted in very small elements, which caused the critical time step to be very small. The critical time step was in the order of 1.8×10^{-9} seconds, which meant that for a simulation time of 1 ms it would have to take 5.5×10^{8} increments to complete the simulation. Computationally this was very expensive. However, the first few simulations were run with this fine mesh. The smaller model was still used and it consisted of only two of the eight stent rings and the balloon was shortened accordingly. The crimp step alone took almost 18 hours to complete. This was definitely not ideal, since changes had to be made to the model after each run, only to wait another 18 hours to see the result of these changes. Due to the limited availability of computers to run these simulations, and the computationally expensive mesh, an alternative option had to be taken.

It was decided to coarsen the mesh in order to increase the critical time step. This would obviously influence the accuracy of the results, but would speed up the simulation run times considerably. With a coarsened mesh, the critical time step was increased to 3.2×10^{-9} seconds. The new time step was almost double the old one and would speed up the simulation by a factor of two. The density of the mesh on the bends of the stent struts and the folds of the balloon could not be decreased by such a large margin, due to the sharpness of the bends and the importance of the stress data of these corner elements.

This meant that there were still fairly small elements in the model, which is why the critical time step only increased by a factor of two. This was however a big improvement and meant that changes to the model could be made at more regular intervals and the smaller model simulation could be perfected, so that the full model could be run with minimal delays and compromises.

5.4.1 Crimp Step

An initial time step of 0.001 seconds was taken for the crimping simulation. The crimping tools were placed a reasonable distance away from the stent itself, about 100 μm. The diameter of the uncrimped stent was about 3200 μm, and this was crimped down by 1200 μm to 2000 μm, meaning that was a 37.5 % reduction in the diameter. It was however observed that the stent gathered more momentum than expected and overshot the displacement of the crimping tool. It was mentioned in Section 4.1 that a smooth step function was chosen to displace the crimping tool. At the end of the crimp step, as the crimping tools started to slow down, the stent kept on moving inwards and away from the crimping tool plates until contact was made with the balloon's outer surface. This was not a true reflection of the real system and it was observed that the kinetic energy of the stent was a lot higher than its internal energy. The reason for the increase of velocity of the stent could be ascribed to the initial hard contact that was made between the crimping tool plates and the stent, as well as speed of the simulation and the mass scaling, as mentioned in Chapter 4.

It was then decided to increase the simulation time to 0.005 seconds and move the crimping tool plates in so that they just touched the outer surface of the stent. Again the simulation was run and the kinetic energy compared to the internal energy of the stent. It was found that the kinetic energy was negligible compared to the internal energy. This can clearly be seen in Figure 5.18. Initially at about 1.2 milliseconds the kinetic energy was higher than the internal energy. This can be ascribed to the initial contact of the crimping tool plates with the outer surface of the stent. This was soon inverted at about 1.45 milliseconds, and now the kinetic energy was less than 2% of the internal energy. Although the new simulation time was still much shorter than the actual time required to crimp the stent, it was justified by the energy investigations. The stent now no longer accelerated faster than the crimping tool plates, but rather slowed down towards the end of the step, insuring a smooth crimp.

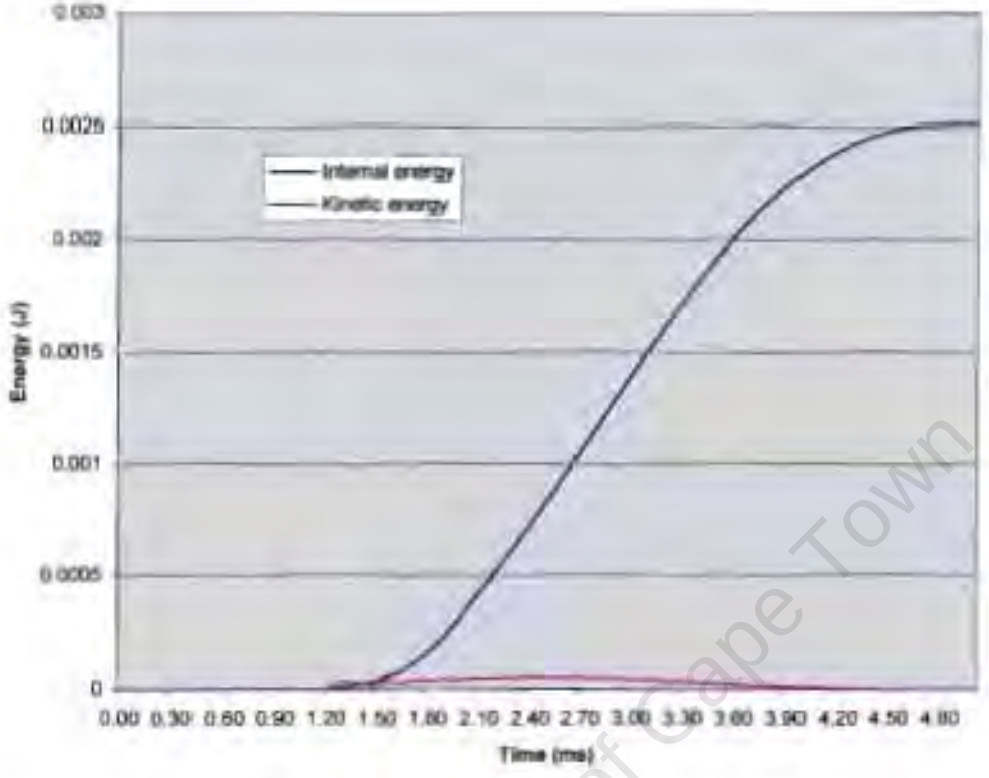

Figure 5.18 Energy development of the system

The kinetic and internal energy values were very low. The energy may be calculated with the following formula:

$$Energy = \int \sigma \varepsilon dV \qquad 5.1$$

meaning that the stress and strain are integrated over the volume. The model is extremely small in size, and therefore the volume is small and the resultant energy values very low. The simulation of the stent crimping from its uncrimped form to the smaller tightly fitting shape on the outside of the stent is shown in Figures 5.19, 5.20 and 5.21.

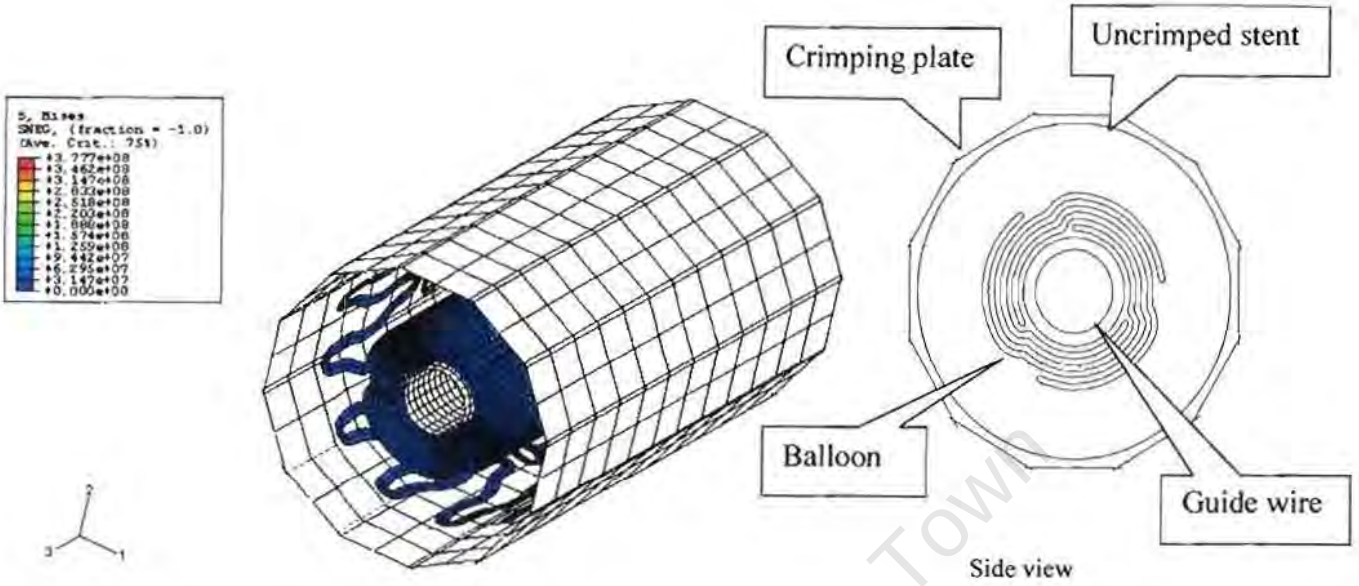

Figure 5.19 Before crimp

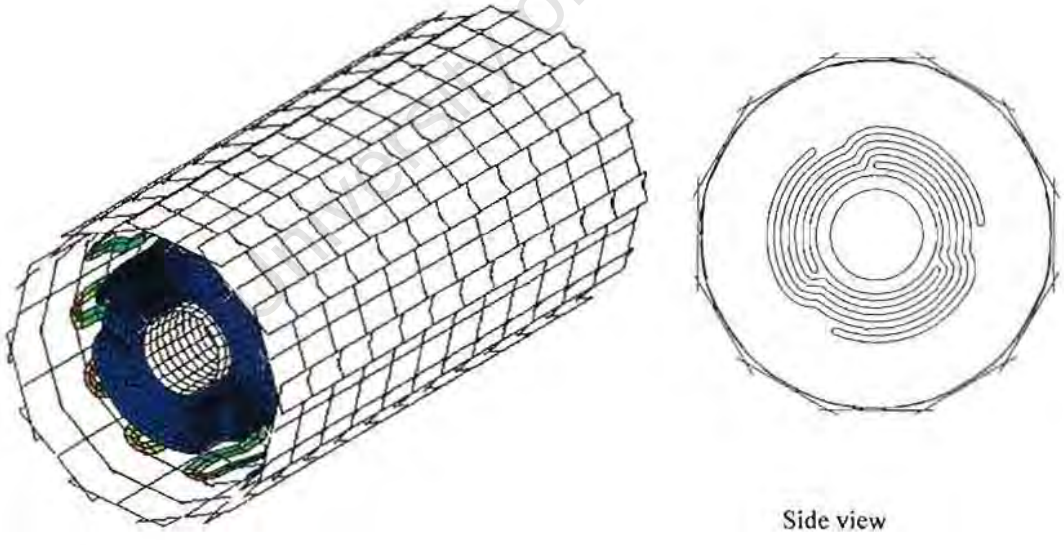

Figure 5.20 Start of actual crimp

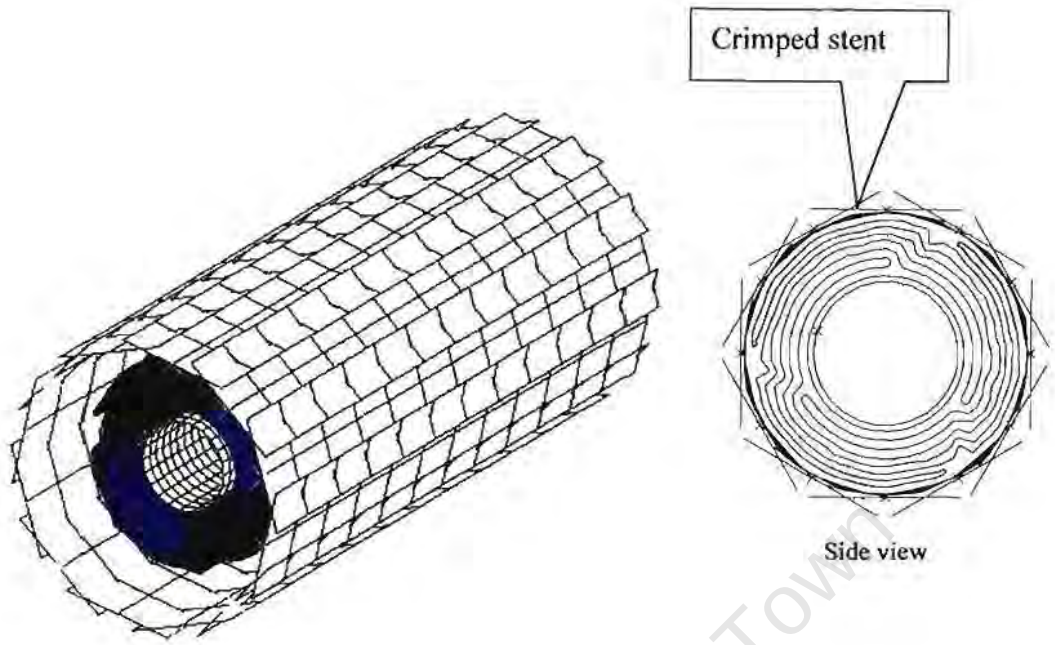

Figure 5.21 End of crimp

Figure 5.22 displays the stent, balloon, inner lumen and guide wire assembly before the beginning of the crimp step. The crimping tool plates had been removed to show the actual development of stress in the stent. The stent was caught within the central canal formed by the crimping tool plates. As these plates moved inward, the stent was crimped smaller and smaller. The crimping of the stent forced the stent struts to move closer to one another and the gaps between them to get smaller with the crimp. This can clearly be seen in Figure 5.23 (a) and (b). Before the crimp the angle between the individual stent struts were about 30^0 as seen in Figure 5.22. At the end of the crimp these angles had almost disappeared completely and the stent struts were more or less parallel to one another (Figure 5.24 (a)).

This shape correlated well with the theoretically anticipated shape of the stent in its crimped formed as calculated by Mr. Markus Lehmann from DISA Vascular (Pty) Ltd. When compared to the crimped stent model, which was used for the first model discussed in Section 5.2, it could be seen that this stent shape was more or less the same. The first model is shown in shown in Figure 5.24 (b) and, when compared to the model in Figure 5.24 (a), a clear resemblance can be seen.

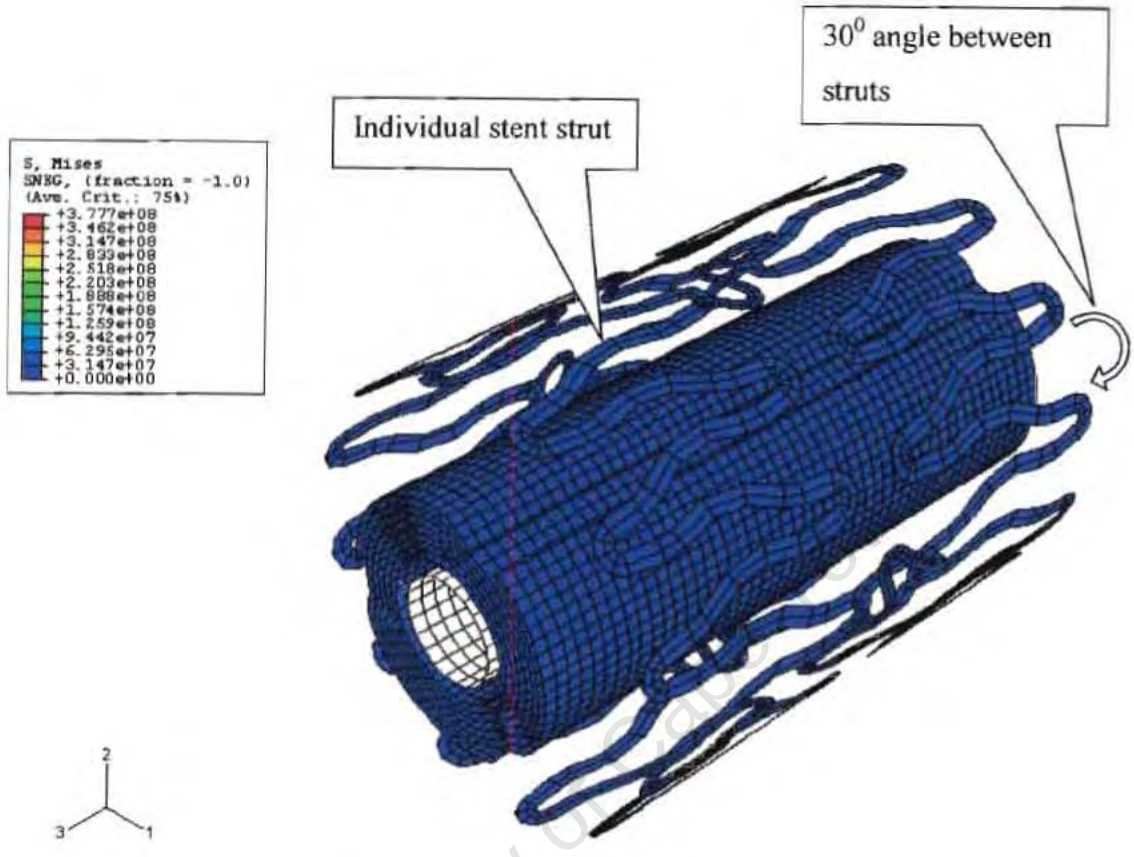

Figure 5.22 Small model crimp simulation: Before the crimp

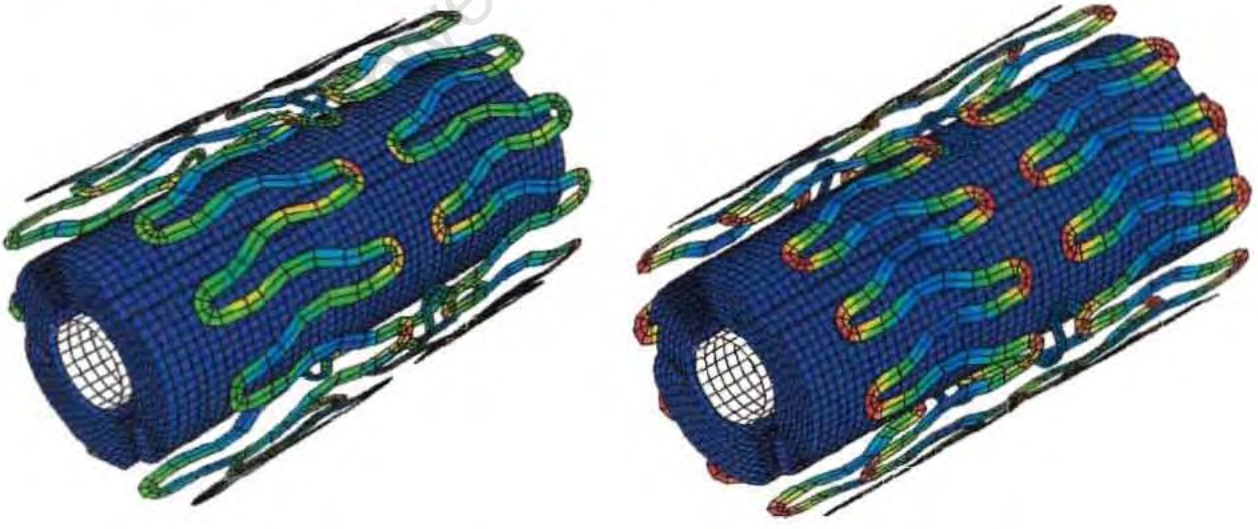

Figure 5.23 Small model crimp simulation: (a) Start of actual crimp, (b) Halfway crimped

(a) (b)

Figure 5.24 Small model crimp simulation: (a) Fully crimped (b) First model before inflation, with no crimping

As the stent was crimped and the struts moved closer to one another, the elements at the bends that connected the struts experienced higher stresses than anywhere else in the stent. This was especially noticed at the outside elements of the bends. This could be ascribed to the closing of the gap between the struts, which caused tension on the outside elements and compression on the inner ones. This stress localisation on the outer elements can be seen in Figure 5.25.

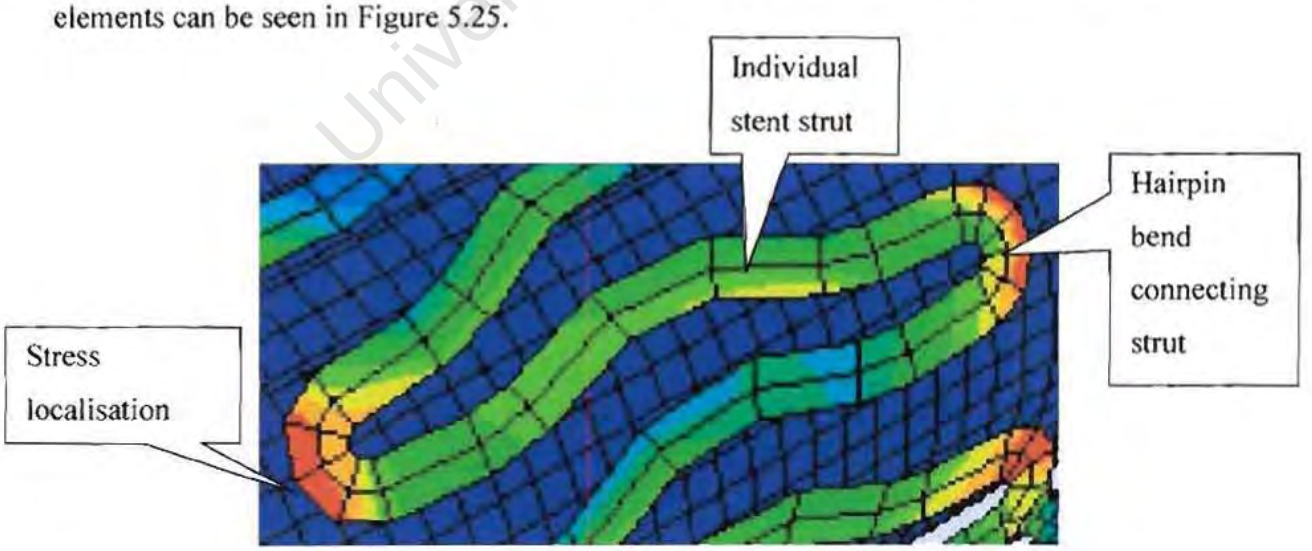

Figure 5.25 Stress localisation on outer elements

The biggest difference between the model where an already crimped stent was used and this model, where the stent was crimped onto the balloon, was the fact that the stent was preloaded after the crimp or before inflation of the balloon. As the crimping tool plates moved radially inwards and the stent was physically crimped to a smaller diameter, stresses developed within the stent, especially in the bends of the stent struts. Figure 5.26 gives a graph of the stress versus the strain for one of the outside elements of the bends. The stress increased linearly until the yield strength was reached. The yield strength now increased even further, meaning that the stent was now work hardened or strain hardened. This curve closely resembled the stress-strain curve for an elasto-plastic material as given by Belytschko *et al.* (2000). The second part of the curve, after initial yield, also correlated well with a typical hardening curve obtained from Belytschko *et al.* (2000). This would indicate that the material model chosen for the stent was correct and that the solution was reliable. The fact that the stent was being work hardened as it was crimped, told us that it got more and more difficult to crimp the stent, as it got smaller and was pushed further past its yield point. This also meant that the stent had gone through some plastic deformation and would retain its crimped shape even after the crimping tools had been removed. The crimping process was thus a success with the stent being crimped onto the outer surface of the folded balloon.

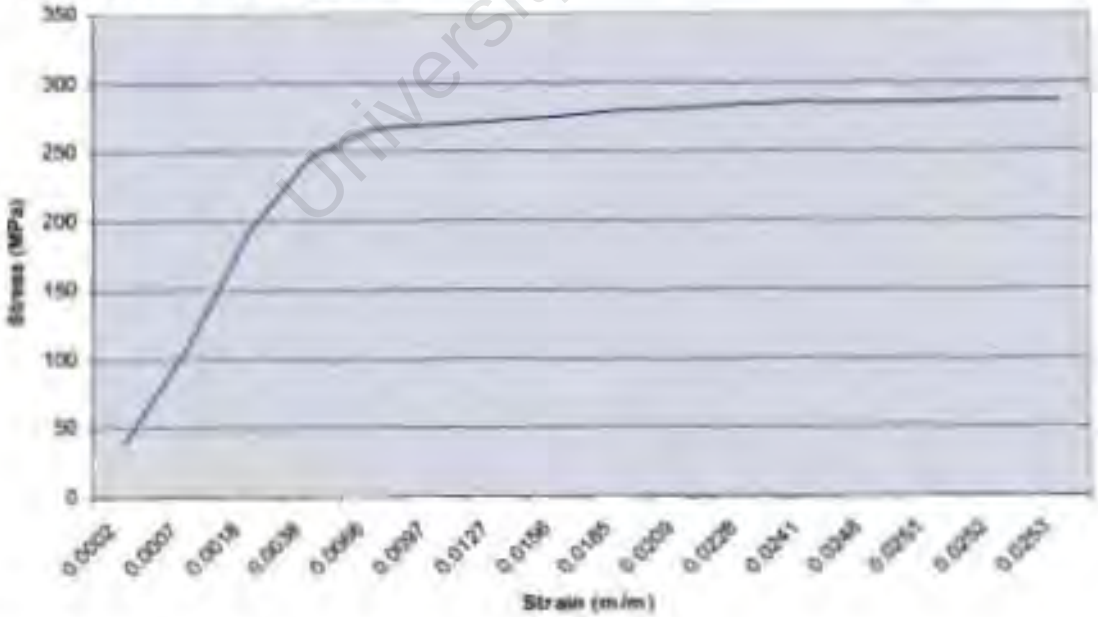

Figure 5.26 Stress versus strain graph for one of outer elements

One of the main difficulties experienced during the simulation of crimping the stent onto the balloon, was to find the correct distance by which the crimping tool plates had to be moved radially inwards. The common idea would be that the stent's inner surface was perfectly circular when crimped, but in fact this was not found to be true. From Figure 5.27 it can be seen that the crimped stent has 12 square facets or square areas all around its inner surface, which caused the stent's inner diameter to be smaller than expected in some areas.

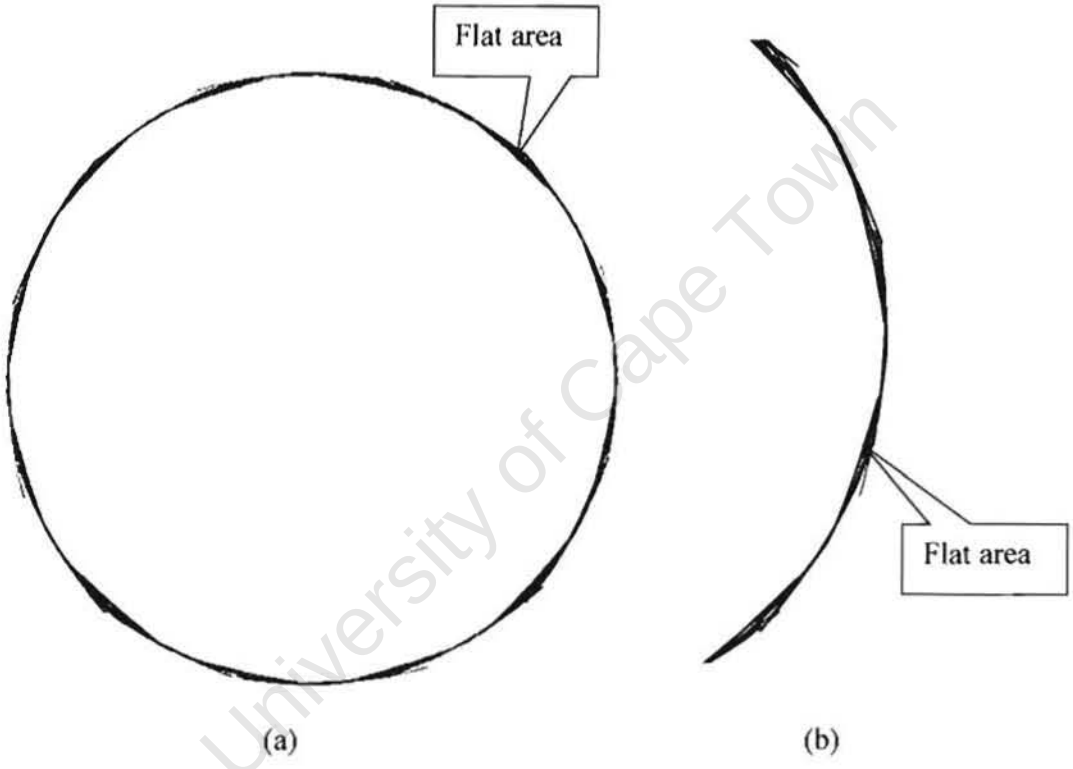

Figure 5.27 (a) Side view of crimped stent (b) Close up of crimped stent section

This provided considerable difficulty in predicting the inner diameter of the crimped stent and thus the distance the crimping tool plates had to be moved inwards. These facets were formed by the bends that connected the individual stent struts as illustrated in Figure 5.25. Due to the fact that no air gap was assumed between the folds of the folded balloon, the stent could not be crimped too far, since this would cause the balloon's surfaces to be pushed through each other and over-closure to occur. In return this would prevent

inflation of the balloon and the simulation would fail. There is a slight gap between the inner lumen and the guide wire, meaning that the stent could be crimped tightly onto the balloon. The balloon would transmit the displacement to the deformable inner lumen, which would then move radially inwards until it touched the guide wire. The difficulty was thus to crimp the stent so that the amount of crimp would be realistic and it would fit tightly on the balloon, but not crimp it too far so that over-closure of the balloon surfaces would occur. The correct crimping distance was eventually obtained after numerous simulations. This non-circular crimp of the stent could also be one of the reasons for the stent shooting off during the deployment of the balloon. Not all of the flat areas were the same size and therefore some parts of the stent made more contact with the balloon than others. This meant that there is more interaction and friction between some parts of the stent and balloon, which causes an uneven distribution of the loads and could initiate an uneven opening of the balloon and stent thus forcing the stent to shoot off.

5.4.2 Zero velocity step

As explained in Section 4.2, the zero velocity step ensured that the inward acceleration of the stent and balloon, due to the inertial effects caused by the mass scaling, were zeroed. This step was necessary to ensure that the balloon and stent would not still have inward velocities with the onset of the inflation step. If they had, it would cause over-closure of the balloon and the simulation would fail at the beginning of the balloon inflation. This step was performed successfully so that the crimping tool plates could be removed.

5.4.3 Release step

Initially it was thought that this step would be a very simple one in that it would only entail the removal of the crimping tool plates. This was however found not to be so simple. With the release or away movement of the plates, the stent also moved radially outwards. It expanded radially outwards for more or less 200 μm before it started to oscillate. It kept on oscillating, by moving inward and outward by small distances. The

only explanation for this oscillation could be the stored energy or inertia of the stent due to the crimping from a large to a small diameter. This inertia might then cause a spring back after the removal of the crimping tool plates. This meant that the stent no longer sat tightly on the outer surface of the folded balloon. This oscillation of the stent was definitely not ideal and with the inflation of the balloon during the deployment step it would cause the balloon to collide hard with the inwardly moving stent. This would result in a failure of the analysis due to the over-closure of the balloon surfaces with the rebound from the stent surface.

The method that was used to try and correct this problem was to move the crimping tool plates out slowly, so that the stent pushed against their inner surfaces. Figures 5.28 and 5.29 show the progression of the release of the crimping tool plates. The force exerted on the inner surface of the crimping tool plates and thus the expansion of the stent caused some of the inertial energy to be dissipated. The plates were moved outwards until the stent reached a point of partial equilibrium where it did not expand any further but rather generated small oscillating movements. The plates were then removed completely (Figure 5.31). The oscillation was considerably smaller than when the crimping tool plates were just removed straight away, meaning that this new approach of crimping tool plate removal was done with some success, but was still not perfectly ideal.

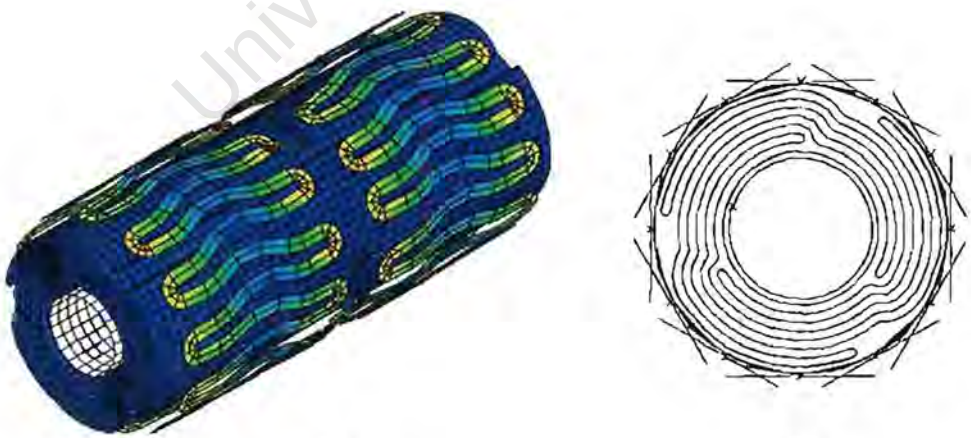

(a) (b)

Figure 5.28 Start of the remove step (a) Isometric view without crimping tool (b) Side view with crimping tool

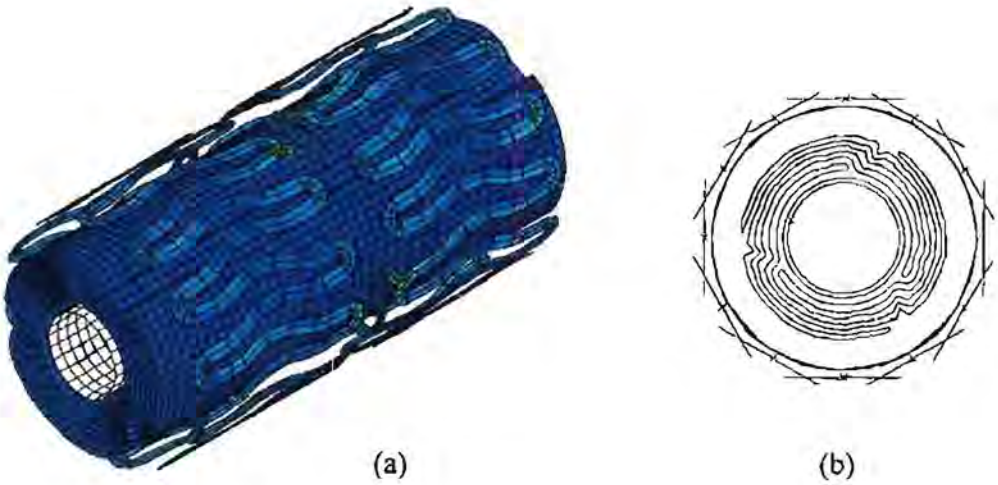

Figure 5.29 Partial equilibrium reached in release step (a) Isometric view without crimping tool (b) Side view with crimping tool

Figure 5.30 illustrates the spatial displacement of the stent in the radial direction during the release step. The displacement values are negative due to the fact that the stent was crimp inwards, in other words the stent was displaced in the negative radial direction. For the first 4.2 milliseconds the stent gradually moves with the outward moving crimping tool plates, being displaced by more or less 215 μm. This is clearly illustrated with the positive displacement of the stent in the radial direction. After that, contact with the crimping tool plates was lost and the stent started to make small oscillating movements. It oscillated with and initial amplitude of about 25 μm, which got smaller with every oscillation as the energy dissipated. The end of the release step the oscillation amplitude was about 15 μm. The spring back of the stent is not unrealistic and in reality the crimping process is repeated three times to ensure a tight fit of the stent on the balloon. This is crucial for the insertion of the stent into the blocked vessel. If the stent is not crimped tightly onto the balloon, it will easily be dislodged during the advancing of the catheter to the site of blockage and could cause serious threats to the patient.

In reality the stent is actually crimped three times to ensure a tight fit. This would imply that the spring back of the stent is not unrealistic at all and happens in real life. It is believed that the only way to eliminate oscillation and spring back would be to recrimp

the stent another two times. With each crimp the stored internal energy would get less and the spring back reduced. In return this would lessen the oscillation and a tightly fitting stent on the folded balloon. Due to computational time limits, the re-crimp could not be simulated, but it is definitely something that has to be done in future to ensure a tightly crimped and non-oscillating stent. The difficulty with the re-crimp will be to calculate the distance through which the crimping tool plates have to move to ensure a tightly crimped stent. As mentioned above, the crimp cannot be too much though, due to the fact that this would cause over-closure of the balloon surfaces and cause the simulation to fail. Another aspect that has to be kept in mind is that the stent gets work hardened as it is crimped and is pushed further past its yield strength. This means that it gets more and more difficult to crimp and that the stress in the outer elements of the bends increases more with every crimp. This increases the risk for stent failure, which could be fatal to the patient. Again this stress the importance of designing the stent strut bends, so that these kinds of stresses could be handled and that the stent could be crimped without the risk of failure.

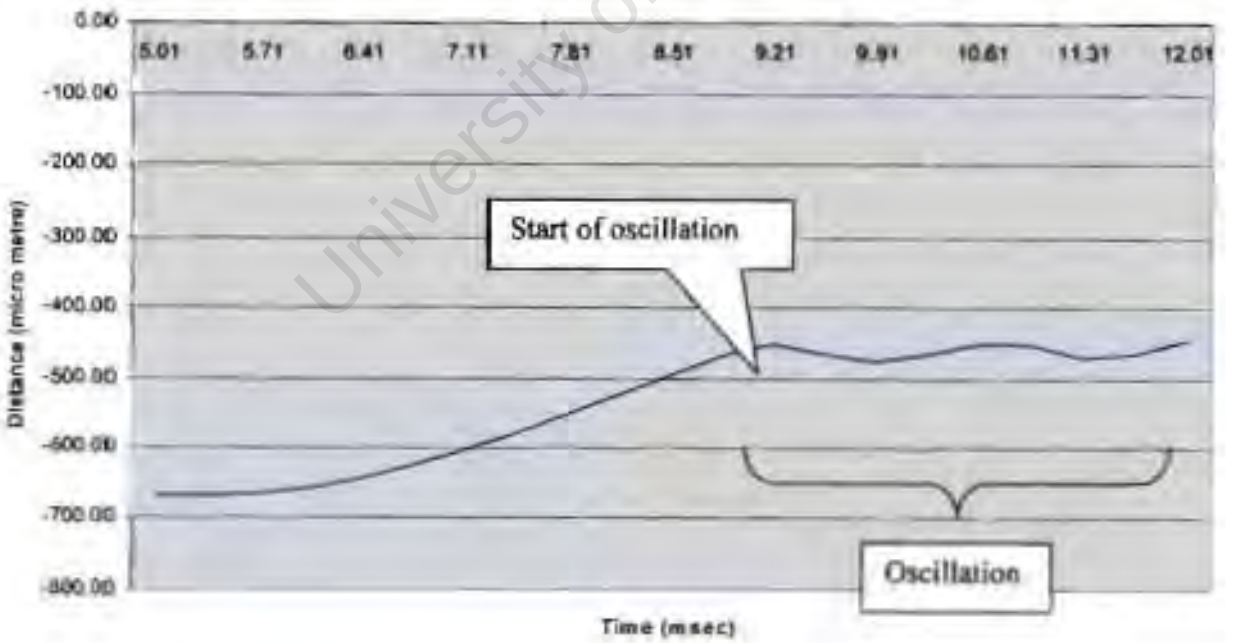

Figure 5.30 Spatial displacement of the stent in the release step

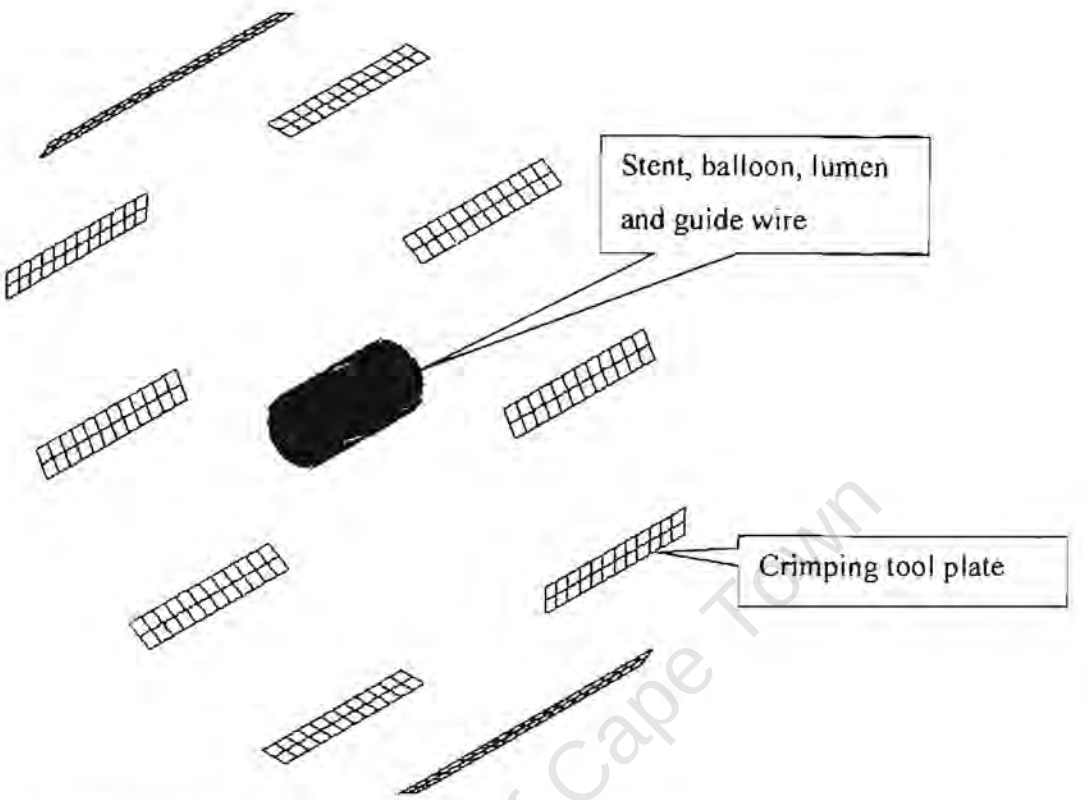

Figure 5.31 Full removal of the crimping tool plates (scaled)

Another possible way for reducing the spring back and oscillation would be to remove all the mass scaling on the model and lengthen the time taken for the crimp and release step. However, computationally this would be just as expensive and due to limited resources this idea could not be pursued. The oscillation was however not that severe and the balloon could now be inflated.

5.4.4 Deployment Step

The pressure step for the increase in pressure inside the balloon was exactly the same as that for the first model assembly as explained in Section 5.2. The "spring back" of the stent caused stress relaxation within the stent. This stress distribution can easily be seen in Figure 5.32. This is obviously not ideal, and there is a need for a another crimp step, to insure a pre-stressed stent, which fits tightly on the outer surface of the balloon. Due to

the computationally expensive nature of this simulation it could not be repeated and would have to be addressed in future studies. The difficulties experienced during the other steps of this simulation, i.e. the crimp step, resulted in a shortage of time to perfect this inflation step. For this reason, I was forced to use a fairly large mass-scaling factor during this step to try and finish the step in the limited time that was available. The inflation step was computationally extremely expensive due to the fact that ABAQUS had to check the stent-balloon and balloon-balloon self-contact, with regular intervals throughout the step to ensure that over-closure or excessive distortion of the balloon and stent elements would not occur. This slowed the simulation down considerably. The use of a big mass-scaling factor could thus not be avoided.

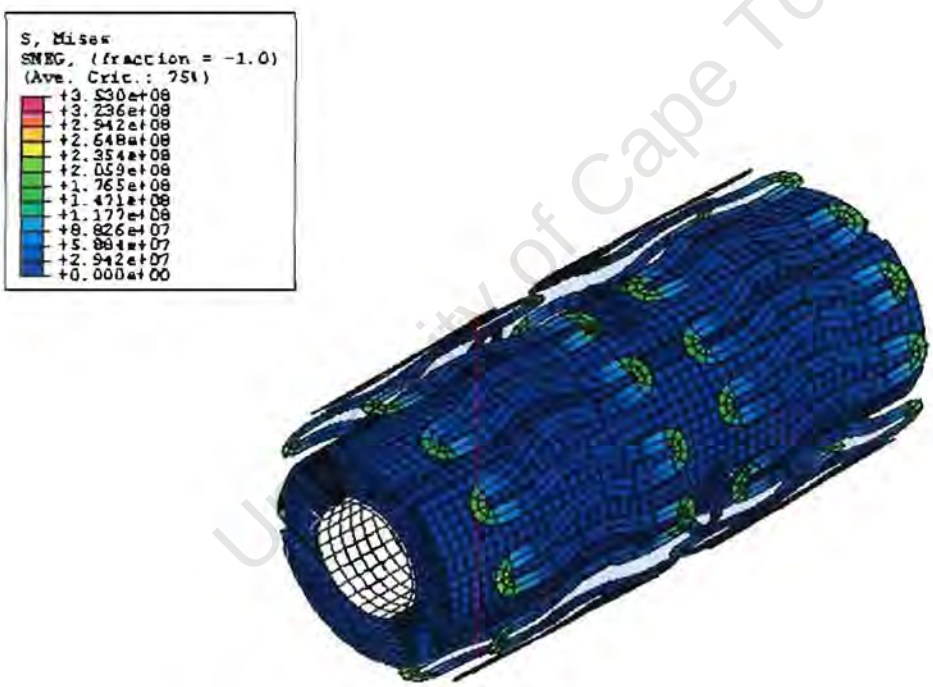

Figure 5.32 Low stresses in stent before inflation

As the pressure started to rise inside the balloon the flaps started to unfold until they made contact with the inner surface of the stent. Due to the fact that the stent was still doing some small oscillating movements, the initial contact between the balloon flaps and

the stent was very hard. The deployment of the balloon flaps halted for a while as the pressure kept on increasing and tried to overcome the reaction forces of the oscillating stent holding down the balloon. Again, the balloon bulged slightly at the ends where it was not held down by the stent. Eventually the reaction force of the stent was overcome and the balloon pushed the stent radially outwards and started deploying the stent (Figure 5.33).

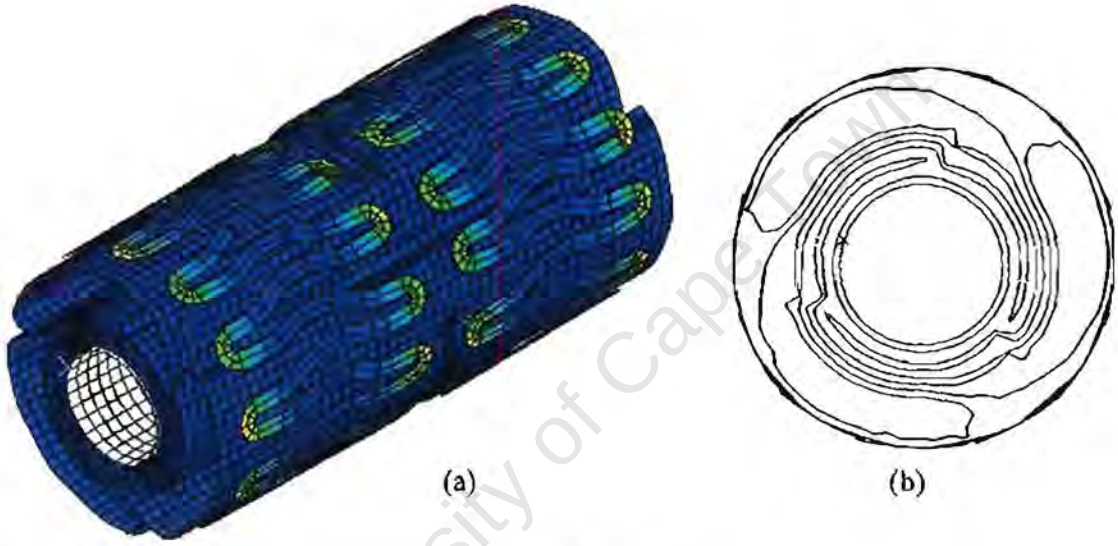

Figure 5.33 Start of inflation (a) isometric view (b) side view

The same out-of-plane deformation phenomenon that was mentioned in Section 5.2 could be observed in the inflation step. The triangular shape of the deploying balloon and stent was not as prominent in this step, due to the fact that the stent sprung back during the release of the crimping tools and was no longer sitting tightly on the folded balloon. This allowed the balloon to open up more before encountering the inner surface of the stent. The inflation of the balloon and resultant deployment of the stent continued in the same fashion as the simulation that was discussed in Section 5.2. However, the big mass-scaling factor resulted in an increased inflation acceleration and thus radial velocity of the balloon. It was also noticed that the oscillation of the stent had not ended and equilibrium of the stent had not been reached. This meant that the stent was still moving radially

inwards and outwards. After a time of about 30 ms the stent was moving inwards, just as the balloon was accelerating radially outwards. The contact between the two resulted in the balloon's surface to overshoot the stent's inner surface and go straight through. This resulted in excessive distortion of the balloon and stent elements and the simulation to be aborted. This is illustrated in Figure 5.34. The only way this could be corrected would be to re-crimp the stent to eliminate its oscillation and to decrease the mass-scaling factor. However, due to the limited availability of computer resources and the computational expense of the simulation, the inflation step could not be corrected in the time that was available for this project.

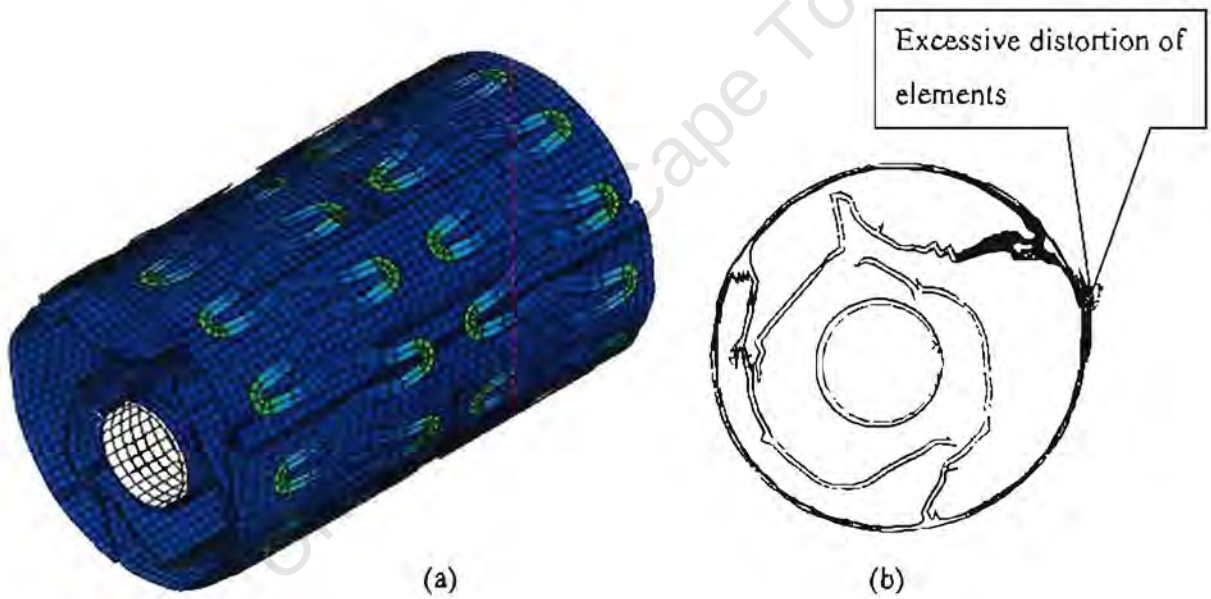

Figure 5.34 Balloon over-shoots stent's inner surfce (a) isometric view (b) side view

5.5 Offset Stent Assembly Simulation

Due to a shortage in time and computational power, the complete model, where the stent is crimped onto the balloon could not be simulated. It was then decided to use the less

computationally demanding complete model, which had the stent, which was modelled in its already crimped form. This was exactly the same model as the one used in Section 5.2, the only difference being the length of the parts. The stent now had the full 8 rings and the balloon was lengthened so that a fair amount stuck out the sides underneath the stent. It is believed that a slightly offset stent could be the reason for the stent to shoot off the delivery balloon during deployment. For this exact reason it was decided to assemble the stent and balloon in such a way that the stent was offset on the balloon and to run the simulation in an attempt to get the stent to shoot off axially. The offset stent position is clearly illustrated in Figure 5.33.

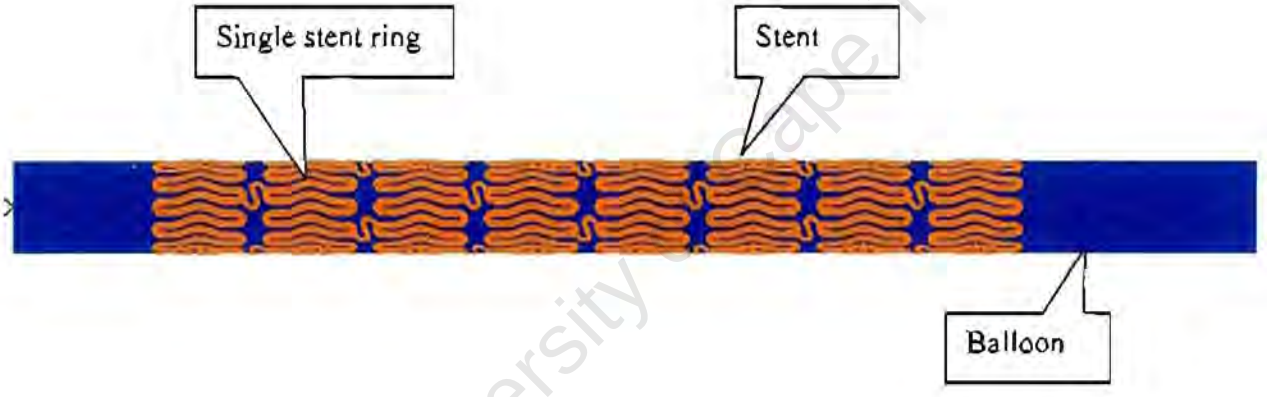

Figure 5.33 Side view of the assembly showing the offset stent

A uniform inflation pressure of 8 bar was applied to the inner surface of the balloon with a smooth step function. With steady increase in pressure the balloon started to flare at its ends, were it was not held down by the stent. Figure 5.34 illustrates the balloon and stent assembly before inflation and from Figure 5.35 it can clearly be seen that the end of the balloon start to flair from the inflation pressure.

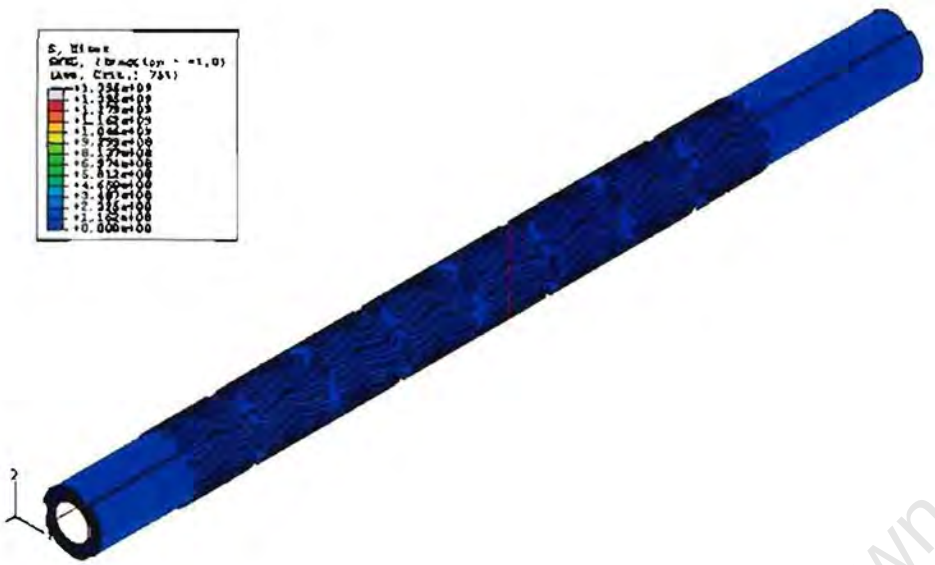

Figure 5.34 Assembly before inflation of the balloon

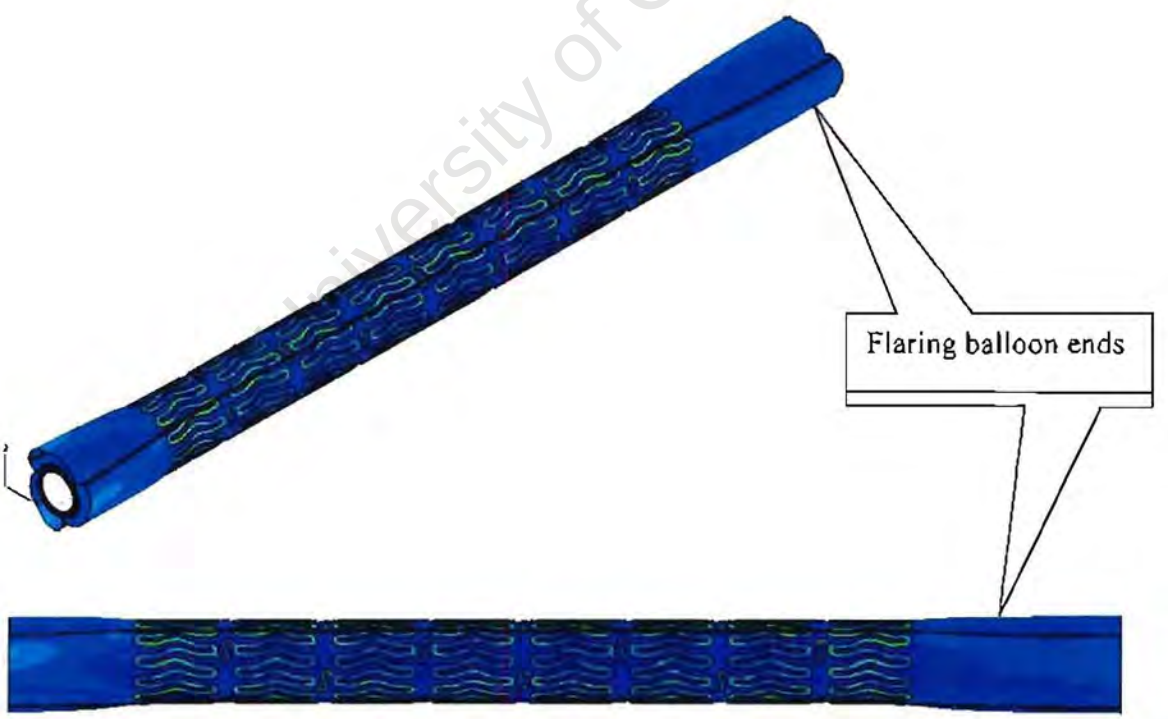

Figure 5.35 Isometric and side view of at start of inflation

As the pressure kept on increasing the flaring of the balloon ends could be seen even more clearly (Figure 5.36). This flaring also caused the ends of the stent to start to flair as the balloon unfolded further and the stent's resistive forces could no longer hold down the inflating balloon. Migliavacca *et al.* (2002) and Tan *et al.* (2000) also noted this so called *Dogboning* effect, where there is stronger expansion of the stent and balloon at its distal ends than in the central region.

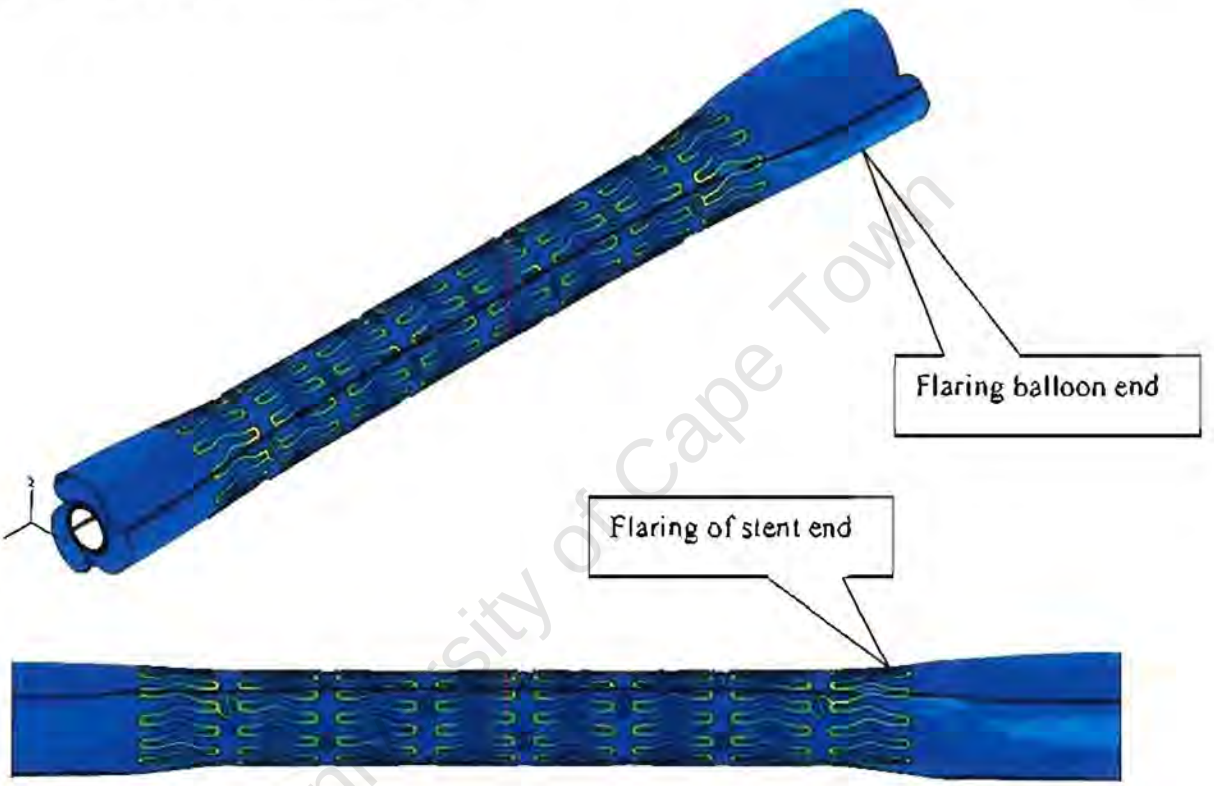

Figure 5.36 Isometric and side view illustrating the progress of the balloon inflation

It was believed that this *Dogboning* of flaring of the balloon ends could be one of the main reasons for the dislodging of the stent. However, as the pressure increased and the balloon inflated further the forces were transmitted towards the centre of the balloon and the force distributed throughout the whole model. The balloon was modelled so that it had fairly large bits sticking out underneath the ends of the stent. This meant that the flaring of the balloon happened at both ends. For this exact reason the stent could not be pushed off the balloon. Although one end flared a bit more than the other, the smaller

flaring was still enough to prevent the stent to shoot off axially. The *dogboning* could still be the reason for the off shooting stent, due to the fact that the bits of balloon sticking out underneath the stent are considerably smaller in reality. This would mean that the stent could be able to almost hold down the one side of the balloon completely and prevent it from flaring. If the other end then still flares, this could cause the stent to be shot of axially. The flaring of the stent ends could also potentially injure the vessel it would be deployed in, as this cause the hairpin bends of the stent to stand up and stick out radially. Again this stresses the importance of the correct polishing of the stent edges, to ensure that injury to the artery is prevented. This phenomenon can clearly be seen in Figure 5.37.

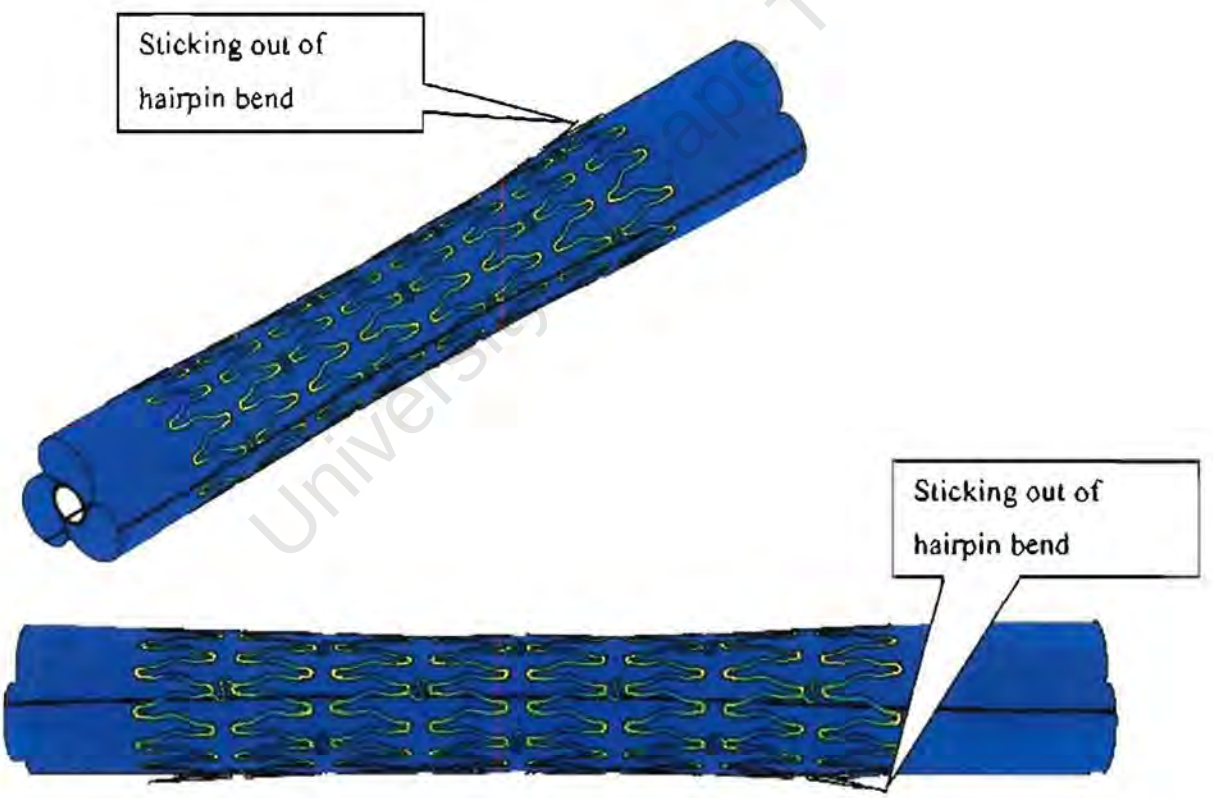

Figure 5.37 Isometric and side view halfway through the inflation process

The rest of the inflation of the balloon and subsequent deployment of the stent progressed in exactly the manner as the inflation for the simulation described in Section 5.2. The balloon expanded fully and deployed the stent to a diameter of more or less 10 mm (Figure 5.38). The attempt to shoot the stent off axially was thus a failure, but important knowledge was gained about changes that could be made to the model for future attempts. Another fact that must be brought the mind is the fact that this was an ideal model, meaning that was are no flaws modelled in the system. The balloon fold was uniform and the stent's inner surface smooth throughout. The stent also made equal contact with the balloon's outer surface all along the length of the model. The ideal will then obviously be to run a simulation on the complete model were the stent is crimped onto the folded balloon. This could introduce uneven contact with the balloon surface, due to the facet forming on the stent's inner surface as explained in Section 5.4.1. The fact that the stent will be crimped tightly onto the balloon means that the balloon would get squashed somewhat, which would in return cause an uneven balloon fold throughout its length. The introduction of some of these factors to the system could mean a dislodging of the stent during the deployment process.

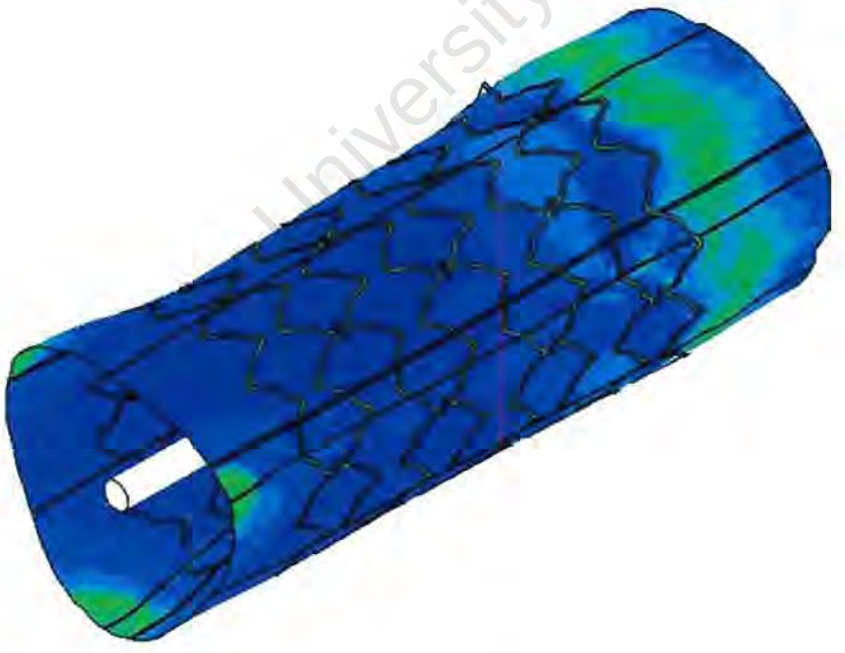

Figure 5.38 Fully deployed stent (scaled)

5.6 Limitations

As already mentioned this simulation was computationally extremely expensive. The first small assembly simulation was done on a 1 GHz Intel Pentium III processor with 512 MB of RAM. The time taken to complete this simulation was more or less 9 hours. Due to the fact that this was novel work and that very little prior knowledge was available to help with the simulation of this problem, this was an iterative process. Meaning that small steps had to be taken at a time to get to the final assembly of the system and subsequent simulation. Small bits were added to the model each time, to try and understand the system and to model it as correctly as possible. This meant that it took at least 9 hours to see the effect of a change or correction to the model. Numerous runs had to be done to insure that the small model assembly simulation worked and that the inflation of the balloon deployed the stent.

The next step was to run the simulation of one quarter of the complete assembly of the system, with the crimping tool. At first a fine mesh was chosen for the model. Due to the large amounts of contact in the model and the small critical time step the simulation was computationally very expensive. A 2.7 GHz ZEON processor with 4 GB of RAM was used to run this simulation. This computer is the property of Finite Element Analysis Services (Pty) Ltd, a company based in Mowbray, South Africa and is used to run all their simulations on. With this computer the run times for this simulation was in region of 6 days or 140 hours. The same iterative approach was taken with this simulation. As mentioned in Section 5.4.1 it took a lot of calculations and reruns to obtain the correct distance by which the stent had to be crimped in order to fit tightly on the balloon. The length duration of the simulations were extremely frustrating and time consuming. The length of these simulations meant that good progress was prevented. Finite Element Analysis Services also made use of this computer to run some of their complex jobs on, which meant that the simulation times were lengthened even more. With time to time the computer was scheduled for other jobs, which meant that this simulation could not be started. It was not feasible to start the simulation on the 1 GHz processor since that would have increased the run time by a large margin.

Accuracy was then forfeited to try and bring down the simulation time, and the mesh was coarsened considerably. This insured that the critical time step increased and that the simulation run time would come down. The simulation with the changed model was again run on the 2.7 GHz ZEON processor with 4 GB of RAM, and it was found that the run time was almost halved to about 3 ½ days or 80 hours. This allowed more regular checkups on changes made to the model and helped the progress of this study somewhat.

The complete model could however not be run on this computer due a fully booked schedule of jobs for Finite Element Analysis Services. The complete model is four times bigger than the smaller one and would thus take four times longer to run. This means that an estimated 2 weeks could be expected per simulation. There were also no other computers available with enough computing power to handle a job of this size. The minimum system requirements for the complete model would be a 2 GHz machine with at least 1.5 GB of RAM. This would still only be half the computing power of the ZEON, meaning that the run time for the simulation would be doubled to 4 weeks per run. For this reason the simulations were carried on the quarter model to ensure that all flaws are eliminated and that these changes could be implemented in the full-scale model. This meant that a simulation of the complete model could be run at a later stage with the right resources and computer power to allow quick and accurate simulations.

5.7 Computer Cluster

Another alternative option was investigated to try and reduce the simulation time.

The UCT-CERN Research Centre in the Physics Department at the University of Cape Town, South Africa, has a cluster of 20 computers that is used to run jobs in parallel. Becker *et al.* (2004) explain that these 20 nodes are stacked on a 5-level rack, capable of 6 boxes per level with 3 switches. Ethernet cables machined into the frame of the rack allow the nodes to connect to the server via a fast Ethernet switch, capable of handling a total of 26 connections. This number is made up of 24 10/100 MBs ports and 2-gigabit

ports to the backplane, which are unused. Typical disk Input/Output rates of Monte-Carlo simulations are about 100 MB/min, per event, which translates to a required bandwidth of 25 MB/s when all nodes are accessing NFS-mounted volumes. This bandwidth is easily saturated on a 10/100 MB/s subnet, and hence the requirement to write data to a local disk, instead of an NFS-mounted one.

From the ABAQUS documentation it can be established that the use of domain parallelization with general contact allows the contact computations to be split across domains so the parallel performance can be greatly improved. The model is split into a number of topological domains. These domains are referred to as parallel domains to distinguish them from other domains associated with the analysis. The domains are distributed evenly among the available processors or "nodes" as they are called. The analysis is then carried out independently in each domain. However, information must be passed between the domains in each time increment because the domains share common boundaries.

The domain-level method divides the model so that the resulting domains take approximately the same amount of computational expense. The load balance is defined as the ratio of the computational expense of the most expensive domain to that of the least expensive domain. Element and node sets are created for each domain and cannot be inspected during the simulation process. The analysis results are independent of the number of processors used for the analysis. However, the results do depend on the number of parallel domains used during the domain decomposition. The number of parallel domains can be set on the command line.

There are however a few limitations concerning the domain decomposition.

Certain features cannot be split across domains. The domain decomposition algorithm automatically takes this into account and forces these features to be contained entirely within one domain. Even if the algorithm succeeds in creating the requested number of domains, the load may be balanced unevenly. Contact pairs that use the penalty contact

algorithm require that the associated nodes be part of a single parallel domain, but these nodes may also be part of other parallel domains. Analyses in which a large percentage of nodes are involved in contact may not scale well when contact pairs are used.

The general contact algorithm has minimal effect on the domain decomposition in most cases. If a rigid body is part of the general contact domain, the entire rigid body is forced into a single parallel domain; however, all rigid bodies having general contact need not be assigned to the same domain. In most cases this restriction for rigid bodies does not cause a load imbalance, although a rigid body with a large number of nodes and faces or that spans a large region of the model, can degrade the load balance.

To run ABAQUS in parallel on a cluster of computers with a message-passing interface (MPI), it may be necessary to install middleware to facilitate inter-processor communication. This would assist in the even distribution of workload over all the nodes and ensure fast and effective simulations.

Permission to use the cluster was obtained from the UCT-CERN Research Centre and ABAQUS was installed on the host computer. Certain alterations had to be made to the ABAQUS environment file to allow it to use the correct version of MPI and Linux (RedHat 9). The first small assembly was used to run a simulation on the cluster. The simulation was first run on a single processor, so that a comparison could be made between the run times of a simulation performed on one processor versus the ones done on a number of nodes. Two simulations were run on the computer cluster, one with 4 nodes and one with 6 nodes. The idea was first to see how the simulation scaled as the number of processors was increased. All hope of using the computer cluster soon vanished due to a memory shortage of the host machine. The host machine had to split the model up into certain domains and then allocate them to different machines. This was done without any difficulty and the simulation started running on all specified nodes. However, the host machine was also used as a domain in order for ABAQUS to recognise its licence throughout the simulation. Output data were also written to a file on the host machine throughout the simulation, meaning that the information froma ll the domains

bottlenecked at the main node. All of this caused memory of the host machine to be used up and the system crashed time after time. The simulation did however manage to get through 4 of the 200 steps and a comparison could be made with the run done on a single processor. Table 5.1 provides a comparison of the three simulations.

Table 5.1 Comparison between cluster and single processor

Number of processors	1	4	6
Weight per domain	100%	± 25%	± 16.5%
Time taken per step	2 min	15 sec.	30 sec.
Estimated completion time	9h 20min	1h 10min	2h 20min

The simulations times come down considerably with the use of the cluster, and parallel processing could definitely be used to run a simulation that is computationally as expensive as this one. What is interesting to note from these comparisons in Table 5.1 is the fact that the simulation was faster with four processors than with six processors. This could be ascribed to the fact that the model consists of so many nodes and elements with a lot of contact between them. These domains have to communicate constantly with each other to check the contact between the elements of the different parts within the model. The use of rigid body parts and the penalty contact algorithm also contributes to the scaling of the simulation. As the number of processors increases, the model is split into more domains, which means that the network traffic increases, as more and more inter-domain communication has to take place. The scaling is thus governed by the speed of the network connecting all the domains. Unfortunately the network speeds of this specific cluster are not very high and the system is quickly saturated. This is why simulations are faster on four nodes than on six. The difficulty is thus to find the optimal number of processors that should be used for a simulation run in parallel. There was no way that this problem could be fixed; neither the memory of the host computer nor the network speed

could be increased and therefore the use of the cluster for this simulation was not feasible.

However, it is still believed that a computer cluster could be used to improve the run times of a job like this. Each node of the cluster would have to be very powerful computationally, especially the host node. It is also crucial that a fast network connection is made between each of the domains, since slow inter-node communication was what reduced the effectiveness of the UCT cluster. Big computer clusters with extremely effective communication between each processor and a high computing power definitely exist and the possibility of using a similar system should definitely be pursued.

CHAPTER SIX

CONCLUSIONS

The use of finite element modelling has been shown to have many advantages with regards to the modelling of complex systems such as the stent delivery mechanism. It has also been shown that this kind of model is computationally extremely expensive and that certain compromises or assumptions have to be made to ensure reasonable run times.

A tri-folded balloon geometry was successfully modelled within ABAQUS/CAE and the 3-D model created with membrane elements. A mapping algorithm was used to map the 2-D coordinates of a flat stent drawing into a 3-D cylindrical coordinate system in order to obtain a round and closed stent. The stent was modelled with shell elements and it was shown that the size of the stent could be changed without any difficulty. Two stents were modelled. The first was in the form of an already crimped stent, meaning that it had the dimensions of a typical stent after crimping. The other was an uncrimped stent model that had the dimensions of a stent in its uncrimped form. The inner lumen was also successfully modelled with shell elements. The guide wire that fits inside the inner lumen was modelled as a discrete rigid body. The crimping machine used to crimp the stents onto the balloons was then successfully modelled as 12 discrete rigid body plates, which were arranged in circumferential fashion. They could be displaced radially to crimp the stent.

Simulations of the balloon inflation were performed and by applying the pressure uniformly on the inner surface of the balloon the stent was successfully deployed. It was shown that the stent first went through an elastic stage and was then past its yield strength to plastically deform into its new shape and diameter. It was also found that the inflating balloon and stent took on a triangular shape during deployment and that out-of-plane bending was experienced at the hairpin bends connecting the stent struts. The uncrimped stent was then successfully crimped onto the folded balloon with the crimping tool. Only one quarter of the complete model was used because of computational limitations due to

shortage of time and processing power. The stent's inner surface created square facets during the crimp, which made it extremely difficult to obtain the correct crimping distance, in order to prevent over-closure of the balloon surfaces. The final shape of the crimped stent correlated well with the predicted form as calculated by DISA Vascular. The velocities of the stent and balloon, generated by the inertial effects due to mass scaling, were successfully equalled to zero after the crimp step. It was found that when the crimping tool plates were removed the stent followed for a short distance. This implied that the stent had stored energy and, with the release of the crimping tool, it sprung back. After this step, the stent started to experience small oscillating movements. The balloon was again successfully inflated and the stent deployed as required.

Although the project was unable to obtain the reasons for the stent shooting off the balloon, it demonstrated that this analysis could be used for stent design and to explore the reasons for the dislodging stent. It has been shown that finite element modelling can be used to understand possible failures in the stent deployment system. The simulation of this system also gave very good insights into possible reasons for the failure of the stent, in that it was shown where the highest stress localisations occur. The shape of the deploying stent and balloon, as well as the out-of-plane deformation of the stent during expansion, were shown to have potentially dangerous implications for a patient receiving a stent to restore blood flow in a blocked vessel. Good insight was also gained about possible reasons for the stent shooting off the balloon although it was found that there could be a number of factors contributing to this phenomenon.

The finite element model can also be used to investigate the effects of certain alterations in the stent design, for instance, changes in stent strut dimensions and material properties, and this could be useful to achieve the optimal stent design.

CHAPTER SEVEN

RECOMMENDATIONS

As mentioned in Section 5.5, the simulation process was computationally very expensive and due to a shortage in computing power and time, the full analysis could not be completed. However, from what was learned by modelling and simulation, a few important recommendations can be made to assist with future work in this field:

- It is very important to have a good understanding of the finite element method and the ABAQUS software package. A combination of these two would ensure that the problem is simulated as realistically as possible.

- Obtain a computer that is computationally powerful enough to handle a job of this size and which could run the job in a more reasonable time. A computer dedicated to this simulation would be ideal.

- Further investigate the possibility of using a parallel computer cluster, which has more memory, and faster network connections between the individual nodes.

- Model a blocked artery around the stent/balloon assembly to simulate the response of the artery to the deploying stent.

- It is believed that by re-crimping the stent another two times, it may be possible minimize or even eliminate the spring back and resultant oscillation of the stent when the crimping tool is removed.

- Model the uneven pressure distribution on the inner-surface of the balloon during its inflation. This could be one of the main reasons for the stent shooting off the balloon during deployment.

- Perform an in-depth investigation of the frictional interaction between the stent and balloon during crimping and deployment.

- Model an air gap between the folded balloon surfaces.

Although the exact reason for the stent shooting off the balloon could not be obtained from this study, valuable insight was gained about possible reasons for this phenomenon. These factors could be incorporated into the stent model to try and induce the dislodging of the stent. The following factors could contribute to a stent shooting off:

- Stent is crimped non-centrally onto the folded balloon

- Internal pressure is not uniform

- Balloon folding is not uniform

- Contact between the stent and the balloon is uneven

- Balloon folds are asymmetrical due to the compressive force exerted by the crimped stent

- Imperfections in the balloon material

- Folding imperfections at the ends where the balloon tapers and is fixed onto the inner lumen

APPENDICES

APPENDIX A: TECHNICAL DRAWINGS

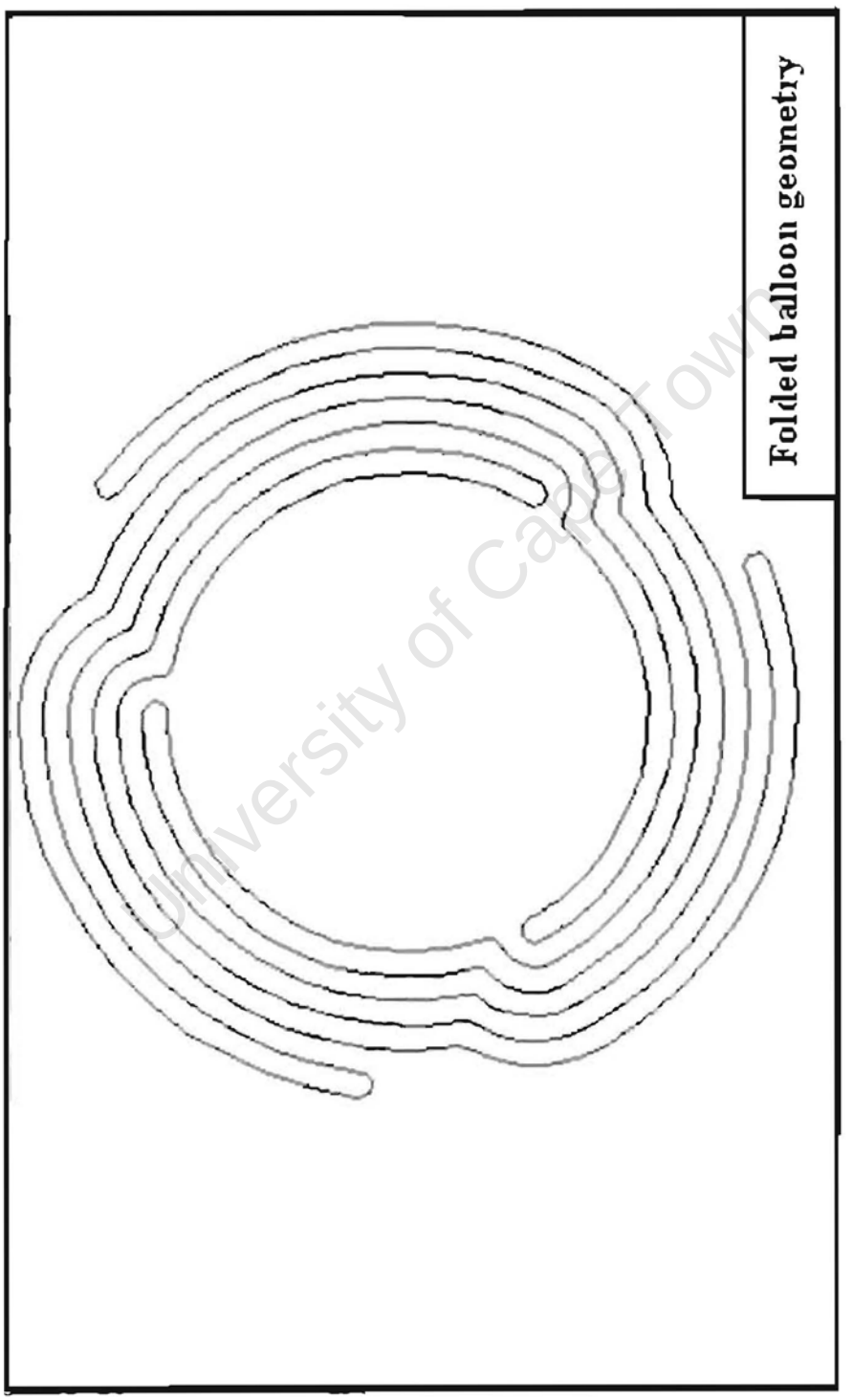

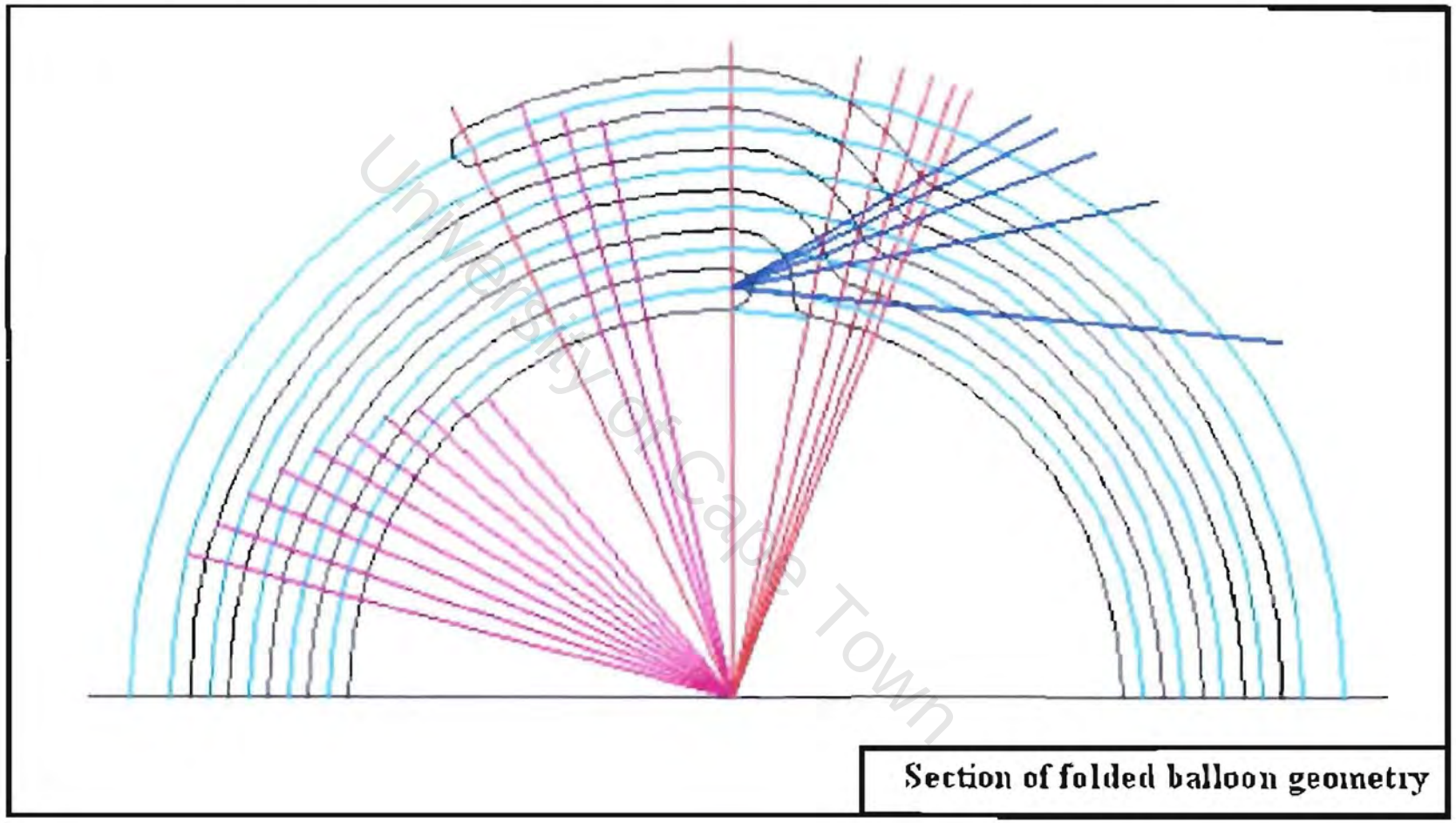

Section of folded balloon geometry

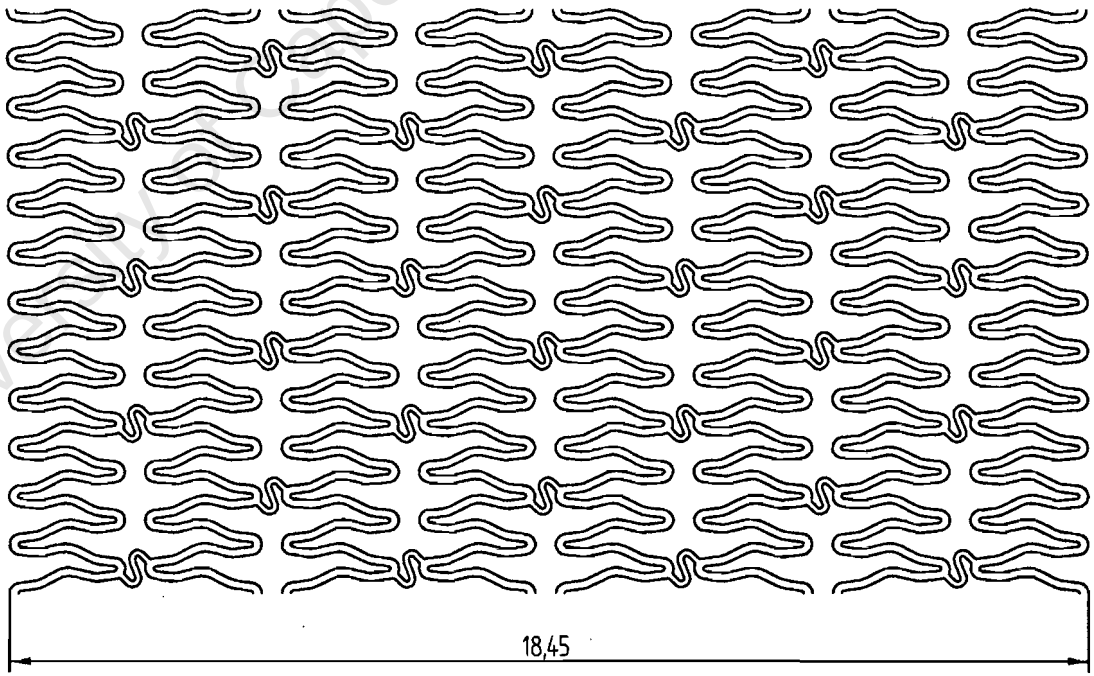

implementation					tolerances		surface	scale 10:1	weight
Peripheral stent/ stent 18mm					+0.02			material SS316L tube, 3.2mm O.D. x 0.16mm	
						date	name	name	
					draft	16.10.02	M. Lehmann	stent 12 cell, 2.0mm rings	
					appr.				
					stand.				
18	b	12 cell	16.10.02	ML	DISA VASCULAR			drawing number D07-01-01stent	sheet of
18	a	corr ring width 2mm	16.10.02	ML					
rev	ind	change	date	name	origin			substitute for	substituted by

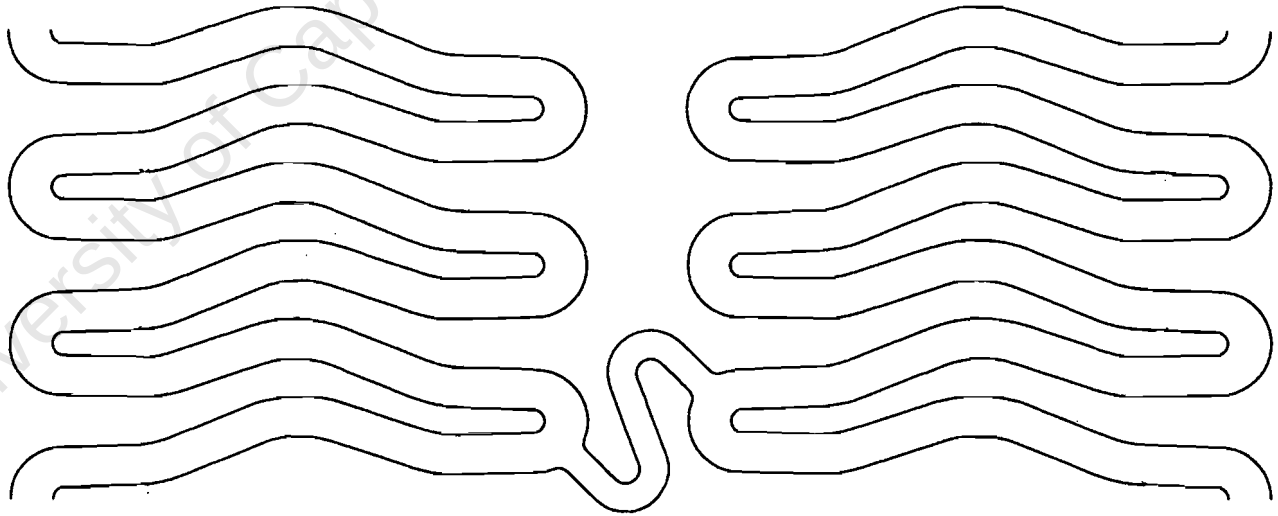

@2.08mm

implementation: Peripheral stent/ stent 18mm					tolerances: +0.02		surface	scale: 50:1	weight
								material: SS316L tube, 3.2mm O.D. x 0.16mm
						date	name	name: stent 12 cell, 2.0mm rings
					draft	16.10.02	M. Lehmann	
					appr.			
					stand.			
18								drawing number: D07-01-01crimp; sheet; of
18	b							
18	a			ML				
rev	ind	change	date	name	origin			substitute for; substituted by

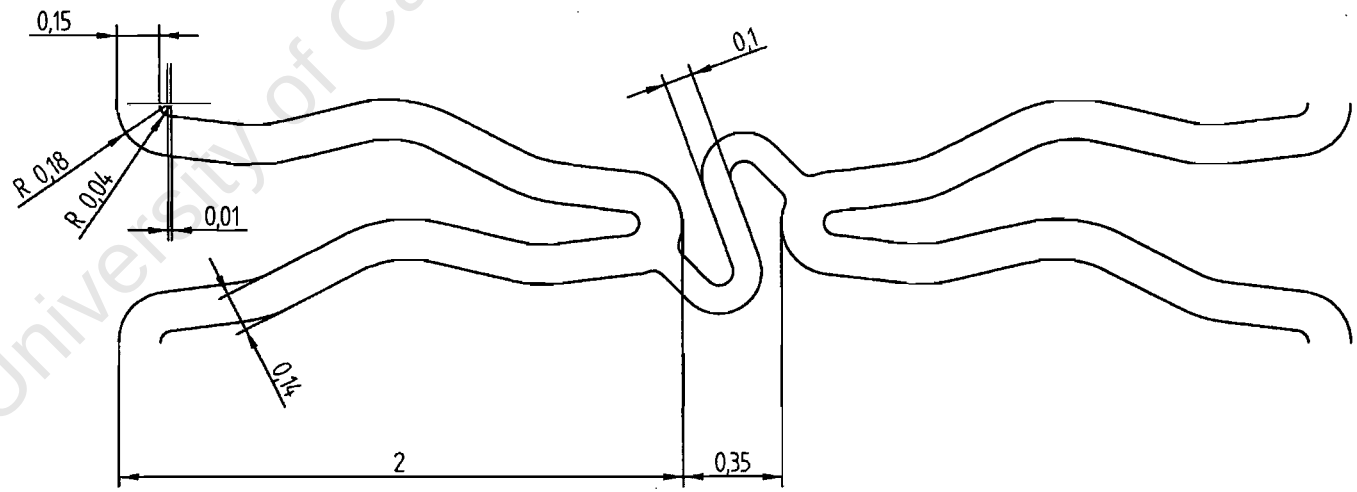

implementation: Peripheral stent/ stent 18mm					tolerances: +0.02		surface	scale 20:1 / weight
					material: SS316L tube, 3.2mm O.D. x 0.16mm			
						date	name	name: stent 12 cell, 2.0mm rings
					draft	16.10.02	M. Lehmann	
					appr.			
					stand.			
18	b	12 cell	16.10.02	ML	DISA VASCULAR			drawing number: D07-01-01dim / sheet
18	a	corr ring width 2mm	16.10.02	ML				of
rev	ind	change	date	name	origin			substitute for / substituted by

APPENDIX B: MATERIAL PROPERTIES

PA11 - Polyamide (Nylon) 11

LEGEND
A = amorphous - Cr = crystalline - C = clear - E = excellent - G = good - P = poor - O = opaque - T = translucent- R = Rockwell - S = Shore

STRUCTURE: Cr

SPECIFIC DENSITY: 1.04

WATER ABSORBTION RATE (%): 0.4

ELONGATION (%): 300

TENSILE STRENGTH (psi): 8000

COMPRESSION STRENGTH (psi): 7900

FLEXURAL STRENGTH (psi): 6000

FLEXURAL MODULUS (psi): 145000

IMPACT (IZOD ft. lbs/in): 1.8

HARDNESS: R108

FABRICATION
- BONDING: G
- ULTRASONIC WELDING: P
- MACHINING: P

DEFLECTION TEMPERATURE (deg. F)
- @ 66 psi: 266
- @ 264 psi: 302

UTILZATION TEMPERATURE (deg. F)
- min: -94
- max: 176

MELTING POINT (deg. F): 365

COEFFICIENT OF EXPANSION: 0.000072

ARC RESISTANCE: 120

DIELECTRIC STRENGTH (kV/mm): 17

TRANSPARENCY: O

UV RESISTANCE: G

Peripheral Angioplasty

Balloon

ClearPAC™ Family of Peripheral Catheters

ClearPAC™ & ClearPAC Bantam™

- Semi-compliant balloon, trifold with memory
- Co-axial shaft for high pushability

ClearPAC™

ClearPAC Bantam™

ClearPAC™

For use with 0.035 guidewires
Shaft Lengths of 150cm, 75cm & 135cm
4F Sheath Compatability for smaller diameters
Tip Lead-in 4F

ClearPAC Bantam™

For use with 0.018 guidewires
Shaft Lengths of 75cm & 135cm
4F Sheath Compatability for smaller diameters
Tip Lead-in 4F

Product Specification

ClearPAC™

Balloon Compliance	
Catheter Length	
Nominal pressure	
Burst pressure	
Average burst pressure	
Monitor Bands	
Guide wire	
Tip Lesion Profile	
Sheath Compatibility	

ClearPAC Bantam™

Balloon compliance	
Catheter length	
Nominal pressure	
Burst pressure	
Average burst pressure	
Monitor bands	
Guidewire	
Tip lesion profile	
Sheath	

clearStream

Technologies Ltd

Mayne Upper, Enniscorthy, Co. Wexford, Ireland.
Tel: +353 (0)54 37100 Fax: +353 (0)54 37200 E: info@clearstream.ie W: www.clearstream.ie

minitubes ☎ [illegible] 📠 [illegible]

03/01 / 145

COPIE CONFORME
NON GEREE

CERTIFICAT D'ANALYSE / CERTIFICAT DE CONFORMITE
CERTIFICATE OF ANALYSIS / CERTIFICATE OF CONFORMITY

ACHETEUR PURCHASER		**N° O. E.** CONFIRMATION'S ORDER N°	13301
N° COMMANDE PURCH. ORDER N°		**SPECIFICATION** PRODUCT STANDARD	FRD018
MATIERE COMMANDEE ORDERED MATERIAL GRADE	Stainless steel tubing according to ASTM F138 (2000) and ISO 5832.1 (1997)		
MATIERE AFFECTEE DELIVERED MATERIAL GRADE	Stainless steel tubing according to ASTM F138 (2000) and ISO 5832.1 (1997)		
DESIGNATION REFERENCE	Ø 3.20 X ± 0.013 X 0.16 -0/+0.01		
QUANTITE COMMANDEE ORDERED QUANTITY	100 mètres	**N° BORDEREAU** NOTE N°	4675 / 4676

LONGUEUR LENGHT	**POIDS** WEIGHT	**NBR PIECES** NBR PARTS	**N° LOT** à rappeler en cas de réclamation / BATCH N° to be mentioned in case of claim	**N° DEROGATION** DISPENSATION N°
51 M 50 M	0.634 Kg 0.642 Kg		[illegible] [illegible]	

ANALYSE DE LA COULEE (%) HEAT ANALYSIS — ☐ N°Matière première / N° Raw material: 3317 — ☒ Produit fini / Finished product

C	Si	P	S	Mn	Ni	Cr	Ti	Mo
0.017	0.41	0.020	< 0.005	1.78	14.52	17.28		2.80
Fe	**Co**	**Cu**	**Mg**	**Al**	**Zn**	**N²**	**H**	**O**
BAL		0.15				0.074		
Sn	**Ca**	**B**	**Ta**	**W**	**Pb**	**Zr**	**Nb**	**As**

CARACTERISTIQUES PHYSIQUES SUR PRODUIT FINI
FINISHED PRODUCT PHYSICAL CHARACTERISTICS
(Lo = 150 mm / Le = 50 mm)

Rm (MPA)	Fm (N)	Rp 0.2 % (MPA)	Fp 0.2 % (N)	A %	Dureté Hardness (HV)	Indice de grain Grain size
888.50	1416.97	730.31	1164.64	7.03 %	320 HV0.3	8

AUTRES TESTS OTHER TESTS

Inclusion's rate in conformity
Intergranular corrosion test in conformity
Free ferrite observation in conformity

Nous certifions que, sauf exceptions ou dérogations [illegible], la fourniture [illegible] a été fabriquée conformément [illegible] spécifications techniques de la commande du client et que, toutes opérations de contrôle et essais effectués, elle répond SOUS TOUS LES ASPECTS aux spécifications particulières [illegible], aux plans ainsi qu'aux normes et règlements en vigueur s'y rapportant.
We certify that, unless exceptions or waivers indicated above, the supplied product has been manufactured in conformity with the technical specifications of the customer's order and that, all inspection and trial operations being made, it corresponds FROM ALL POINTS OF VIEW to the indicated particular specifications, to the drawings and also to the corresponding standards and regulations into effect.

SERVICE QUALITE QUALITY DEPARTMENT	**VISA** :	**DATE**

Document [illegible]

[illegible]

Arkema Pebax® MX 1205 SN 01 Polyether Block Amide (PEBA) (Dry)

Subcategory: Elastomer, TPE; Polyether Block Amide (PEBA); Polymer; Thermoplastic
Close Analogs:
Arkema, formed in 2004, was formerly Atofina Chemicals and before that Elf Atochem.
Key Words: Thermoplastic Elastomer, TPE
Material Notes:
POLYETHER BLOCK AMIDE (PEBA) hardness 40 shore D Non plasticized flexible Polyamide Outstanding mechanical properties at low temperature (-40°C) Applications: molded parts for sport goods (softness, nice touch feeling...) Industrial (damping properties, overmolding, resiliency...)
ISO data provided by the manufacturer, Arkema.

Physical Properties	Metric	English	Comments
Density	1.01 g/cc	0.0365 lb/in³	
Water Absorption	1.5 %	1.5 %	
Moisture Absorption at Equilibrium	0.4 %	0.4 %	Humidity Absorption
Melt Flow	14 g/10 min	14 g/10 min	235°C/1 kg load
Mechanical Properties			
Hardness, Shore D	40	40	
Tensile Strength, Yield	6.9 MPa	1000 psi	at 50% Strain; 50 mm/min
Tensile Modulus	0.065 GPa	9.43 ksi	1 mm/min
Electrical Properties			
Electrical Resistivity	1.57e+013 ohm-cm	1.57e+013 ohm-cm	
Surface Resistance	6.98e+012 ohm	6.98e+012 ohm	
Dielectric Strength	43 kV/mm	1090 kV/in	
Dissipation Factor	0.00059	0.00059	1 MHz

Dissipation Factor, Low Frequency	0.00085	0.00085	100 Hz
Comparative Tracking Index	600 V	600 V	
Thermal Properties			
Melting Point	147 °C	297 °F	10°C/min
Flammability, UL94	HB	HB	1.6 mm
Optical Properties			
Transmission, Visible	80 %	80 %	Mfr. reports 'Transparent' but doesn't quantify.

APPENDIX C: INPUT DECKS FOR ABAQUS

The nodes and elements are not displayed in these input decks, but are included in the complete input deck files written to CD.

C1 Test model

```
Heading
 Job name: Test model Model name: Model-1
Preprint, echo=NO, model=NO, history=NO, contact=NO

 ----------------------------------------------------------------

 PARTS

Part, name=balloon
End Part
Part, name=stent
End Part

 ----------------------------------------------------------------

 MATERIALS

Material, name=Rubber
Density
 990.,
Elastic
 1e+10, 0.3
Material, name=Steel
Density
 7850.,
Elastic
 1.69e+11, 0.3
Plastic
 3e+08,  0.
 4.8e+08, 0.3

 ----------------------------------------------------------------

 INTERACTION PROPERTIES

Surface Interaction, name=Balloon-contact
```

```
Friction
 0.,
Surface Behavior, pressure-overclosure=HARD
Surface Interaction, name=Balloon-shell
Surface Behavior, pressure-overclosure=HARD

  ------------------------------------------------------------

  BOUNDARY CONDITIONS

  Name: x-symmetry Type: Symmetry/Antisymmetry/Encastre
Boundary
x-symm, XSYMM
  Name: y-fix Type: Displacement/Rotation
Boundary
y-symm, 2, 2

  ------------------------------------------------------------

  INTERACTIONS

  Interaction: Balloon-balloon
Contact, op=NEW
Contact Inclusions, ALL ELEMENT BASED
Contact property assignment
, , Balloon-contact

  ------------------------------------------------------------

  STEP: Contact

Step, name=Contact
Balloon surface on shell
Dynamic, Explicit
 , 0.2
Bulk Viscosity
 0.06, 1.2
Mass Scaling: Semi-Automatic
          Whole Model
Fixed Mass Scaling, factor=1000.

  ------------------------------------------------------------

  LOADS

  Name: Pressure   Type: Pressure
```

```
Dsload, amplitude=Amp-1
balloon-inner, P, 2.045e+06

  ------------------------------------------------------------

  OUTPUT REQUESTS

Restart, write, number interval=1, time marks=NO

  FIELD OUTPUT: F-Output-1

Output, field, variable=PRESELECT

  HISTORY OUTPUT: H-Output-1

Output, history, variable=PRESELECT
End Step
```

C2 First small assembly

```
Heading
  Job name: First small assembly Model name: model-1
Preprint, echo=NO, model=NO, history=NO, contact=NO

  ------------------------------------------------------------

  PARTS

Part, name=Circular-stent-correct
End Part
Part, name=balloon
End Part
Part, name=lumen_1
End Part

  ------------------------------------------------------------

  MATERIALS

Material, name=Nylon
Density
 1040.,
Elastic
 4.65e+08, 0.4
Material, name="Stainless Steel"
```

```
Density
 7850.,
Elastic
 1.93e+11, 0.3
Plastic
 3.3e+08,   0.
 6.7e+08, 0.48

  ----------------------------------------------------------------

  INTERACTION PROPERTIES

Surface Interaction, name=Contact
Friction
 0.1,
Surface Behavior, pressure-overclosure=HARD

  ----------------------------------------------------------------

  BOUNDARY CONDITIONS

  Name: fix lumen Type: Symmetry/Antisymmetry/Encastre
Boundary
"lumen rp", ENCASTRE
  Name: fixed Type: Displacement/Rotation
Boundary
 Edges-1, 3, 3
  Name: fixed 2 Type: Displacement/Rotation
Boundary
 edges-2, 3, 3

  ----------------------------------------------------------------

  INTERACTIONS

  Interaction: Balloon-balloon
Contact, op=NEW
Contact Inclusions, ALL ELEMENT BASED
Contact property assignment
, , Contact
  ----------------------------------------------------------------

  STEP: Blow up balloon

Step, name="Blow up balloon"
Blow up baloon
```

```
Dynamic, Explicit
 , 0.032
Bulk Viscosity
 0.06, 1.2
Mass Scaling: Semi-Automatic
          Whole Model
Fixed Mass Scaling, factor=100000.

  ----------------------------------------------------------------

  LOADS

Name: Load-1   Type: Pressure
Dsload, amplitude=Amp-1
Balloon-inner, P, 910600.

  ----------------------------------------------------------------

  OUTPUT REQUESTS

Restart, write, number interval=1, time marks=NO

  FIELD OUTPUT: F-Output-1

Output, field, variable=PRESELECT, number intervals=200

  HISTORY OUTPUT: H-Output-1

Output, history, variable=PRESELECT
End Step
```

C3 Full Assembly

```
Heading
  Job name: full assembly Model name: full assembly
Preprint, echo=NO, model=NO, history=NO, contact=NO

  ----------------------------------------------------------------

  PARTS

Part, name=balloon
End Part
Part, name=corr-course-stent
End Part
```

```
Part, name=crimping-tool-1
End Part
Part, name=crimping-tool-10
End Part
Part, name=crimping-tool-11
End Part
Part, name=crimping-tool-12
End Part
Part, name=crimping-tool-2
End Part
Part, name=crimping-tool-3
End Part
Part, name=crimping-tool-4
End Part
Part, name=crimping-tool-5
End Part
Part, name=crimping-tool-6
End Part
Part, name=crimping-tool-7
End Part
Part, name=crimping-tool-8
End Part
Part, name=crimping-tool-9
End Part
Part, name="guide wire"
End Part
Part, name=lumen
End Part

  ----------

 MATERIALS

Material, name=PEBAX
Density
 1010.,
Elastic
 3.38e+08, 0.35
Material, name=rubber
Density
 990.,
Elastic
 1e+10, 0.3
Material, name="stainless steel"
Density
 7850.,
```

```
Elastic
 1.69e+11, 0.3
Plastic
 3.3e+08,  0.
 6.7e+08, 0.48

 ---------------------------------------------------------------

 INTERACTION PROPERTIES

Surface Interaction, name=contact
Friction
 0.1,
Surface Behavior, pressure-overclosure=HARD

 ---------------------------------------------------------------

 BOUNDARY CONDITIONS

Name: lumen_edge Type: Displacement/Rotation
Boundary
lumen_edge, 3, 3
Name: wire-edge fix-2 Type: Symmetry/Antisymmetry/Encastre
Boundary
guide-wire-refpnt, ENCASTRE

 ---------------------------------------------------------------

 INTERACTIONS

Interaction: contact
Contact, op=NEW
Contact Inclusions, ALL ELEMENT BASED
Contact property assignment
 ,  , contact
Surface property assignment, property=THICKNESS
stent-inner , ORIGINAL , 1.
stent-outer , ORIGINAL , 1.
balloon-outer , ORIGINAL , 1.
balloon-inner , ORIGINAL , 1.

 ---------------------------------------------------------------

 STEP: pressure

Step, name=pressure
```

Dynamic, Explicit
, 0.005
Bulk Viscosity
0.06, 1.2
Mass Scaling: Semi-Automatic
Whole Model
Fixed Mass Scaling, factor=100.

BOUNDARY CONDITIONS

Name: disp-1 Type: Displacement/Rotation
Boundary, amplitude=Amp-1
crimpingtool_refpt-1, 1, 1, -0.00065
crimpingtool_refpt-1, 2, 2
crimpingtool_refpt-1, 3, 3
crimpingtool_refpt-1, 4, 4
crimpingtool_refpt-1, 5, 5
crimpingtool_refpt-1, 6, 6
Name: disp-10 Type: Displacement/Rotation
Boundary, amplitude=Amp-1
crimpingtool_refpt-10, 1, 1, -0.00065
crimpingtool_refpt-10, 2, 2
crimpingtool_refpt-10, 3, 3
crimpingtool_refpt-10, 4, 4
crimpingtool_refpt-10, 5, 5
crimpingtool_refpt-10, 6, 6
Name: disp-11 Type: Displacement/Rotation
Boundary, amplitude=Amp-1
crimpingtool_refpt-11, 1, 1, -0.00065
crimpingtool_refpt-11, 2, 2
crimpingtool_refpt-11, 3, 3
crimpingtool_refpt-11, 4, 4
crimpingtool_refpt-11, 5, 5
crimpingtool_refpt-11, 6, 6
Name: disp-12 Type: Displacement/Rotation
Boundary, amplitude=Amp-1
crimpingtool_refpt-12, 1, 1, -0.00065
crimpingtool_refpt-12, 2, 2
crimpingtool_refpt-12, 3, 3
crimpingtool_refpt-12, 4, 4
crimpingtool_refpt-12, 5, 5
crimpingtool_refpt-12, 6, 6
Name: disp-2 Type: Displacement/Rotation
Boundary, amplitude=Amp-1
crimpingtool_refpt-2, 1, 1, -0.00065

```
crimpingtool_refpt-2, 2, 2
crimpingtool_refpt-2, 3, 3
crimpingtool_refpt-2, 4, 4
crimpingtool_refpt-2, 5, 5
crimpingtool_refpt-2, 6, 6
 Name: disp-3 Type: Displacement/Rotation
Boundary, amplitude=Amp-1
crimpingtool_refpt-3, 1, 1, -0.00065
crimpingtool_refpt-3, 2, 2
crimpingtool_refpt-3, 3, 3
crimpingtool_refpt-3, 4, 4
crimpingtool_refpt-3, 5, 5
crimpingtool_refpt-3, 6, 6
 Name: disp-4 Type: Displacement/Rotation
Boundary, amplitude=Amp-1
crimpingtool_refpt-4, 1, 1, -0.00065
crimpingtool_refpt-4, 2, 2
crimpingtool_refpt-4, 3, 3
crimpingtool_refpt-4, 4, 4
crimpingtool_refpt-4, 5, 5
crimpingtool_refpt-4, 6, 6
 Name: disp-5 Type: Displacement/Rotation
Boundary, amplitude=Amp-1
crimpingtool_refpt-5, 1, 1, -0.00065
crimpingtool_refpt-5, 2, 2
crimpingtool_refpt-5, 3, 3
crimpingtool_refpt-5, 4, 4
crimpingtool_refpt-5, 5, 5
crimpingtool_refpt-5, 6, 6
 Name: disp-6 Type: Displacement/Rotation
Boundary, amplitude=Amp-1
crimpingtool_refpt-6, 1, 1, -0.00065
crimpingtool_refpt-6, 2, 2
crimpingtool_refpt-6, 3, 3
crimpingtool_refpt-6, 4, 4
crimpingtool_refpt-6, 5, 5
crimpingtool_refpt-6, 6, 6
 Name: disp-7 Type: Displacement/Rotation
Boundary, amplitude=Amp-1
crimpingtool_refpt-7, 1, 1, -0.00065
crimpingtool_refpt-7, 2, 2
crimpingtool_refpt-7, 3, 3
crimpingtool_refpt-7, 4, 4
crimpingtool_refpt-7, 5, 5
crimpingtool_refpt-7, 6, 6
 Name: disp-8 Type: Displacement/Rotation
```

```
Boundary, amplitude=Amp-1
crimpingtool_refpt-8, 1, 1, -0.00065
crimpingtool_refpt-8, 2, 2
crimpingtool_refpt-8, 3, 3
crimpingtool_refpt-8, 4, 4
crimpingtool_refpt-8, 5, 5
crimpingtool_refpt-8, 6, 6
  Name: disp-9 Type: Displacement/Rotation
Boundary, amplitude=Amp-1
crimpingtool_refpt-9, 1, 1, -0.00065
crimpingtool_refpt-9, 2, 2
crimpingtool_refpt-9, 3, 3
crimpingtool_refpt-9, 4, 4
crimpingtool_refpt-9, 5, 5
crimpingtool_refpt-9, 6, 6

  OUTPUT REQUESTS

Restart, write, number interval=1, time marks=NO

  FIELD OUTPUT: F-Output-1

Output, field, variable=PRESELECT

  HISTORY OUTPUT: H-Output-1

Output, history, variable=PRESELECT
End Step

  ----------------------------------------------------------------

  STEP: zero velocity

Step, name="zero velocity"
Dynamic, Explicit
 , 1e-05
Bulk Viscosity
 0.06, 1.2
Mass Scaling: Semi-Automatic
              Whole Model
Fixed Mass Scaling, factor=100.

  BOUNDARY CONDITIONS

 Name: zero velocity-balloon Type: Velocity/Angular velocity
Boundary, type=VELOCITY
```

```
balloon, 1, 1
balloon, 2, 2
balloon, 3, 3
 Name: zero velocity-stent Type: Velocity/Angular velocity
Boundary, type=VELOCITY
stent, 1, 1
stent, 2, 2
stent, 3, 3

 OUTPUT REQUESTS

Restart, write, number interval=1, time marks=NO

 FIELD OUTPUT: F-Output-1

Output, field, variable=PRESELECT, number intervals=1

 HISTORY OUTPUT: H-Output-1

Output, history, variable=PRESELECT
End Step

 ----------------------------------------------------------------

 STEP: release

Step, name=release
Dynamic, Explicit
 , 0.007
Bulk Viscosity
 0.06, 1.2
Mass Scaling: Semi-Automatic
              Whole Model
Fixed Mass Scaling, factor=100.

 BOUNDARY CONDITIONS

 Name: disp-1 Type: Displacement/Rotation
Boundary, op=NEW, amplitude=Amp-2
crimpingtool_refpt-1, 1, 1, 1.
crimpingtool_refpt-1, 2, 2
crimpingtool_refpt-1, 3, 3
crimpingtool_refpt-1, 4, 4
crimpingtool_refpt-1, 5, 5
crimpingtool_refpt-1, 6, 6
 Name: disp-10 Type: Displacement/Rotation
```

```
Boundary, op=NEW, amplitude=Amp-2
crimpingtool_refpt-10, 1, 1, 1.
crimpingtool_refpt-10, 2, 2
crimpingtool_refpt-10, 3, 3
crimpingtool_refpt-10, 4, 4
crimpingtool_refpt-10, 5, 5
crimpingtool_refpt-10, 6, 6
 Name: disp-11 Type: Displacement/Rotation
Boundary, op=NEW, amplitude=Amp-2
crimpingtool_refpt-11, 1, 1, 1.
crimpingtool_refpt-11, 2, 2
crimpingtool_refpt-11, 3, 3
crimpingtool_refpt-11, 4, 4
crimpingtool_refpt-11, 5, 5
crimpingtool_refpt-11, 6, 6
 Name: disp-12 Type: Displacement/Rotation
Boundary, op=NEW, amplitude=Amp-2
crimpingtool_refpt-12, 1, 1, 1.
crimpingtool_refpt-12, 2, 2
crimpingtool_refpt-12, 3, 3
crimpingtool_refpt-12, 4, 4
crimpingtool_refpt-12, 5, 5
crimpingtool_refpt-12, 6, 6
 Name: disp-2 Type: Displacement/Rotation
Boundary, op=NEW, amplitude=Amp-2
crimpingtool_refpt-2, 1, 1, 1.
crimpingtool_refpt-2, 2, 2
crimpingtool_refpt-2, 3, 3
crimpingtool_refpt-2, 4, 4
crimpingtool_refpt-2, 5, 5
crimpingtool_refpt-2, 6, 6
 Name: disp-3 Type: Displacement/Rotation
Boundary, op=NEW, amplitude=Amp-2
crimpingtool_refpt-3, 1, 1, 1.
crimpingtool_refpt-3, 2, 2
crimpingtool_refpt-3, 3, 3
crimpingtool_refpt-3, 4, 4
crimpingtool_refpt-3, 5, 5
crimpingtool_refpt-3, 6, 6
 Name: disp-4 Type: Displacement/Rotation
Boundary, op=NEW, amplitude=Amp-2
crimpingtool_refpt-4, 1, 1, 1.
crimpingtool_refpt-4, 2, 2
crimpingtool_refpt-4, 3, 3
crimpingtool_refpt-4, 4, 4
crimpingtool_refpt-4, 5, 5
```

```
crimpingtool_refpt-4, 6, 6
 Name: disp-5 Type: Displacement/Rotation
Boundary, op=NEW, amplitude=Amp-2
crimpingtool_refpt-5, 1, 1, 1.
crimpingtool_refpt-5, 2, 2
crimpingtool_refpt-5, 3, 3
crimpingtool_refpt-5, 4, 4
crimpingtool_refpt-5, 5, 5
crimpingtool_refpt-5, 6, 6
 Name: disp-6 Type: Displacement/Rotation
Boundary, op=NEW, amplitude=Amp-2
crimpingtool_refpt-6, 1, 1, 1.
crimpingtool_refpt-6, 2, 2
crimpingtool_refpt-6, 3, 3
crimpingtool_refpt-6, 4, 4
crimpingtool_refpt-6, 5, 5
crimpingtool_refpt-6, 6, 6
 Name: disp-7 Type: Displacement/Rotation
Boundary, op=NEW, amplitude=Amp-2
crimpingtool_refpt-7, 1, 1, 1.
crimpingtool_refpt-7, 2, 2
crimpingtool_refpt-7, 3, 3
crimpingtool_refpt-7, 4, 4
crimpingtool_refpt-7, 5, 5
crimpingtool_refpt-7, 6, 6
 Name: disp-8 Type: Displacement/Rotation
Boundary, op=NEW, amplitude=Amp-2
crimpingtool_refpt-8, 1, 1, 1.
crimpingtool_refpt-8, 2, 2
crimpingtool_refpt-8, 3, 3
crimpingtool_refpt-8, 4, 4
crimpingtool_refpt-8, 5, 5
crimpingtool_refpt-8, 6, 6
 Name: disp-9 Type: Displacement/Rotation
Boundary, op=NEW, amplitude=Amp-2
crimpingtool_refpt-9, 1, 1, 1.
crimpingtool_refpt-9, 2, 2
crimpingtool_refpt-9, 3, 3
crimpingtool_refpt-9, 4, 4
crimpingtool_refpt-9, 5, 5
crimpingtool_refpt-9, 6, 6
 Name: lumen_edge Type: Displacement/Rotation
Boundary, op=NEW
lumen_edge, 3, 3
 Name: wire-edge fix-2 Type: Symmetry/Antisymmetry/Encastre
Boundary, op=NEW
```

```
guide-wire-refpnt, ENCASTRE
 Name: zero velocity-balloon Type: Velocity/Angular velocity
Boundary, op=NEW, type=VELOCITY
balloon, 1, 1
balloon, 2, 2
balloon, 3, 3
 Name: zero velocity-stent Type: Velocity/Angular velocity
Boundary, op=NEW

 OUTPUT REQUESTS

Restart, write, number interval=1, time marks=NO

 FIELD OUTPUT: F-Output-1

Output, field, variable=PRESELECT

 HISTORY OUTPUT: H-Output-1

Output, history, variable=PRESELECT
End Step

 ----------------------------------------------------------


 STEP: expand

Step, name=expand
Dynamic, Explicit
 , 0.08
Bulk Viscosity
 0.06, 1.2

 BOUNDARY CONDITIONS

 Name: disp-1 Type: Displacement/Rotation
Boundary, op=NEW, amplitude=Amp-2
crimpingtool_refpt-1, 1, 1, 1.
crimpingtool_refpt-1, 2, 2
crimpingtool_refpt-1, 3, 3
crimpingtool_refpt-1, 4, 4
crimpingtool_refpt-1, 5, 5
crimpingtool_refpt-1, 6, 6
 Name: disp-10 Type: Displacement/Rotation
Boundary, op=NEW, amplitude=Amp-2
crimpingtool_refpt-10, 1, 1, 1.
crimpingtool_refpt-10, 2, 2
```

```
crimpingtool_refpt-10, 3, 3
crimpingtool_refpt-10, 4, 4
crimpingtool_refpt-10, 5, 5
crimpingtool_refpt-10, 6, 6
 Name: disp-11 Type: Displacement/Rotation
Boundary, op=NEW, amplitude=Amp-2
crimpingtool_refpt-11, 1, 1, 1.
crimpingtool_refpt-11, 2, 2
crimpingtool_refpt-11, 3, 3
crimpingtool_refpt-11, 4, 4
crimpingtool_refpt-11, 5, 5
crimpingtool_refpt-11, 6, 6
 Name: disp-12 Type: Displacement/Rotation
Boundary, op=NEW, amplitude=Amp-2
crimpingtool_refpt-12, 1, 1, 1.
crimpingtool_refpt-12, 2, 2
crimpingtool_refpt-12, 3, 3
crimpingtool_refpt-12, 4, 4
crimpingtool_refpt-12, 5, 5
crimpingtool_refpt-12, 6, 6
 Name: disp-2 Type: Displacement/Rotation
Boundary, op=NEW, amplitude=Amp-2
crimpingtool_refpt-2, 1, 1, 1.
crimpingtool_refpt-2, 2, 2
crimpingtool_refpt-2, 3, 3
crimpingtool_refpt-2, 4, 4
crimpingtool_refpt-2, 5, 5
crimpingtool_refpt-2, 6, 6
 Name: disp-3 Type: Displacement/Rotation
Boundary, op=NEW, amplitude=Amp-2
crimpingtool_refpt-3, 1, 1, 1.
crimpingtool_refpt-3, 2, 2
crimpingtool_refpt-3, 3, 3
crimpingtool_refpt-3, 4, 4
crimpingtool_refpt-3, 5, 5
crimpingtool_refpt-3, 6, 6
 Name: disp-4 Type: Displacement/Rotation
Boundary, op=NEW, amplitude=Amp-2
crimpingtool_refpt-4, 1, 1, 1.
crimpingtool_refpt-4, 2, 2
crimpingtool_refpt-4, 3, 3
crimpingtool_refpt-4, 4, 4
crimpingtool_refpt-4, 5, 5
crimpingtool_refpt-4, 6, 6
 Name: disp-5 Type: Displacement/Rotation
Boundary, op=NEW, amplitude=Amp-2
```

```
crimpingtool_refpt-5, 1, 1, 1.
crimpingtool_refpt-5, 2, 2
crimpingtool_refpt-5, 3, 3
crimpingtool_refpt-5, 4, 4
crimpingtool_refpt-5, 5, 5
crimpingtool_refpt-5, 6, 6
 Name: disp-6 Type: Displacement/Rotation
Boundary, op=NEW, amplitude=Amp-2
crimpingtool_refpt-6, 1, 1, 1.
crimpingtool_refpt-6, 2, 2
crimpingtool_refpt-6, 3, 3
crimpingtool_refpt-6, 4, 4
crimpingtool_refpt-6, 5, 5
crimpingtool_refpt-6, 6, 6
 Name: disp-7 Type: Displacement/Rotation
Boundary, op=NEW, amplitude=Amp-2
crimpingtool_refpt-7, 1, 1, 1.
crimpingtool_refpt-7, 2, 2
crimpingtool_refpt-7, 3, 3
crimpingtool_refpt-7, 4, 4
crimpingtool_refpt-7, 5, 5
crimpingtool_refpt-7, 6, 6
 Name: disp-8 Type: Displacement/Rotation
Boundary, op=NEW, amplitude=Amp-2
crimpingtool_refpt-8, 1, 1, 1.
crimpingtool_refpt-8, 2, 2
crimpingtool_refpt-8, 3, 3
crimpingtool_refpt-8, 4, 4
crimpingtool_refpt-8, 5, 5
crimpingtool_refpt-8, 6, 6
 Name: disp-9 Type: Displacement/Rotation
Boundary, op=NEW, amplitude=Amp-2
crimpingtool_refpt-9, 1, 1, 1.
crimpingtool_refpt-9, 2, 2
crimpingtool_refpt-9, 3, 3
crimpingtool_refpt-9, 4, 4
crimpingtool_refpt-9, 5, 5
crimpingtool_refpt-9, 6, 6
 Name: lumen_edge Type: Displacement/Rotation
Boundary, op=NEW
lumen_edge, 3, 3
 Name: wire-edge fix-2 Type: Symmetry/Antisymmetry/Encastre
Boundary, op=NEW
guide-wire-refpnt, ENCASTRE
 Name: zero velocity-balloon Type: Velocity/Angular velocity
Boundary, op=NEW
```

```
 Name: zero-velocity-balloon-2 Type: Velocity/Angular velocity
Boundary, op=NEW, type=VELOCITY
balloon-edge, 3, 3

 LOADS

 Name: pressure  Type: Pressure
Dsload, amplitude=Amp-3
balloon-inner, P, 600000.

 OUTPUT REQUESTS

Restart, write, number interval=1, time marks=NO

 FIELD OUTPUT: F-Output-1

Output, field, variable=PRESELECT, number intervals=40

 HISTORY OUTPUT: H-Output-1

Output, history, variable=PRESELECT
End Step

  ----------
```


C4 Offset stent simulation

```
Heading
 Job name: offset stent assembly Model name: offest stent assembly
Preprint, echo=NO, model=NO, history=NO, contact=NO

  ----------

 PARTS

Part, name=balloon
End Part
Part, name=full-stent-correct
End Part
Part, name=lumen_1
```

```
End Part

  ------------------------------------------------------------

 MATERIALS

Material, name=Nylon
Density
 1040.,
Elastic
 4.65e+08, 0.4
Material, name=Rubber
Density
 990.,
Elastic
 1e+10, 0.3
Material, name="Stainless Steel"
Density
 7850.,
Elastic
 1.93e+11, 0.3
Plastic
 3.3e+08,  0.
 6.7e+08, 0.48
Rate Dependent
40.,5.

  ------------------------------------------------------------

 INTERACTION PROPERTIES

Surface Interaction, name=Contact
Friction
 0.1,
Surface Behavior, pressure-overclosure=HARD

  ------------------------------------------------------------

 BOUNDARY CONDITIONS

  Name: Balloon-fix-1 Type: Displacement/Rotation
Boundary
"Balloon edges-2", 3, 3
  Name: Balloon-fix-2 Type: Displacement/Rotation
Boundary
"Balloon edges-1", 3, 3
```

```
 Name: fix lumen Type: Symmetry/Antisymmetry/Encastre
Boundary
"lumen rp", ENCASTRE

 ---------------------------------------------------------------

 INTERACTIONS

 Interaction: Balloon-balloon
Contact, op=NEW
Contact Inclusions, ALL ELEMENT BASED
Contact property assignment
 ,  , Contact

 ---------------------------------------------------------------

 STEP: Blow up balloon

Step, name="Blow up balloon"
Blow up baloon
Dynamic, Explicit
 , 0.032
Bulk Viscosity
 0.06, 1.2
Mass Scaling: Semi-Automatic
              Whole Model
Fixed Mass Scaling, factor=100000.

 LOADS

 Name: Load-1   Type: Pressure
Dsload, amplitude=Amp-1
Balloon-inner, P, 910600.

 OUTPUT REQUESTS

Restart, write, number interval=1, time marks=NO

 FIELD OUTPUT: F-Output-1

Output, field, variable=PRESELECT, number intervals=200

 HISTORY OUTPUT: H-Output-1

Output, history, variable=PRESELECT
End Step
```

REFERENCES

Bathe K-J (1976), *Numerical methods in finite element analysis,* Prentice-Hall, Inc., Englewood Cliffs, New Jersey 07632

Bathe K-J (1982), *Finite element procedures in engineering,* Prentice-Hall, Inc., Englewood Cliffs, New Jersey 07632

Becker B, Horner MJN (2004), "C.A.R.M.E.N.: A General-Purpose Computing Facility For Scientific Research Using OSCAR", *Proceedings of the 2nd Annual OSCAR Symposium (OSCAR2004)*, Winnipeg, Manitoba Canada, 16-19 May, 2004

Belytschko T, Liu WK, Moran B (2000), *Nonlinear finite elements for continua and structures*, John Wiley & Sons, Inc., The Atrium, Southern Gate, Chichester, West Sussex PO19 8SQ, England

David Chua SN, Mac Donald BJ, Hashmi MSJ (2001), "Finite-element simulation of stent expansion", *Journal of Materials Processing Technology,* Vol.120, pp. 335-340

David Chua SN, Mac Donald BJ, Hashmi MSJ (2003), "Finite element simulation of stent and balloon interaction", *Journal of Materials Processing Technology,* Vol.143-144, pp. 591-597

Cook RD, Malkus DS, Plesha ME, Witt RJ (2002), *Concepts and applications of finite element analysis, Fourth Edition,* John Wiley & Sons, Inc., Canada

Cook RD (1995), *Finite element modelling for stress analysis*, John Wiley & Sons, Inc., Canada

Cebral JR, Löhner R, Choyke PL, Yim PJ (2001), "Merging of intersections for finite element modeling", *Journal of Biomechanics,* Vol. 34, pp. 815-819

Cook RD (1995), *Finite Element modelling for stress analysis,* John Wiley & Sons Inc., USA

Dumoulin C, Cochelin B (2000), "Mechanical behaviour modelling of balloon-expandable stents", *Journal of Biomechanics,* Vol. 33, pp. 1461-1470

Etave F, Finet G, Boivin M, Boyer J-C, Rioufol G, Thollet G (2001) "Mechanical properties of coronary stents determined by using finite element analysis", *Journal of Biomechanics,* Vol.34, pp. 1065-1075

Migliavacca F, Petrini L, Colombo M, Auricchio F, Pietrabissa R (2002), "Mechanical behaviour of coronary stents investigated through the finite element method", *Journal of Biomechanics,* Vol. 35, pp. 803-811

Oh S, Kleinberger M, McElhaney JH (1994), "Finite-Element analysis of balloon angioplasty", *Medical and Biological Engineering and Computing,* Vol.32, pp. S108-S114

Prendergast PJ, Lally C, Dally S, Reid AJ (2003), "Analysis of Prolapse in Cardiovascular Stents: A Constitutive Equation for Vascular Tissue and Finite-Element Modelling", *Transactions of the ASME*, Vol. 125, pp. 692-699

Rockey KC, Evans HR, Griffiths DW, Nethercot DA (1975), *The finite element method,* William Clowes & Sons, Limited, London, Beccles and Colchester

Rogers C, Tseng DT, Squire JC, Edelman ER (1999), "Balloon-Artery Interactions During Stent Placement: A Finite Element Analysis Approach to Pressure, Compliance, and Stent Design as Contributors to Vascular Injury", *Circulation Research,* Vol. 84, pp. 378-383

Tan LB, Webb DC, Kormi K, Al-Hassani STS (2001), "A method for investigating the mechanical properties of intracoronary stents using finite element numerical simulation", *International Journal of Cardiology,* Vol.78, pp. 51-67